# THE **ASEAN JOURNAL** OF **RADIOLOGY**

# Letter from editorial board

Over the years, the Asean Journal of Radiology has published the papers on Radiological Sciences, such as research work, reviews articles, case reports, and innovations in medical sciences related to all branches of Radiology, in a hard copy or printed articles. We currently have online tool which is more effective of delivery method, all members and readers can assess and participate easily.

On behalf of the editorial staffs of The Asean Journal of Radiology, we encourage all readers to submit scientific works on aforementioned specialty areas. We thank you for all authors and all peer reviewers for participating in our Asean Journal of Radiology. Your responses will provide continually improve our journal. If you have any suggestions, you may e-mail to us at Pusjeckchon@hotmail.com

**Anchalee Churojana, MD**

*Editor in Chief, Asean Journal of Radiology*

*Royal College of Radiologists of Thailand and Radiological Society of Thailand*

# Contents

## Original Article

## Case Report

Original Article

# Prediction for Risk of Recurrence and Delayed Metastases of Nasopharyngeal Carcinoma: An evaluation of CT scan

**Umasan Phuprasat, M.D.**
**Anchalee Churojana, M.D.**
**Kullathorn Thepmongkol, M.D.**

*Division of General Radiology, Department of Radiology, Faculty of Medicine, Siriraj Hospital, Mahidol University,*
*2 Prannok Road, Bangkok Noi, Bankok, Thailand 10700*

## Abstract

**Purpose:** To analyze the imaging characteristic on CT scan of the primary nasopharyngeal carcinoma which predict the locoregional recurrence.

**Materials and Methods:** A retrospective review of 464 patients who had nasopharyngeal carcinoma at Siriraj Hospital, during 2004-2009 was performed. The treatment options were radiation therapy and concurrent chemotherapy corresponding to the staging, which were assessed by using CT. The patients who had no available initial imaging studies, incomplete treatment or had follow up less than 1 year were excluded. The imaging studies were analyzed for primary tumor size, direct tumor extension, and cervical lymph node involvement. The vascular invasion was defined as the obliteration more than half of the circumferential fat surrounding internal carotid artery. The regional nodes were evaluated for the levels of involvement and size of the largest one.

**Results:** There were 99 patients (68 male, 31 female, mean age at 50 years) with the TNM classifications as follows:  T1 5.2%, T2 39.4%, T3 24.2%, T4 21.2%, N0 18.2%, N1 14.1%, N2 46.5% and metastasis 11.76%. The extensions were prevertebral space (54.5%), masticator space (30.3%), skull base destruction (18.2%), and vascular invasion (42.4%). Nodal involvement was found in 81.8%. The most frequency of the largest lymph node was at ipsilateral level V (38.4%) and II (41.4%). Recurrence was found in 40.4% with averaged at 24 months after complete treatment (95%CI). Vascular invasion and skull base invasion had significant associated to predictive the risk of recurrence (P=0.04 and <0.001, respectively). The size of the tumor or lymph node showed no relation to the local regional recurrence or metastasis.

**Conclusion:** The risks of NPC recurrence have been correlated to TNM staging, skull base, and carotid space involvement. Skull base invasion has been identified to be the predictive sign for tumor recurrence. Skull base invasion and carotid space involvement have also a statistically significant prognostic factor for overall survival.

# Introduction

Nasopharyngeal carcinoma (NPC) is an aggressive cancer which is endemic in Southern China and South East Asia, which has the incidence accounting 2-10 per 100,000 person-years[1-3]. The gross mortality of NPC is reported about 1.34 per 100 000, comprises 1.61% of tumor caused deaths and ranks ninth in China[4-5].

In Thailand, according to the statistics database of Siriraj Cancer Institute Registry in 2008, new cases of NPC were accounted for 3.28% and 1.21% which were ranking at the eighth and thirteenth common cancer in male and female patients, respectively[6].

Although NPC is very radiosensitive and the treatment outcome have improved in the recent decades, but rate of local regional failure and tumor recurrence can occur in 19%-56% of patients within 2-5 years after definite radiotherapy[4,5,7,8]. The prognosis following local recurrence is rather poor without retreatment[8,9]. Moreover, after treatment, clinical examination for detection of residual or recurrence may be inconclusive; imaging studies may be equivocal due to the presence of diffuse soft tissue edema. In such cases, tumor recurrence should be confirmed by biopsy[4,5].

Thus, it is essential to be able to predict the therapeutic response of the patients with NPC from the initial imaging study which CT scan is widely common used[4,8-10]. Those patients may be need more closely follow up for the early detection of tumor recurrence. In this regard, early retreatment may be benefit to achieve better tumor control and improve patient survival[4,5,7-10].

The purpose of this paper is to analyze whether any characteristics or sign on initial CT scan which may predict the risk of tumor recurrence in the patients with NPC after receiving complete treatment.

# Materials and Methods

## Patient characteristics

A number of 464 patients who had pathological proven of nasopharyngeal carcinoma (NPC) at Siriraj Hospital, Mahidol University, between January 2004 and April 2009 were retrospectively reviewed, under the approval of the ethic committee of our hospital.

All patients received definite standard radiation treatment with or without concurrent chemotherapy corresponding to their own primary stage. Our radiation therapy protocol for primary NPC was achieved from external-beam radiation, either conventional radiotherapy or integrated moderator radiotherapy (IMRT) at a mean dose of 70 Gy in 33 fractions (range, 65-80 Gy), which were 1.8 to 2.0 Gy per fraction for 5 fractions at a weekly interval.

After complete treatment, the patients had scheduled to follow up with evaluation of the treatment response by the joint clinics of otolaryngology, radiotherapy, and oncology for every 6-8 weeks in the first year, every 3 months in the second year, once every 4-6 months in the third year, and once every 6-9 months, thereafter. Endoscopic examination of the nasopharynx was evaluated at 6-8 weeks. The follow-up imaging was performed within 3-12 months or whenever there was clinical suspicion of tumor recurrence.

**The exclusion criterias were included**

1. The patients who had unavailable initial imaging study.

2. The patients who had incomplete treatment or loss to follow up.

3. The patients who had less than 12 months

follow up after complete treatment.

4. The patients who had history of other underlying malignancy with cervical lymph node metastasis.

5. The patients who had advanced staging or distant metastasis at the presenting diagnosis which included intracranial extension, and/or metastases to mediastinal lymphnode, lung, skeleton, liver, and miscellaneous (bone marrow, skin, other viscera and soft tissue).

6. The patients who had progressive disease or distant metastasis during or immediate after complete treatment.

## Tumor response and recurrence

The patients who were enrolled in this study were divided into 2 groups; recurrent and non recurrent groups.

The recurrent group included those patients who had increase or newly detectable one or more of the following lesions; 1. loco-regional or primary site, 2. cervical lymph node, 3. distant metastases during the follow up period for at least one year, after initial document of tumor free-period or at least stable disease after complete treatment. The recurrent disease was diagnosed by information of physical examination, endoscopic findings, imaging feature and histopathology.

The non-recurrent group was defined as the patients who had responded to the treatment or at least stable disease after complete treatment without evidence of new lesions or recurrence over one year period.

The patients who had progressive disease after treatment, either at the primary site or cervical lymph nodes were excluded from the study.

## CT scan analysis

The initial CT scans were reviewed by one neuroradiologist who had more than 10 years experience and blinded from the follow up outcome of the patients. The CT images were retrieved from the picture archiving and communication system (PACS) for evaluation of the primary tumor in term of side, size (averaged diameter), extension and tumor staging using TNM staging according to AJCC 2002 guideline[11]. The side was observed to be one or both sides of tumor involvement. The tumor size was calculated in the averaged diameter which measured in two maximal dimensions with perpendicular axes to each other on the cross sectional CT image (figure 1) and classified as less than 5 mm, 5-10 mm, 11-15 mm and more than 15 mm. The direct extension of the primary tumors are categorized into many regions as parapharyngeal space, masticator space, parotid space, prevertebral space, skull base, internal carotid artery (ICA) or vascular invasion and presence of retropharyngeal lymph nodes.

Our criteria for ICA invasion was at least demonstration of obliteration of the circumferential fat plane between ICA and tumor more than 180 degrees.

The cervical lymph nodes were interpreted as the level system according to 1977 AJCC nodal classification[12]. However, the supraclavicular group was named separately. They were documented as positive if the short axis was longer than 10 mm.

## Statistical analysis

All the statistical analyses in this study were carried out using SPSS for Windows software version 13.0 (SPSS; statistical software version 13.0).
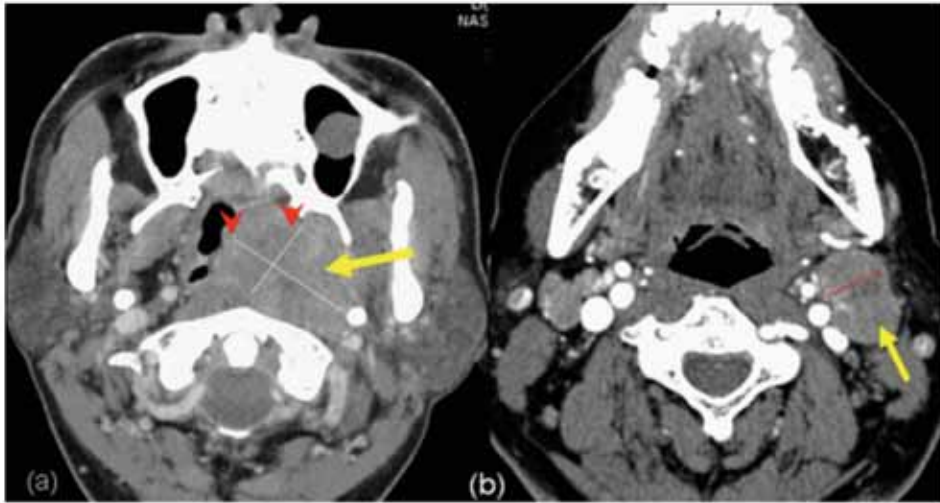
**Fig. 1** Demonstrated of primary tumor and lymph node measurements

(a) The primary tumor (arrow) measurement on contrast enhanced CT image in the axial plane was obtained by the averaged measurement in two greatest dimensions in perpendicularly axes to each other (arrow head) and classified into 4 groups as less than 5 mm, 5-10 mm, 11-15 mm and more than 15 mm.

(b) The regional nodal measurement was performed by single maximal diameter in short axis.

The univariate analysis was using the log rank test and multivariate analysis was using the Cox proportional hazards model. Survival analysis were performed using estimation method of Kaplan and Meier. Overall survival (OS) in this study was defined as the time from NPC diagnosis to death resulting from any cause or at the time of last follow-up. P values less than 0.05 was considered statistically significant.

## Results

Of 464 patients with NPC, there were 99 patients (68 men, and 31 women) who met our criteria. All patients had mean time of follow up at 24 months. Recurrent disease was found in 40/99 (40.4%) including locoregional recurrence at primary site and/or cervical lymph node in 19 cases (19.2%) and distance metastasis in 21 cases (21.2%), with

a relapse time range from 6 to 58 months (mean 12 months) after complete treatment. The comparison of the demographic data and tumor characteristics of recurrent and non recurrent groups were shown in table 1, which showed no significant statistically difference between both groups.

Concerning characteristics of primary lesion of NPC (table 2), the T stage of primary tumor according to AJCC 2002 TNM classification had statistically significant correlation to risk of tumor recurrence (P=0.044), whereas the higher T stage had higher risk of recurrence. The lateralization and size of the primary tumor showed no statistically significant to predict risk of recurrence of NPC.

With respect to direct extension of the NPC to other neck spaces (table 3), there were significant association of tumor recurrence with the involvement of carotid space or vascular invasion

**Table 1:** Patient and tumor characteristics of recurrence and non recurrence groups

| Character | Total n = 99 | Number of patients | |
|---|---|---|---|
| | | Recurrent n = 40 | Non recurrent n = 59 |
| Sex: Men | 68 | 30 (44.12%) | 38 (55.88%) |
| Women | 31 | 10 (29.03%) | 21 (70.96%) |
| Age range ( Mean age: years) | 18–82 (50.23) | 18–74 (48.61) | 33–82 (50.30) |
| Pathological Feature (WHO) | | | |
| Type I: NK,SCC | 11 | 4 (36.36%) | 7 (63.64%) |
| Type II: SCC(mod-poor diff) | 45 | 21 (46.66%) | 24 (53.33%) |
| Type III: Undifferentiated, SCC | 43 | 15 (34.88%) | 28 (65.12%) |
| Treatment | | | |
| Definite Radiation Therapy | 4 | 1 (25%) | 3 (75%) |
| Concurrent chemoradiation | 95 | 55 (55.56%) | 44 (44.44%) |
| Mean radiation dose | 68 $\pm$ 2 Grey | 68 $\pm$ 2 Grey | 68 $\pm$ 2 Grey |
| Mean time of follow up (months) | 24 $\pm$ 2 | 24 $\pm$ 2 | 24 $\pm$ 2 |

**Table 2:** Comparison of feature of primary NPC between recurrence and non recurrence groups

| Parameter | Total Number n = 99 (100%) | Number of patients | | p-value |
|---|---|---|---|---|
| | | Recurrent group n =40 (40.4%) | No recurrent group n = 59 (59.6%) | |
| Location [a] of NPC | | | | |
| One side of NP | 69 (70) | 24 (63.13) | 31 (36.87) | 0.452 |
| Both side of NP | 30 (30) | 16 (53.33) | 14 (46.67) | |
| Primary tumor size [b] | | | | |
| < 5 mm. | 6 (6.06) | 4 (66.67) | 2 (33.33) | 0.385 |
| 5 – 10 mm. | 5 (5.05) | 2 (40.00) | 3 (60.00) | |
| 11 – 15 mm. | 13 (13.13) | 7 (53.85) | 6 (46.15) | |
| > 15 mm. | 75 (75.76) | 27 (36.00) | 48 (64.00) | |
| TNM Classification [c] | | | | |
| T stage: T1 | 15 (15.15) | 7 (46.67) | 8 (53.33) | 0.044 |
| T2 | 39 (39.39) | 7 (17.95) | 32 (82.05) | |
| T3 | 24 (24.24) | 14 (58.33) | 10 (41.67) | |
| T4 | 21 (21.21) | 12 (57.14) | 9 (42.86) | |

Using Cox regression Analysis and significant p-value was less than 0.05

n: Number of cases in each group

a: Lateralization of primary nasopharyngeal cancer (NPC) which was stratified as involved one side of NP included midline lesion, or involved both side of NP

b: Primary tumor size measured from initial CT image

c: TNM tumor classification according to AJCC 2002 guideline

**Table 3:** Comparison of tumor extension between recurrence and non recurrence groups

| Direction of NPC spreading | Total n = 99 (100%) | Number of patients | | p-value |
|---|---|---|---|---|
| | | Recurrent group n =40 (40.4%) | No recurrent Group n = 59 (59.6%) | |
| Parapharyngeal space invasion | 22/99 (22.22) | 8 (36.36) | 14 (63.64) | 0.41 |
| Masticator space invasion | 30/99 (33.33) | 13 (43.33) | 17 (56.67) | 0.40 |
| Prevertebral space invasion | 54/99 (54.55) | 20 (37.04) | 34 (62.96) | 0.39 |
| Parotid space invasion | 7/99 (7.10) | 4 (57.14) | 3 (42.86) | 0.56 |
| Vascular invasion | 42/99 (42.42) | 23 (54.76) | 19 (45.24) | 0.04 [1] |
| Skull base invasion | 18/99 (18.18) | 14 (77.78) | 4 (22.22) | < 0.001 [2] |

Using Cox regression analysis and significant p-value was less than 0.05

1: The hazard risk was 2.05 with 95% Confidential Interval 1.03-4.06.

2: The hazard risk was 0.26 with 95% Confidential Interval = 0.13-0.52.

**Table 4:** Nasopharyngeal carcinoma: 6th edition TNM Classification (2002) according to AJCC staging system guideline [11]

| T stage | |
|---|---|
| T1 | Tumor confined to nasopharynx |
| T2 | Tumor extends to soft tissue |
| T2a | Tumor extends to oropharynx and/or nasal cavity without parapharyngeal extension |
| T2b | Any tumor with parapharyngeal extension |
| T3 | Tumor invades bony structures and/or paranasalsinuses |
| T4 | Tumor with intracranial extension and/or involvement of cranial nerves, infratemporal fossa, hypopharynx, orbit, or masticator space |
| **N stage** | |
| N0 | No regional lymph node (LN) metastasis |
| N1 | Unilateral metastasis in LN (s), $\leq$6 cm in greatest dimension, above supraclavicular fossa |
| N2 | Bilateral metastasis in LN (s), $\leq$6 cm in greatest dimension, above supraclavicular fossa |
| N3 | Metastasis in LN (s) >6 cm and/or to supraclavicular fossa |
| N3a | Metastasis in LN (s) >6 cm in dimension |
| N3b | Metastasis in LN (s) with extension to supraclavicular fossa |
| **Stage group** | |
| I | T1N0M0 |
| IIA | T2aN0M0 |
| IIB | T2bN0M0 or T1-T2N1M0 |
| III | T1-T3N2M0 or T3N0-N1M0 |
| IVA | T4N0-N2M0 |
| IVB | Any T N3, M0 |
| IVC | Any T, any N, M1 |

**Table 5:** Comparison of the feature of lymph nodes between recurrent and non recurrent groups

| Parameter | Total n = 99 (100%) | Number of patients | | p-value |
|---|---|---|---|---|
| | | Recurrent group n =40 (40.4%) | No recurrent n = 59 (59.6%) | |
| N stage : N0 | 18 (18.2) | 5 (27.78) | 13 (72.22) | 0.002 |
| N1 | 14 (14.1) | 10 (71.42) | 4 (28.57) | |
| N2 | 46 (46.5) | 13 (28.26) | 33 (71.74) | |
| N3 | 21 (21.2) | 12 (57.14) | 9 (42.86) | |
| Cervical nodes involvement | | | | |
| Ipsilateral side of NPC | 59 (59.6) | 23 (38.98) | 36 (61.01) | 0.690 |
| Contralateral side NPC | 40 (40.4) | 17 (42.50) | 23 (57.50) | |
| Level of nodal involvement | | | | |
| Cervical LN group II | 41 (41.4) | 27 (65.8) | 14 (34.2) | 0.954 |
| Cervical LN group III | 5 (5.1) | 3 (60.0) | 2 (40.0) | |
| Cervical LN group IV | 1 (1.0) | 0 (0.0) | 1 (100) | |
| Cervical LN group V | 38 (38.4) | 20 (52.6) | 18 (47.4) | |
| All II - V levels | 8 (8.1) | 5 (62.5) | 3 (37.5) | |
| RPLN | 39 (39.4) | 19 (48.7) | 20 (51.3) | |
| SPC | 6 (6.1) | 4 (66.7) | 2 (33.3) | |
| Maximal diameter of LN | | | | |
| Less than 1.0 cm | 17 (17.2) | 4 (23.5) | 13 (76.5) | 0.064 |
| 1.0 -1.5 cm | 25 (25.3) | 6 (6.1) | 19 (93.9) | |
| > 1.5 – 2.0 cm | 20 (20.2) | 11 (55.0) | 9 (45.0) | |
| > 2.0 cm | 24 (24.2) | 11 (45.8) | 13 (54.2) | |
| Matted lymph node | 13 (13.1) | 8 (61.5) | 5 (38.5) | |
| (Averaged diameter of LN) | - | 3.6 cm | 1.5 cm | 0.178 |

**Table 6:** Multivariate Cox regression analysis of significant factors

| Predictive Factors | Recurrent NPC n=40 (40.4%) | No recurrent NPC n=59 (59.6%) | P-values* | HR[1] [95%CI] |
|---|---|---|---|---|
| Primary T stage | 40/99 (40.4) | 59/99 (59.6) | 0.637 | - |
| Primary N stage | 40/99 (40.4) | 59/99 (59.6) | 0.657 | - |
| Vascular invasion | 23/99 (23.23) | 19/99 (19.19) | 0.285 | - |
| Skull base invasion | 14/99 (14.14) | 4/99 (4.04) | < 0.001 | 0.259 [0.13-0.59] |

*Using Cox regression analysis and significant p-value was less than 0.05

1 Harzard Risk (HR) value of Cox regression analysis

[P-value=0.04 and 95%CI; 1.03-4.06, HR=2.05] and skull base extension [P-value=<0.001 and 95%CI; 0.13-0.52, HR=0.26]. In our study, extension to other adjacent spaces such as parapharyngeal space, masticator space or parotid space had no correlation with the risk of recurrence.

All patients had cervical lymph node enlargement at presentation. The distribution of lymph nodes which were classified according to level system, the nodal stage according to AJCC 2002 TNM classification and nodal size were demonstrated in table 4 and 5. According to our data, the only lymph node feature that had statistically significant to associate with the risk of recurrent NPC was correlated with nodal stage of TNM classification (P=0.007). Similar to T stage, the risk of recurrence was increased with the higher N stage. In our study, the mean nodal size was 3.6 cm in the short axis of recurrent group whereas it was 1.5 cm in the non recurrent group. However, there was no statistically significant to prognostic risk of recurrence between these 2 groups. (P=0.064).

However, after using multivariate analysis by Cox proportion and hazard model of statistically significant factors (as shown in table 6), which were associated with tumor recurrence, including primary T and N stage, vascular invasion and skull base invasion. The result showed only skull base invasion that is persistent statistically significant feature (P <0.001), whereas another features showed no statistically significant (P >0.05). Thus, the skull base invasion was a predictive sign to determine risk of recurrent NPC and another feature was undetermined.

In our study, twenty-one of 40 patients with recurrent disease had distant metastases, 13 patients was found metastases to lung, 7 to liver, 3 to skeleton, and 2 had subcutaneous nodules, which the further tissues biopsy showed metastasis carcinoma. Three of them had both lung and bony metastases and one of them had progressive liver involvement after lung metastasis at the time of last follow up. The interval duration from post complete treatment to metastases was averaged at 24 months.

When correlation between the follow up time and evidence of recurrent NPC, overall survival rate for all 99 NPC patients were 85%, 71%, 56%, and 50% in first, second, third, and fourth-year after diagnosis, respectively (figure 2). The median overall survival rate was 39 months.

Apart of direct extension of the NPC to other neck spaces, there were two spaces of direct extension that had profound influence of the patient's survival rate. The first one was a vascular invasion (figure 3); the patient who had a vascular invasion will be the time of recurrence NPC rapidly more than the patient, who did not have the vascular invasion. Median time of recurrence was 34 months in patient with vascular invasion and 43 months in patient without this feature (P value = 0.032).

Similarly to survival time analysis of skull base invasion (figure 4); the patient who had a skull base invasion will have recurrence more rapidly than the patient who did not have the skull base invasion. Median time of recurrence were 24 and 44 months in patient with and without skull base invasion, respectively (P value =< 0.001).

In another parameter, included primary tumor size, location, the rest of primary extension, nodal size, and nodal levels, had similarly in median time of recurrence and no statistically significant difference within groups.

**Fig. 2** Overall survival rate of patient's entire group at mean of covariates (n= 99).



Survival Function at mean of covariates

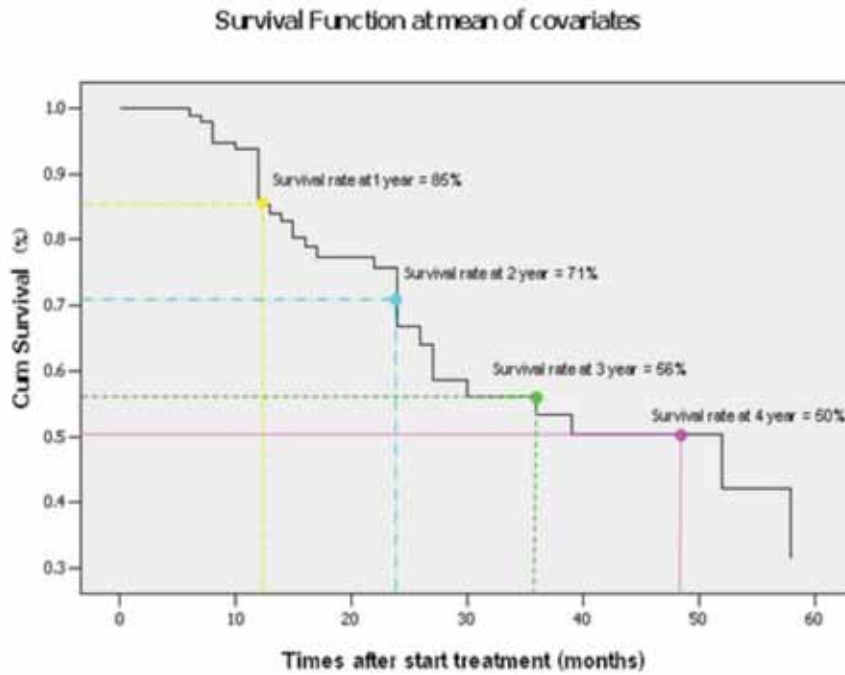**Fig. 3** Survival of patients for the different levels of vascular/carotid space invasion



Survival Functions

| Vascular invasion | Total | Median time of recurrence (months) |
|---|---|---|
| No vascular space invasion | 57 | 42.74 |
| Vascular space invasion | 42 | 34.32 |
| Overall | 99 | 39.02 |

Kaplan-Meier analysis was defined significant p value less than 0.005
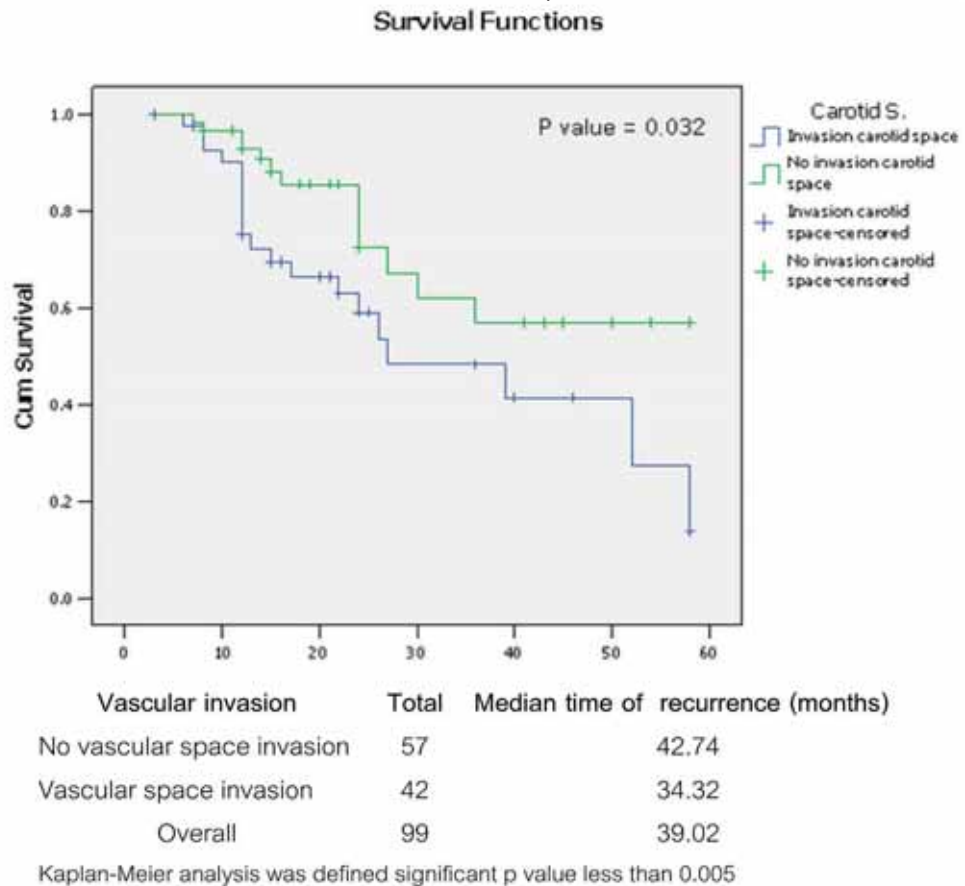
**Fig. 4** Survival of patients by skull base invasion



Survival Functions
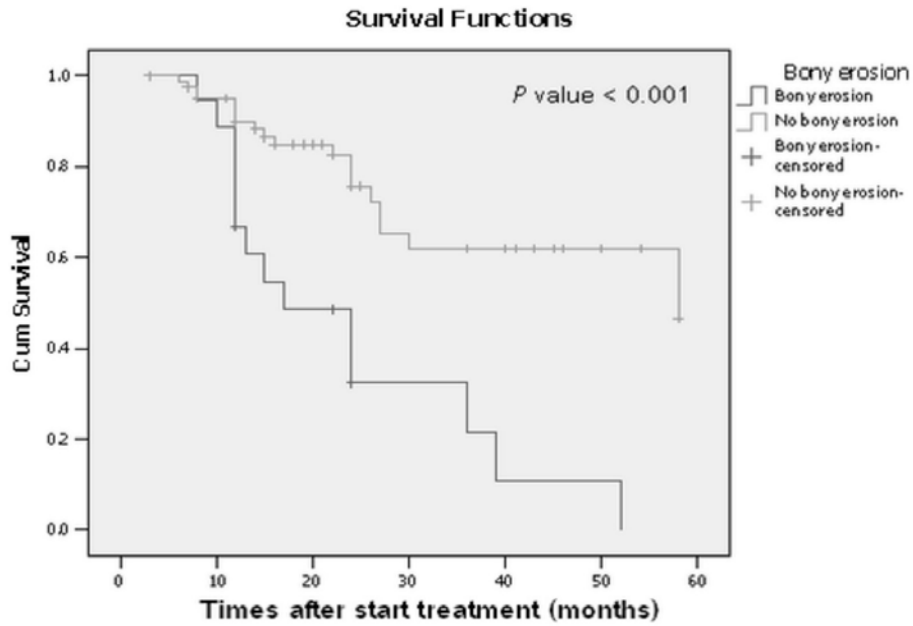
| Bony skull invasion | Total | Median time of recurrence (months) |
|---|---|---|
| No bony skull invasion | 81 | 43.564 |
| Bony skull invasion | 18 | 23.956 |
| Overall | 99 | 39.017 |

Kaplan-Meier analysis was defined significant p value less than 0.005

**Fig. 5** Vascular or Carotid space invasion
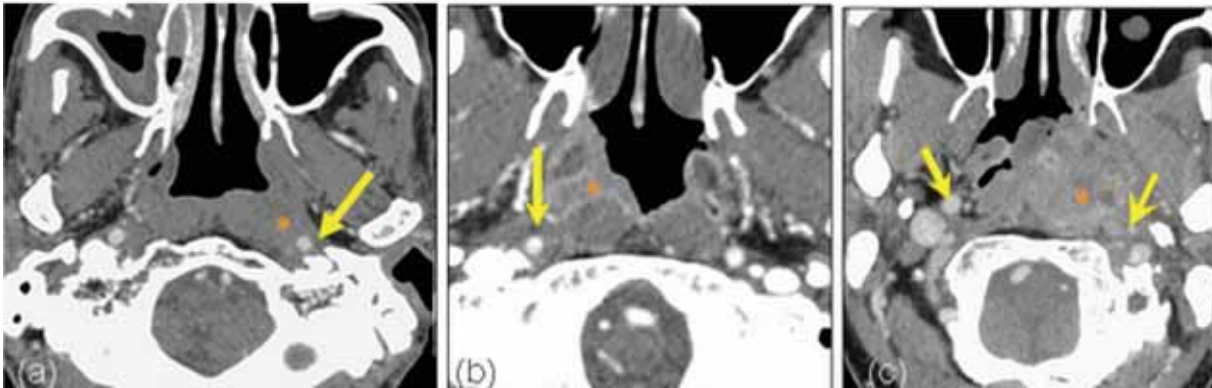


(a)     Axial contrast-enhanced CT scan of the nasopharynx in a patient with NPC. There is an enhancing tumor at left nasopharynx (*), which extension caused obliterate the circumferential fat plane of left internal carotid artery or internal jugular vein more than half of diameter (arrow). Comparisons to the right sided, which preserves normal fat plane.

(b)     Axial contrast-enhanced CT scan of the nasopharynx in a different patient with NPC. There is an enhancing tumor at right nasopharynx (*), which extension to across midline and caused obliterate the circumferential fat plane of right ICA more than half of diameter (arrow). Comparisons to the left sided, which preserves the normal fat plane.

(c)     Axial contrast-enhanced CT scan of the nasopharynx in a different patient with NPC. The enhancing tumor mainly occupies at left nasopharynx and across midline to the right side (*), cause obliterate the circumferential fat plane of both ICA more than 180 degrees (arrow). Narrowing of left ICA is also noted.

**Fig. 6**  A 57 years man known case of right nasopharyngeal cancer
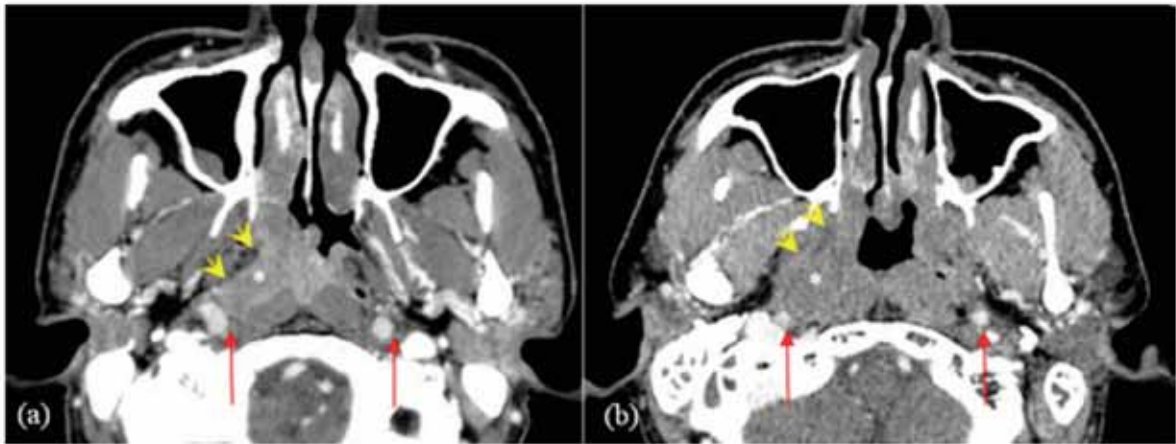


(a)     Axial contrast-enhanced CT scan of the nasopharynx showed enhancing NPC at right NP (*) and extension to right parapharyngeal space; PPS (arrow head) but still preserves the normal fat plane of bilateral vascular spaces (arrow).

(b)     Axial contrast-enhanced CT scan of the other patient with right NPC (*), revealed the NPC extends to right PPS (arrow head) and encase right carotid space nearly half of its diameter, but still preserves the normal fat plane of left vascular spaces (arrow).

**Fig. 7**  A 57 years old man known case of right nasopharyngeal cancer
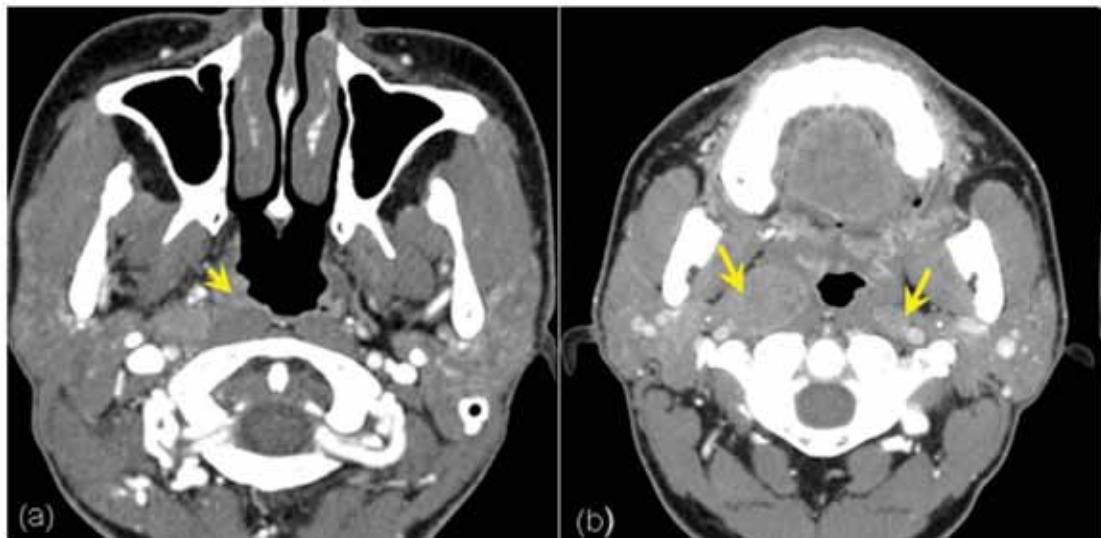


(a)     Axial contrast-enhanced CT scan of this patient at level of nasopharynx show enhancing tumor at right nasopharynx (arrow head).

(b)     Axial contrast-enhanced CT scan of the same patient at lower level has shown bilateral enlarged retropharyngeal lymph nodes (arrow).

**Fig. 8** A 49 years man known case nasopharyngeal cancer
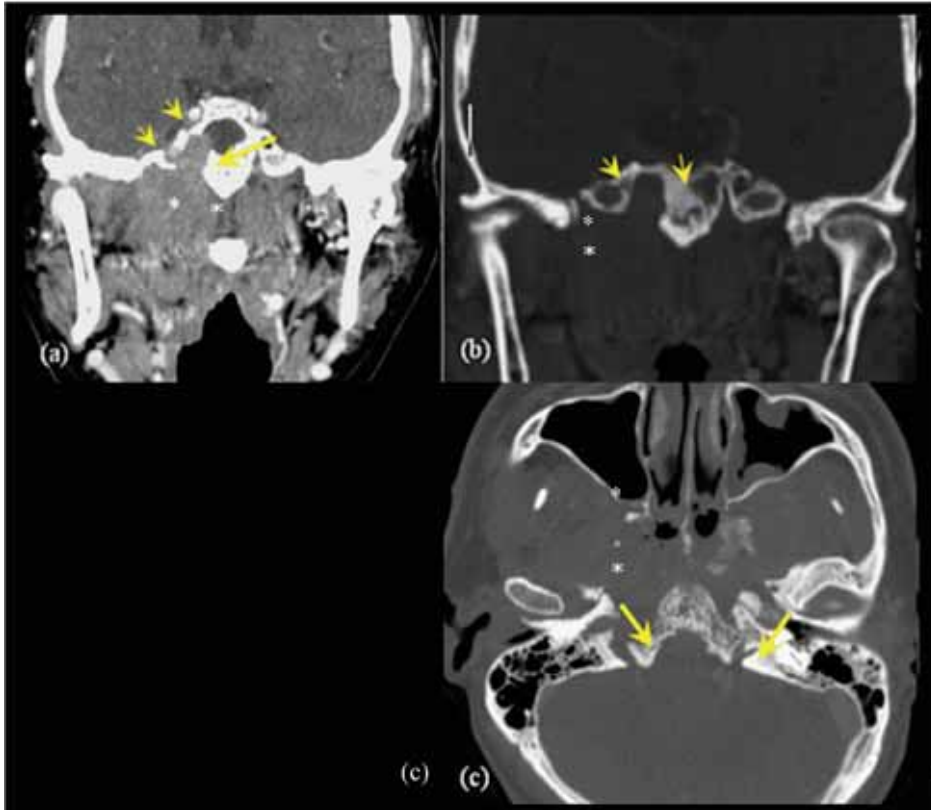


(a)    Coronal view of contrast-enhanced CT scan with soft tissue window and bone window (b) shows enhancing NPC at both NP, which extended into cavernous sinus with predominate in the right sided, resulting of bony destruction at right petrous, right pterygoid plate and clivus.

(b)    Axial view of contrast-enhanced CT scan with bone window showed extensive bony destruction of petrous bones, pterygoid plates, clivus and widening of both foramen lacerum, foramen ovale and foramen spinosum.

## Discussion

Local recurrence and distant metastasis are the common mode of treatment failure of a nasopharyngeal cancer, which are determinant of survival. Locoregional control of NPC remains a significant factor of local recurrence. It has been accepted that the primary tumor, nodes and metastases (according to the TNM staging) is the most important prognostic factor. Different patterns of treatment failure had been defined across stages. T3-4 No-1 mostly has local failure; any T with N2-3 has risk of locoregional and distant failure[13]. In addition, some investigators suggested that tumor volume had a close relationship with survival rates and recurrence rates. The NPC with large tumor volume was associated with more recurrence and poor survival rate[14]. Moreover, De-hong et al had described the relationship between post-radiation changes and recurrent diseases and suggested, that If the nasopharyngeal walls remained moderately thick (greater than 3 mm) on a CT scan beyond 6 months after radiotherapy, the risk of relapse would increase15.

In our study, which initially excluded metastases, by using univariate analyses primary tumors, nodes, skull base erosion, and carotid space invasion were independent risk factors of tumor

recurrence. According to TNM staging, the skull base involvement was corresponding to T4 stage. In term of prognostic factors, our results were in accordance with various studies, in which the higher T stage had increased risk of local failure with consequently increased risk of recurrence[16]. However, in our data tumor size had no statistically significant correlation with the risk of recurrence. This finding was disagreed with those reports which promoted the value of tumor volume in predicting local control. This might imply that the tumor size which was measured on the single axial image was not represented the tumor volume. Although, volumetric analysis of the primary tumor has been shown to be an important prognostic value in predicting local control, but tumor volume measurement techniques is complicated and less applicable in routine work. Furthermore, NPCs tend to be infiltrative and irregularly resulting to difficult to assessment. Accurate measurement of tumor volume requires a detailed outlining of the tumor extent from imaging, and a calculation of tumor volume from a three-dimensional perspective[17].

For early detection of skull base erosion, multidetector CT scan has been the reliable and the most cost-effectiveness imaging tool for evaluation. MRI should be performed when subtle lesions adjacent to the skull base or subtle intracranial invasion is suspicious. Comparison the capacity between CT scan and MRI was not the purpose of this study.

Carotid space invasion had been recognized which showing significant correlation with tumor recurrence in our analysis. Generally speaking, carotid space is post styloid compartment of parapharyngeal space. Its involvement indicates posterolateral tumor extension in the parapharyneal

space which is corresponding to T2b stage of TNM staging. The parapharyngeal space was the most commonly infiltrated region.

Involvement of parapharyngeal space was shown to be associated with prognostic factor and poor local control in several reports[16]. Kalogera-Fountzila A et al[16] demonstrated that the degree of the tumor extension into the parapharyngeal space was an independent prognostic factor for overall survival. Our data suggested that invasion of the carotid space which was indicated by loss of fat plane surrounding the internal carotid artery was more important sign than invasion of parapharyngeal space alone. To evaluate infiltration of perivascular fat plane, MRI is more accurate and preferred to be diagnostic method particularly if it is not extensive involvement, however, multidetector CT scan can be applied. Based on our result, skull base erosion and carotid space involvement had statistically significant, thus, posterior extension of the NPC may confer the worse prognosis.

The incidence of presence of cervical lymph node involvement in patients with NPC is quite high. About 75% of patients have enlarged cervical nodes at presentation[18], 80% are bilateral. Nodal metastasis shows an orderly inferior spread and the affected nodes are larger in the upper neck[19]. It was found 100% in our study. There was correlation between lymph node involvement according to TNM staging and risk of tumor recurrence (p=0.02), however, the size and the nodal levels had no significant effect.

Our data revealed metastatic retropharyngeal lymph node at 39.4%, but no difference between recurrent and non recurrent groups. It is considered to be primary station of NPC and may be seen in 65% of patients with cervical lymph node metastases, 35% of metastasis bypasses this node to reach the

cervical nodes[20]. Some authors had also reported that the distant failure for these lymph node metastases was similar to level II lymph node involvement. In the staging system of NPC, involvement of retropharyngeal lymph node has not been mentioned routinely. How its abnormality influence on prognosis of NPC is still not well understood. The reports of no significant influence of retropharyngeal lymph node on predicting outcome[21] are in agreement with our results.

Concerning the lymph node size, although we found that the averaged diameter of the largest lymph node of recurrent group was larger than the other group (3.6 cm and 1.5 cm respectively) but it was no significant difference (p valve <0.05) in relation to the risk of recurrence. However, there has been controversy over the prognostic significance of the size and various features of lymph node involvement. Lee et al[22] found that maximum lymph node size was independently significant in predicting survival, but in contrast, many investigators found that it was not a significant prognostic factor[23,24]. Furthermore, Teo et al[23] reported that fixed lymph nodes, and contralateral neck lymph nodes were independently significant in predicting survival, rather than maximal lymph node size.

Among the other factor that were significant, only skull base invasion had been identified to be an independent factor for prediction of NPC recurrence in multivariate analysis. However, those findings may be correlated with one another. Because of late local recurrences, even after five years are not rare, and those patients who had developed distant metastases after primary radiotherapy had a better prognosis[22], thus, early detection of recurrent disease or distant metastases after complete treatment is very important. For NPC patients who have those suggestive findings, particularly, skull base invasion should be followed up closely.

## Conclusion

The risks of NPC recurrence after complete treatment have been correlated to TNM staging, skull base invasion, and carotid space involvement. Neither tumor size, lymph node size, parapharyngeal space invasion alone nor retropharyngeal lymph nodes have been shown to be significant prognostic factors. Skull base invasion has been identified to be the predictive sign for tumor recurrence. Skull base invasion and carotid space involvement have a statistically significant prognostic factors for overall survival. Carotid space involvement is indicated by infiltration of perivascular fat plane of the internal carotid artery.

## Acknowledgements

and overall radiology residents who have supported my work. I thank you all from the bottom of my heart.

**Umasan Phuprasat,** M.D.

# References

1.  Parkin DM, Bray F, Ferlay J, Pisani P. NP Screen(r) Assay Risk Assessment for Nasopharyngeal Carcinoma (NPC). Global Cancer Statistic, 2002. Cancer J Clin. 2005 Mar-Apr: 55(2);74-108.

2.  Chang ET and Hans-Olov Adami. Review The Enigmatic Epidemiology of Nasopharyngeal Carcinoma. Cancer Epidemiology Biomarkers Prev. 2006(10) October:15.

3.  Nguyen MQ, Nguyen CH, Parkin DM. Cancer Incidence in Ho Chi Minh City, Viet Nam (1995-1996). Int J Cancer: 1998;76:472-9.

4.  LUO De-hong, ZHOU Chun-wu, Er-ni LI and WEN Bi-xiu. Post radiation CT changes and recurrent nasopharyngeal carcinoma. Chinese Medical Journal 2008;121(10):916-22.

5.  Comoretto et al. Detection and Restaging of Residual and/or Recurrent Nasopharyngeal Carcinoma after Chemotherapy and Radiation Therapy: Comparison of MR Imaging and FDG PET/CT: Radiology. 2008 October: 249(1).

6.  สถาบันมะเร็งโรงพยาบาลศิริราช (Siriraj cancer center) www.si.mahidol.ac.th/th/department/cancer/dept__history.asp-11k:

7.  Isles M.G, McConkey and Mehanna H.M. A systematic review and meta-analysis of the role of positron emission tomography in the follow up of head and neck squamous cell carcinoma following radiotherapy or chemoradiotherapy. Clinical Otolaryngology 2008;33(3): 210-22.

8.  Carlos Suárez, Juan P, Rodrigo, Alessandra Rinaldo, Johannes Langendijk A et al. Current treatment options for recurrent nasopharyngeal cancer: Eur Arch Otorhinolaryngol (2010);267:1811-24.

9.  Teo PM, Kwan WH, Lee WY, Leung, Johnson PJ. Prognostic factors Determining Survival Subsequent to Distant Metastasis from Nasopharyngeal Carcinoma Clinical Oncology Department, Prince of Wales Hospital, Shatin, and Hong Kong Cancer. 1996 Jun 15;77(12):2423-31.

10. Ragab S.M, Faerfan, Makhalifa. The Journal of Laryngology and Otology. 2008 March; 27(22):1230-4.

11. Cooper J, Fleming I.D and Henson D.E. American Joint Committee on Cancer manual for staging of cancer (6th ed.), JB Lippincott, Philadelphia (2002).

12. Frederick L. Greene et al. 1977 AJCC nodal classification, American Joint Committee on Cancer manual for staging of cancer (6th edition), JB Lippincott, Philadelphia (2002).

13. Wei WI, Chua DT, Sham JS, Ho WK, Au GK et al. Current Management Strategy of Nasopharyngeal Carcinoma. The predictive value of the 1997 American Joint Committee on Cancer stage classification in determining failure patterns in nasopharyngeal carcinoma. Cancer (2001): 92; 2845-55.

14. Jia-Yin Zhou, Vincent F. H. Chong, James B. K. Khoo, Kap-Luk Chan, Jing Huang. The relationship between nasopharyngeal carcinoma tumor volume and TNM T-classification: a quantitative analysis. Eur Arch Otorhinolaryngol (2007) 264:169-74.

15. LUO De-hong, ZHOU Chun-wu, LI Er-ni and WEN Bi-xiu. Post-radiation CT changes and recurrent nasopharyngeal carcinoma. Chin Med J 2008;121(10):916-22.

16. Anna Kalogera-Fountzila, Dimitrios Karanikolas, Nikos Katodritis, Epaminodas Samantas, Apostolos Sarafopoulos, Ippoliti Ikonomou et al. Prognostic Factors and Significance of the Revised 6th Edition of the AJCC Classification in Patients with Locally Advanced Nasopharyngeal Carcinoma. Strahlenther Onkol 2006;182:458-66.

17. Jeong-Hyun Kim and Joon-Kyoo Lee. Prognostic Value of Tumor Volume in Nasopharyngeal Carcinoma. Yonsei Medical Journal 2005 (46):2;221-7.

18. Chong VF, Fan YF. Skull base erosion in nasopharyngeal carcinoma: detection by CT and MRI. Clin Radiol. 1996; 51:625-31.

19. Sham JST, Wei WI, Kwan WH, Chan CW, Kwong WK, Choy D. Nasopharyngeal carcinoma: Pattern of tumor regression after radiation. Cancer 1990;65:216-22.

20. Chong V. F. H., Fan J. B. K, and Khoo. Retropharyngeal lymphadenopathy in nasopharyngeal carcinoma. European Journal of Radiology December 1995 (21),2:15; 100-5.

21. Li-Zhi Liu, Guo-Yi Zhang, Chuang0Miao Xie, Xue-Wen Liu, Chun-Yan Cui et al. MRI of retropharyngeal node

metastasis in nasopharyngeal cancer: pattern of spread. Radiation Oncology Biol. Phys. 2006 (66), No. 3; 721-30.

22. Lee WY, Teo PM, Kwan WH, Leung SF, Johnson PJ. Prognostic factors Determining Survival Subsequent to Distant Metastasis from Nasopharyngeal Carcinoma Clinical Oncology Department, Prince of Wales Hospital, Shatin, Hong Kong. Clinical Onco (1996) Jun 15; 77(12):2423-31.

23. Chen HH, Prevost TC, and Duffy SW. Prognostic Factors in 677 Patients in Singapore with Nondisseminated Nasopharyngeal Carcinoma. Cancer, November 15, 1999 (86):1912-1920

24. Sham JST, Wei WI, Kwan WH, Chan CW, Kwong WK, Choy D. Nasopharyngeal carcinoma: Pattern of tumor regression after radiation. Cancer, 1990;65;216-22.

# Functional MRI During Memory Recognition in Healthy Adults

**Theeraphol Panyaping, MD**
**Lojana Tuntiyatorn, MD**
**Chakrit Sugying, MD**
**Witaya Sungkarat, MD, PhD**

*Department of Radiology, Faculty of Medicine Ramathibodi Hospital, Mahidol University, Bangkok, Thailand*

## Abstract

**Purpose:** To localize the functional cortices enrolled during abstract picture recognition task that might be a baseline study to provide Thais standard paradigm for future research.

**Material and methods:** The protocol study was approved by institutional review broad and local ethics committee. Informed written consent was obtained from all participants after character of the experimental study was fully explained. Twenty healthy subjects underwent functional MRI and axial T1 weighted image, the latter was anatomic reference image. Abstract picture recognition task as block paradigm was used. Statistic analysis of fMRI datas were analyzed as a whole group analysis and using sample t test random effect analysis model, RFx (corrected P value <0.01). BOLD activities on brain surface rendering images were displayed as color from red (less activity) to yellow (strong activity). The anatomic reference image was loaded to overlay the colored maps and the anatomy of the cerebral cortical lobes and gyri and hippocampal formation were defined. In addition, BOLD activities are also displayed as color overlays on axial, coronal and sagittal views of T1W reference anatomic images, gradual change from dark blue (less activity) to red (most strong activity).

**Results:** Activation for abstract picture recognition was observed at the both-sided cerebellum, bilateral parietal lobes, left hippocampus, bilateral occipital lobes including calcarine cortices, left motor cortex, bilateral premotor cortices, supplementary motor area and left superior temporal gyrus (Wernicke's area). There is asymmetry of the activities in both hemispheres with left-sided predominance. Bilateral parietal and occipital lobes showed the most intense activities.

**Conclusion:** Abstract picture recognition task showed activation in multiple areas of cortical brain, which correlates with the human memory processing.

## Background

Functional MR imaging has been proved to be powerful non-invasive research technique to aid in identifying regions of brain activation by particular stimuli and tasks. By using blood oxygenated level-dependent (BOLD) technique that based on the detection of local alteration in cerebral blood flow (CBF) and blood oxygenation in response to brain activity and the effect of those oxygenation changes on the MR signal[1,2].

Functional MR imaging activation patterns during various memory tasks have been studied in healthy volunteers. Two main groups of structures involved in working memory and secondary memory include the prefrontal cortex and medial temporal lobe. Hence, these regions have been the focus of prior functional MR imaging studies of normal memory. In prior functional MR imaging studies[1-5] the prefrontal cortex has consistently been found to be involved in learning and recall. In those studies, specific regions or hemispheres have been localized on the basis of the cognitive paradigm used. Activation in the prefrontal cortex is greater with increasing memory loads and is more pronounced during initial, as opposed to repeated, attempts at learning[5]. Increased activation during learning is associated with more successful subsequent recall[5]. Authors of functional MR imaging studies have also documented the role of the medial temporal lobe in learning and recall. The medial temporal lobe structures most often implicated in these studies are the hippocampus and parahippocampal gyrus[6].

In the prior functional MRI study during memory recognition in healthy volunteers using words and common nameable objects showed cortical activation at hippocampi with left-sided predominance[7].

Corresponding with the recent functional MRI study in patients with mild cognitive impairment, which showed decreased cortical activation in bilateral frontal cortices, hippocampus, and left cerebellum compared with control subjects (P <.001).[8] Hence, functional MRI study during memory recognition can be the sensitive tool in detecting cortical deactivation in mild cognitive impairment patients or early Alzheimer's disease with benefit in early diagnosis correlating with the clinical finding and psychological test, whereas no detectable abnormality on conventional MR imaging.

To date, no study of functional MRI during memory recognition task has been established in Thailand. This is the first study being and using abstract picture recognition paradigm. The purpose of this study is to localization of the functional cortices during working memory task in healthy subjects.

In addition, it will provide standard Thais paradigm for future more advanced research in memory functional MRI, especially in patients with mild cognitive impairment or early Alzheimer's disease.

## Materials and Methods

### Subjects

Twenty volunteer subjects (11 males, 9 females) were included in the study. Their age varies from 25 to 59 years old, mean age: 32 years. All of them are right-handed, healthy subjects without history of neurological and psychiatric episodes. The health status of the subjects was evaluated by interviewing and normal finding on their routine axial T1-weighted images. All volunteers performed MMSE (Mini Mental State Examination) and their results were normal. Informed written consent was obtained

from all participants after character of the experimental study was fully explained. The institutional review broad and local ethics committee approved the study protocol.

## Data acquisition and post processing analysis

Functional MR imaging was performed using a 3.0-Tesla whole body imager (Acheiva; Phillips Medical Systems, Best, the Netherlands) and sense head coil was used. An automatic shimming method enhanced the signal-to-noise ratio and reduced the functional MR susceptibility artifacts. Preliminary set up and localizing scan required about 30 sec. In vivo's Eloquence system was used to control what the patient see inside the scanner. By using the Experiment Presentation Computer (EPC), the stimuli were presented via the Patient display hood (PDH), which contains a 15-inch LCD, 1025x768 resolution and 30 degree visual field coverage. The PDH was mounted on the head coil and the subjects were positioned in the scanner in supine position. The patients were instructed to look at the screen whether they can see the entire screen. Synchronization of the fMRI scan with the stimuli from the EPC was manually performed, and then time delay will be corrected.

Axial T1 weighted image {repetition time (TR) = 200 milliseconds, echo time (TE) = 2.3 milliseconds, in phase} will be the first step to provide image for anatomical localization of the activation maps.

Then functional MR imaging will be performed using a gradient-echo, echo planar sequence with following parameters; TR/TE=3000/35 milliseconds; flip angle, 90 degree; matrix size, 128x128; field of view, 240x240 mm; section thickness, 5 mm; no gap intersection. Echo-planar images were position perpendicular to the long axis of the whole brain.

Imaging preprocessing and data analyses will perform with SPM2 software (Welcome Department of Cognitive Neurology, London, England). Data preprocessing are done in a standardized fashion by using the following established procedures: section timing correction, motion correction and spatial normalization of the resection volumes to a based on the Montreal Neurological Institute (MNI) reference brain space. After spatial normalization, images will smooth with an 8-mm full-width-at-half-maximum isotropic Gaussian kernel.

## Statistic consideration

Results of all subjects will be analyzed as a whole group analysis applying the general linear model and data will be analyzed by using the one-sample t test random effect analysis model, RFx (corrected P value <0.01).

The results were displayed in tile viewers, showing images with an overlay of colored maps (SPMs). Pixels with a value at or above the threshold value (corrected P value <0.01) were displayed as part of colored overlay. BOLD activities are displayed as brain surface rendering images with an overlay of colored maps, gradual change from red (pixels at threshold level) to yellow (pixels at greater threshold level). In addition, BOLD activities are also displayed as color overlays on axial, coronal and sagittal views of T1W reference anatomic images, gradual change from dark blue (less activity) to red (most strong activity).

The anatomic reference image was loaded to overlay the colored maps and the anatomy of the hemispheric lobes, cortical gyri and hippocampal

formation were defined according to supratentorial cortical anatomy and anatomy of the hippocampal formation on elsewhere[9]. Two neuroradiologists localized anatomy of areas of activation in consensus.

## Cognitive task

### *Paradigm:*

All participants will be trained to perform the functional MR imaging tasks by power point presentation, which will take about 10 minutes per person immediately before imaging.

### Step 1

There are eight blocks of abstract pictures and each block contained six pictures. During picture encoding, the pictures will be projected on a computer screen at outside the imaging room and subjects will view the total 48 abstract pictures sequentially. Each block will be presented with 3 seconds per picture and 3 sec interval time for each block. These pictures will run sequentially and three round each. In total 48 images with three rounds each will acquire per subject and take time about 7.2 minutes. The subjects will be instructed to view the pictures carefully and memorize them.

### Step 2: two sequential tasks

After finish the step 1, subjects will be positioned on the imaging table with a specially molded foam pad to restrict motion of the head. The pictures were projected on the small overhead LCD of

the PDH.

### Task 1: Recognition

There are eight blocks of abstract pictures. Each block consists of six abstract pictures previously seen on step 1 and following by four gray screen pictures (control condition). Each block will be presented, sequentially with 3 seconds per picture.

### Task 2: New picture

There are eight blocks of unseen abstract pictures. Each block consists of six new abstract pictures, which are not seen on step 1 and following by four solid gray screen pictures (control condition). Each block will be presented, sequentially with 3 seconds per picture.

The sequential tasks will perform with each block of task 1 (recognition condition) alternating with task 2 (new picture) in same fashion for all subjects. The functional MRI will be performed during task 1 and task 2 in 8 minutes. The subject will press the bottom on the right hand if there is any picture in the step 1.

## Results

Twenty healthy subjects were included in the study, 11 males and 9 females, ages from 25 to 59 years old, mean age: 32 years. (Table 1)
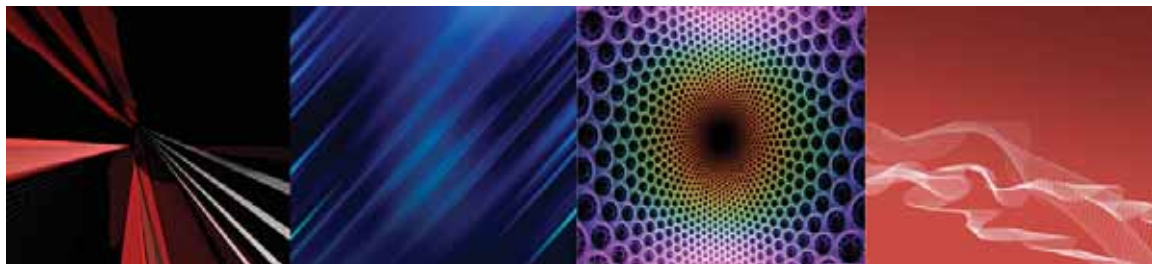
BOLD activities are displayed as brain sur-



**Fig. 1**   Example of abstract pictures

face rendering images with an overlay of colored maps from red (less activity) to yellow (strong activity) as well as color overlays on axial, coronal and sagittal views of T1W reference anatomic image from dark blue (less activity) to red (strong activity).

The activity for task 1 (recognition ) and task 2 (new picture ) versus baseline are observed mainly at the both-sided cerebellum, bilateral occipital and parietal lobes as well as some activities at frontal lobes including supplementary motor area (Figure 1).

Using the statistical procedures as described above ( corrected P value <0.01), activation for abstract pictures recognition versus new abstract pictures viewing was observed at the both-sided cerebellum, bilateral parietal lobes, bilateral occipital lobes including calcarine cortices, left hippocampus, left precentral gyrus, bilateral premotor cortices (posterior aspect of middle frontal and inferior frontal gyri), supplementary motor area and left superior temporal gyrus (Wernicke's area). (Figure 2) The BOLD signal at the left hippocampus is present at anterior aspect. (Figure 3) No activation of the right hippocampus is observed. Activities at the bi-

lateral caudate nuclei and left thalamus are also observed. (Figure 4) Bilateral parietal and occipital lobes showed the most intense activities. Note asymmetry of the activities in both hemispheres with left-sided predominance.

Comparing with activity during abstract picture recognition, the activity during viewing new abstract pictures showed the same location but significant lower in intensity (corrected P<0.01).

## Discussion

Functional MRI is superior to other functional imaging techniques (SPECT and PET) because it can evaluate both structural and functional anatomy in the single imaging with less time consuming and no contrast administration. Different type of stimuli and paradigm activates different cortical regions. Hence, functional MRI may be an aid powerful tool for evaluation of structure and function of the specific brain areas.

In prior functional MR imaging studies[1-5], the prefrontal cortex has been found to be activated in learning and recall. Also, there are many studies of prefrontal cortex lateralization on memory working.

**Table 1** Demographic data of the subjects

| Subject | Age | Sex | Subject | Age | Sex |
|---------|-----|-----|---------|-----|-----|
| 1 | 30 | F | 11 | 25 | M |
| 2 | 31 | M | 12 | 27 | F |
| 3 | 40 | F | 13 | 30 | M |
| 4 | 42 | F | 14 | 28 | M |
| 5 | 27 | F | 15 | 28 | F |
| 6 | 30 | M | 16 | 53 | F |
| 7 | 28 | M | 17 | 59 | M |
| 8 | 32 | M | 18 | 28 | M |
| 9 | 28 | M | 19 | 25 | M |
| 10 | 30 | F | 20 | 30 | F |
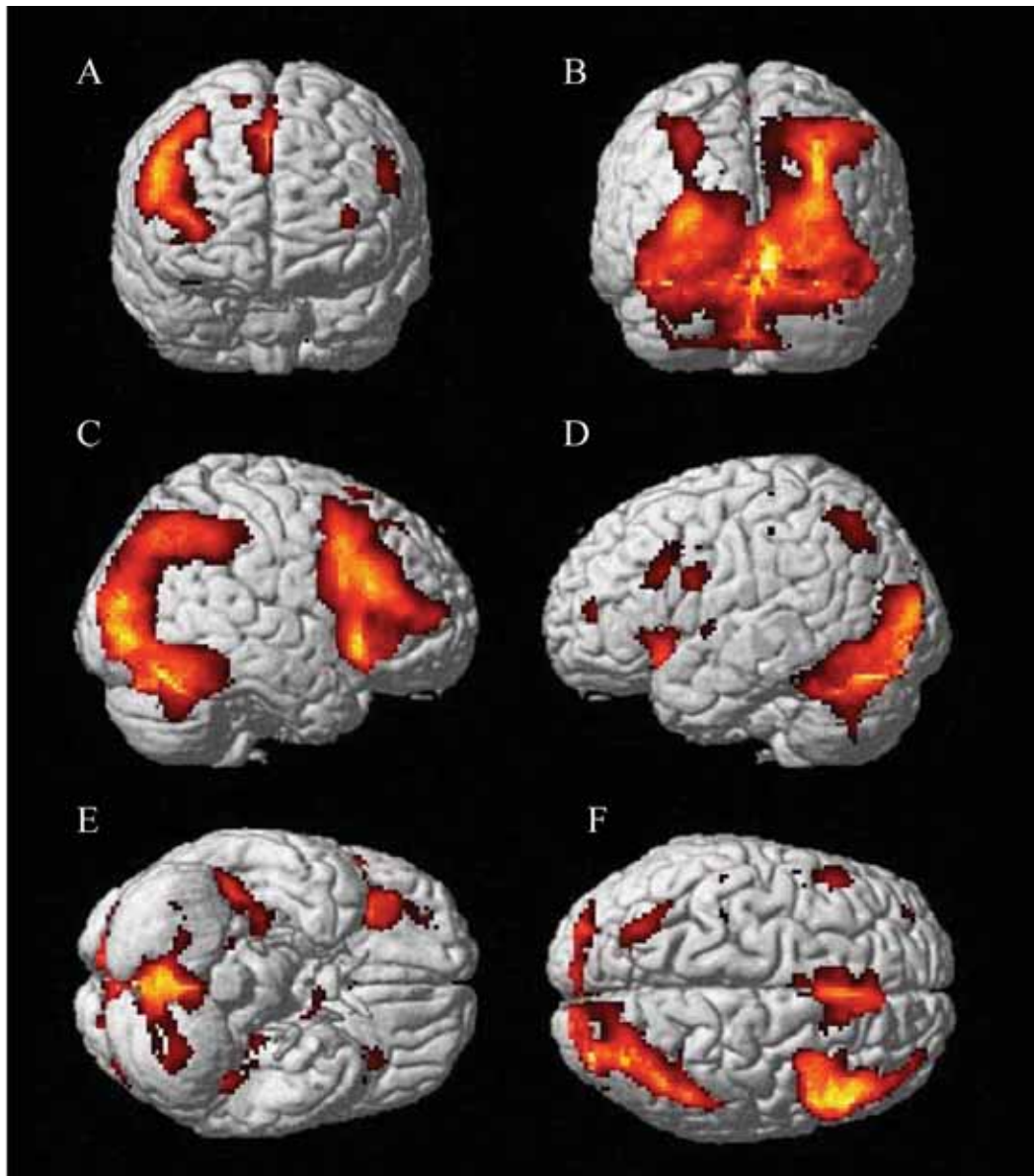
**Fig. 1** Brain surface rendering images with an overlay of colored maps. A; anterior view, B; posterior view, C; right lateral view, D; left lateral view, E; inferior view, F; superior view Intensity of activation was displayed as color from red(less activity) to yellow (strong activity). The pictures showed activation for task 1(recognition) and task 2(new picture) versus baseline (control condition) at the both-sided cerebellum, bilateral parietal lobes, occipital lobes and some area of frontal lobes including supplementary motor area.
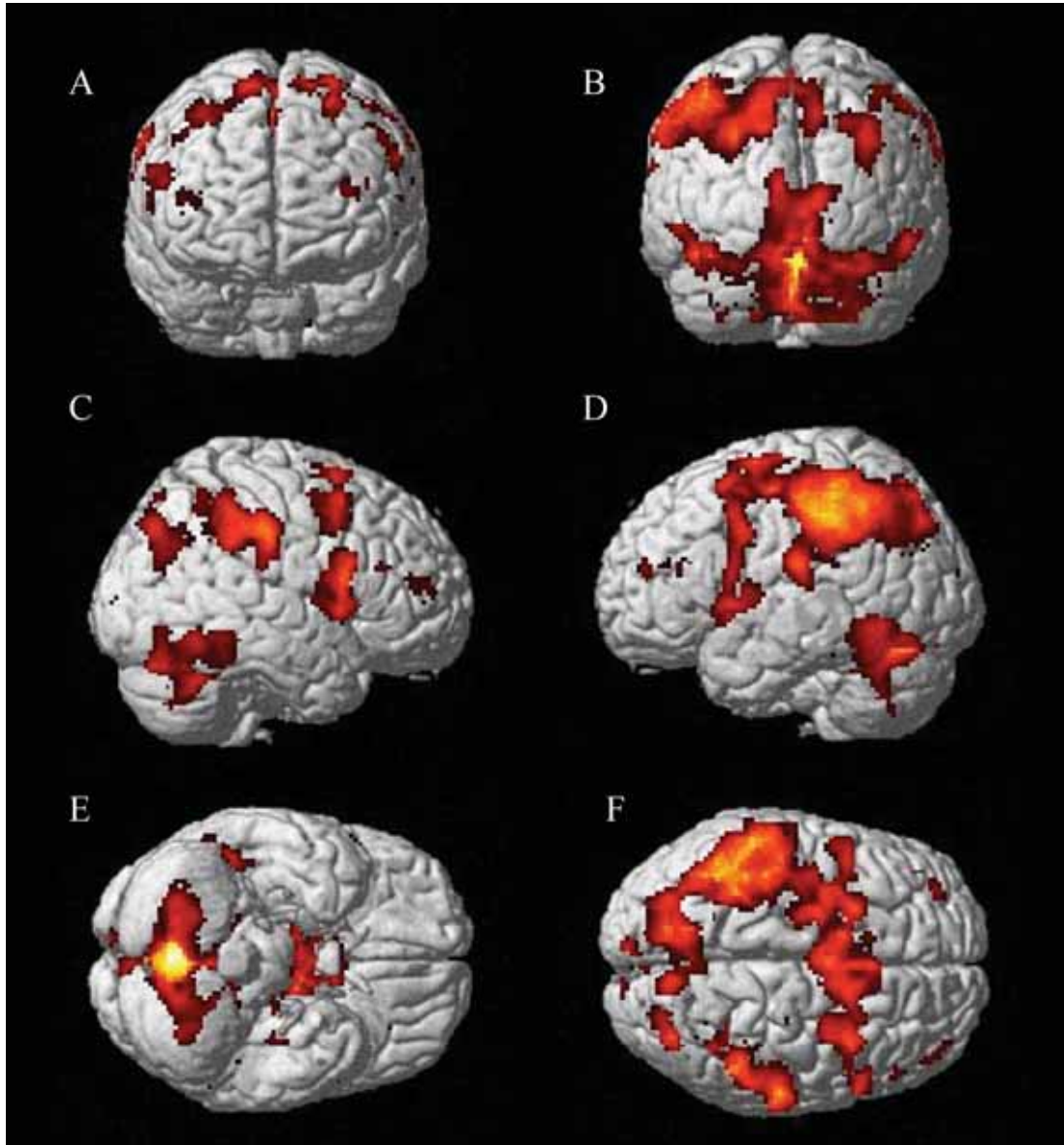
**Fig. 2** Brain surface rendering images with an overlay of colored maps. A; anterior view, B; posterior view, C; right lateral view, D; left lateral view, E; inferior view, F; superior view  Intensity of activation was displayed as color from red(less activity) to yellow (strong activity). The pictures showed activation during abstract picture recognition at the both-sided cerebellum, bilateral parietal lobes, left hippocampus, bilateral occipital lobes, left motor cortex, bilateral premotor cortices, supplementary motor area and left superior temporal gyrus (Wernicke's area). These activities are predominant on the left side. Note the most intense activities at bilateral parietal and occipital lobes.
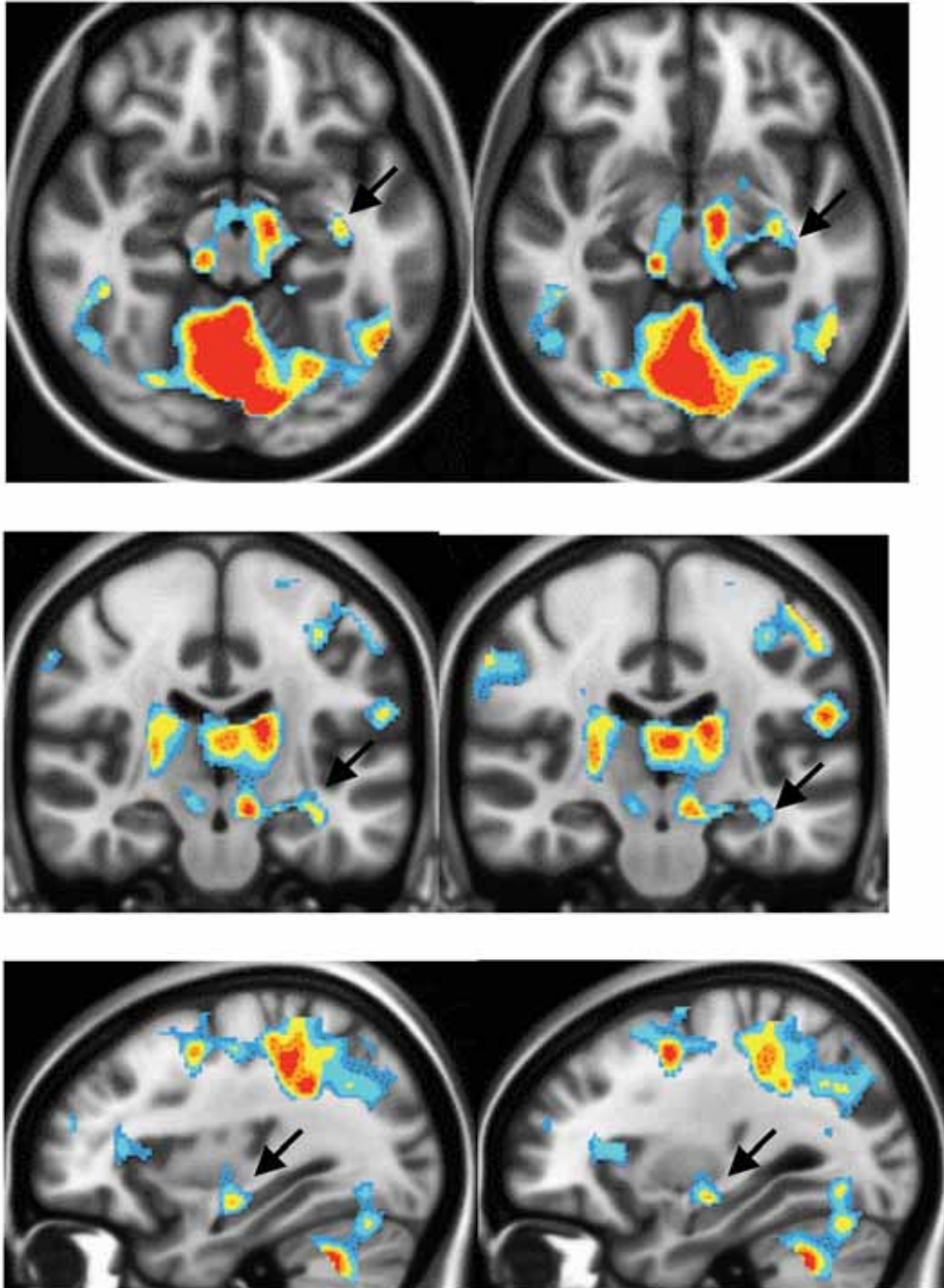
**Fig. 3** Results at hippocampus level during abstract picture recognition are displayed as color overlays on axial (A), coronal (B) and sagittal (C) views of T1-weighted images. Intensity of activation was displayed as color, gradual change from dark blue (less activity) to red (strong activity). The pictures showed activation at the anterior aspect of left hippocampus (black arrow). Note no activation of the right hippocampus.
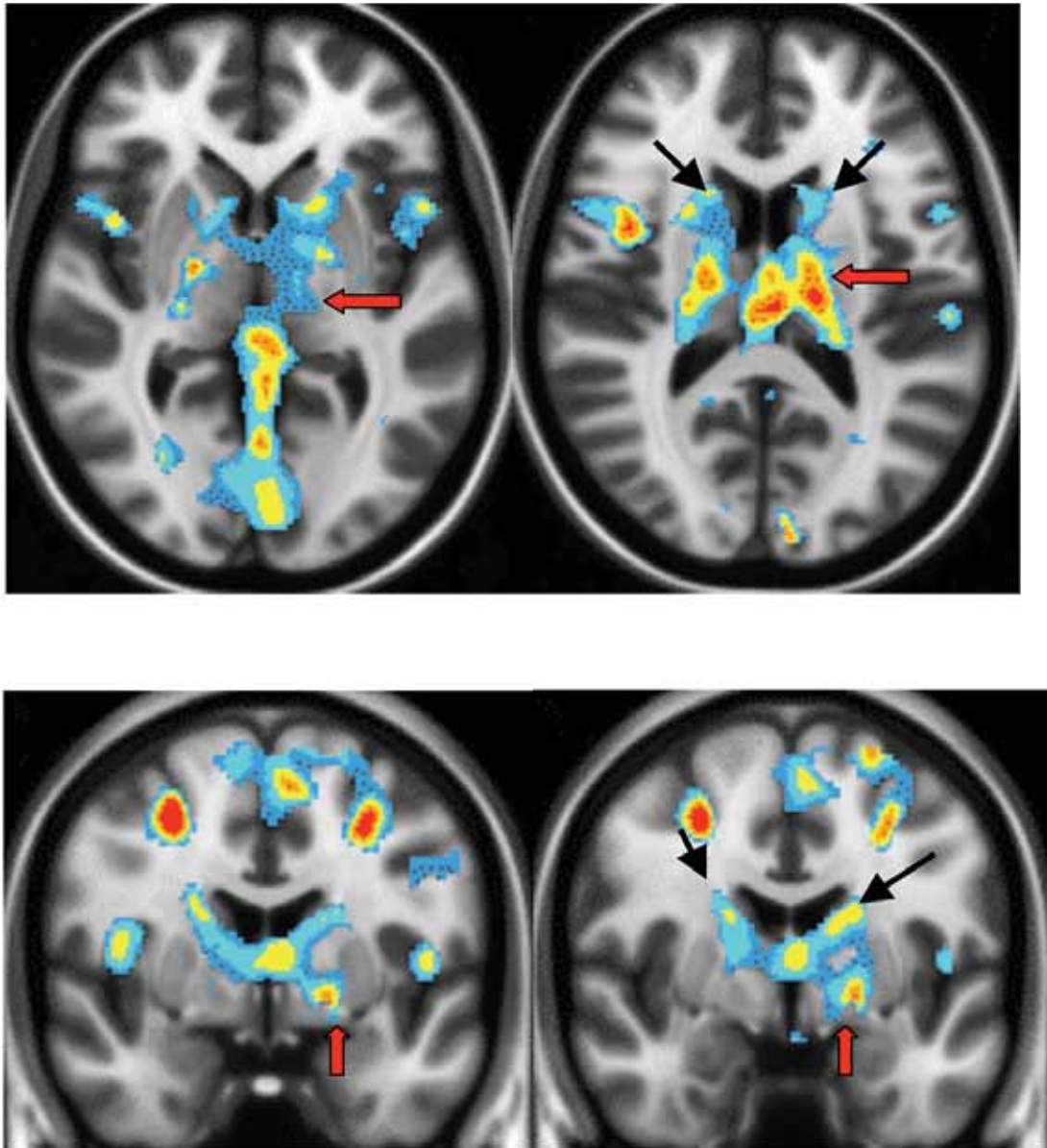
**Fig. 4** Color overlays on axial (A) and coronal (B) views of T1-weighted images at the basal ganglia and thalamic regions. Intensity of activation was displayed as color, gradual change from dark blue (less activity) to red (strong activity). The pictures showed activities at the bilateral caudate nuclei (black arrow) and left thalamus (red arrow).

Grady et al studied brain activity during encoding pictures of objects and words using positron emission tomographic scans (PET). They found that differentiated stimulus type and the different encoding strategies yielded different brain activity with left prefrontal and bilateral medial temporal regions enrolled in deep processing and intentional learning of pictures[6].

Task-activated BOLD signal at the left hippocampus in our study was anterior predominance, as has been previously reported in the prior functional MRI study during memory recognition in healthy volunteers using words and common nameable objects[7]. There was claimed that verbal/semantic memory is usually attributed to the left medial temporal structure and anterior aspect of hippocampus also supports the executive frontal lobe activity[8]. And corresponding with the recent functional MRI study in patients with mild cognitive impairment, which showed decreased cortical activation in the bilateral frontal cortices and left hippocampus during recognition (P <.001).[9] Thus, it should be support that the left hippocampus plays the crucial role in memory recognition.

There has been known that cortical eye fields including occipitotemporal, occipitoparietal, parietal and prefrontal cortices[11]. Furthermore, there are projections from visual cortex to the parietal, temporal and frontal lobes in pathway of memory processing and learning[12]. Therefore, the most intense activation at parietal and occipital lobes as well as frontal lobes in our study could be associated with visual stimulation and memory pathway. Moreover, inferior parietal lobule has been implicated in the guidance of spatial attention and acts as a multifaceted behavioral integrator that binds visuospatial, motor and cognitive information into a topographically salience. It may be said that the parietal cortex act as a bridge to link perception, action and cognition[13].

The activity observed in the left thalamus is also consistent with the data in monkeys and humans at medial thalamus in previous study (Aggleton and Brown 1999) that indicates a role of the thalamus in memory recognition[14].

The caudate nucleus is generally considered to be involved in the learning of more gradually acquired visual discrimination tasks (i.e., visual habit formation; Teng et al. 2000)[15]. Thus, activities at bilateral caudate nuclei in our study can be described with visual discrimination of the different abstract pictures in our memory task.

In addition, we found intense activation in the cerebellum and this finding confirms results of a previous study with 1.5-T MR imaging in healthy elderly subjects[16]. And corresponding with the result of decreased cortical activation at the left cerebellum in recent functional MRI study in patients with mild cognitive impairment[9], which supports role of cerebellum in memory pathway.

There is also activation at the Wernicke's area, which may be due to receiving sensory input from visual and auditory cortices.

In this study, we have some limitation due to contamination of activity at the bilateral premotor cortices from activation of motor and sensory cortices during memory task.

The pictures using in this paradigm were not meaningful, resulting in no bias of the results due to effect of remote or long term memory. These our observations were based on group analysis with adequate sample size and statistically significance. So these results can be used as a reference of the

whole population. Thus, these results from healthy volunteers can also be used as control group reference for further research in the patients with mild cognitive impairment or early Alzheimer's disease. However, there is some limitation in age range of the subjects in our study that is too young comparing with age group of the patients with mild cognitive impairment or Alzheimer's disease.

Thus, further research of functional MRI during memory recognition in normal cognitive elderly subjects, with or without comparison to the patients with mild cognitive impairment or early Alzheimer's disease will get more benefit in early diagnosis combined with the clinical finding and psychological test. In addition, this functional MRI with abstract picture recognition paradigm could have benefit in follow up the patient with MCI or Alzheimer's disease by comparison of activation at specific areas between pre and post treatment.

## Conclusion

The functional MR imaging of abstract picture recognition task in this study showed multiple sites of cortical activation. Significant activations were observed at the cerebellum, bilateral parietal lobes, occipital lobes, frontal lobes, left hippocampus, bilateral caudate nuclei, left thalamus and left superior temporal gyrus (Wernicke's area). There are asymmetric activities in both hemispheres with left-sided predominance.

## Acknowledgement

## References

1. Courtney SM, Ungerleider LG, Keil K, Haxby JV. Transient and sustained activity in a distributed neural system for human working memory. Nature 1997;386:608-11.

2. Ojemann JG, Buckner RL, Corbetta M, Raichle ME. Imaging studies of memory and attention. Neurosurg Clin N Am 1997;8:307-9.

3. Gabrieli JD, Poldrack RA, Desmond JE. The role of left prefrontal cortex in language and memory. Proc Natl Acad Sci U S A 1998;95:906-13.

4. Wagner AD, Desmond JE, Glover GH, Gabrieli JD. Prefrontal cortex and recognition memory: functional-MRI evidence for context-dependent retrieval processes. Brain 1998;121:1985-2002.

5. Buckner RL, Kelley WM, Petersen SE. Frontal cortex contributes to human memory formation. Nat Neurosci 1999; 2:311-4.

6. Cohen NJ, Ryan J, Hunt C, Romine L, Wszalek T, Nash C. Hippocampal system and declarative (relational) memory: summarizing the data from functional neuroimaging studies. Hippocampus 1999;9:83-98.

7. Craig E, L. Stark, Larry R. Squire. Functional magnetic resonance imaging (fMRI) activity in the hippocampal region during recognition memory. The Journal of Neuroscience, October15, 2000, 20(20):7776-81.

8. Bellgowan PS, Binder JR, Swanson SJ. Side of seizure focus predicts left medial temporal lobe activation during verbal encoding. Neurology 1998;51:479-84.

9. Petrella JR, Krishnan S, Slavin MJ, Tran TT, Murty L, Doraiswamy PM. Mild cognitive impairment: evaluation with 4-T functional MRimaging. Radiology 2006;240:177-86.

10. Burton PD, Thomas PN, Tarek AY. Neuroimaging Clinical of North America. Anatomic basic of functional MR imaging. 2001;11:305-41.

11. Puce A, Allison T, Gore JC, McCarthy G. Face-sensitive regions in human extrastriate cortex studied by functional MRI. J Neurophysiol 1995;74:1192-9.

12. Anthony D., Benjamin J., Itamar K. Parietal lobe contributions to episodic memory retrieval. TRENDS in Cognitive Sciences 2005;9:445-53.

13. Gottlieb J. From thought to action: the parietal cortex as a bridge between perception, action and cognition. Neuron 2007;53:9-16.

14. Aggleton, J.P. and Brown, M.W. 1999. Episodic memory, amnesia and the hippocampal-anterior thalamic axis. Behav. Brain Sci. 22: 425-89.

15. Teng, E., Stefanacci, L., Squire, L.R., and Zola, S.M. 2000. Contrasting effects on discrimination learning after hippocampal lesions and conjoint hippocampal-caudate lesions in monkeys. J. Neurosci. 20:3853-63.

16. Rombouts SA, Barkhof F, Veltman DJ, et al. Functional MR imaging in Alzheimer's disease during memory encoding. AJNR Am J Neuroradiol 2000;21:1869-75.

Original Article

# Predictive Factors for Successful Percutaneous Sclerotherapy of Venous and Lymphatic Malformations

**Anchalee Churojana, MD**
**Laksanawadee Mahiwan, MD**
**Dittapong Songsaeng, MD**
**Rujimas Khumtong, MD**
**Saowanee Homsud**

*Diagnostic Division, Department of Radiology, Faculty of Medicine Siriraj Hospital, Mahidol University, Bangkok, Thailand*

## Abstract

**Objectives:** To determine the predictive factors for good response outcome of venous (VMs) and lymphatic malformations (LMs) by percutaneous sclerosing therapy and to compare the complications associated with bleomycin versus alcohol treatment.

**Methods:** A retrospective analysis of 225 patients with lymphatic and venous malformation who had treated by percutaneous sclerotherapy using alcohol and/or bleomycin was performed The treatment outcome was graded from 0-3, in orderly of clinical responsiveness by using visual assessment of changing in size and subjective improvement of symptoms. Predictive factors of good treatment outcome were determined by uni- and multivariate analysis which were conducted on sex, age, onset of disease, location, type, characteristic of lesion and sclerosant usage.

**Results:** Of 225 patients, 87.6% were VMs and 12.4% were LMs. VMs were predominating in female (6.2:3.8). Between ethanol and bleomycin, there was no statistical significant of treatment sessions, dose and treatment outcome. (p= .42) Sclerosing therapy provided better response on VMs than LMs. (49.2% and 21.4% respectively, p=.002), and had more effective on focal lesions than diffuse patterns (64.9% and 26.1% respectively p<.001) The gender, onset of disease, locations, characteristic on venography and preceding treatment showed no correlation with treatment result. Major complications of ethanol occurred in 38.6%,including hematuria, gangrene, facial paralysis, pulmonary embolism and death. Minor adverse reactions of bleomycin encountered in 19.8% with hyperpigmentation, flu-like symptom and localized fibrosis.

**Conclusion:** Both absolute alcohol and bleomycin were effective sclerosing agents for percutaneous treatment of venous malformations, but no serious complications encountered with bleomycin. The characteristic of focal single lesion, at any region of body part, can be a predictor for good response.

## Introduction

Venous malformation (VM) and lymphatic malformation (LM) are benign congenital abnormalities. They grew proportionately with the patients and did not regress[1]. Although presented at birth, they may appear clinically at any age throughout the life. The presentations of VM and LM are variable including asymptomatic, swelling, pain, ulcerate, bleed, and cosmetic concerns. The clinical severity is related to their location and extension. If located within the oral cavity, these lesions may lead to dysphagia, difficulties with speech or swallowing, orthodontic concerns, and airway obstruction[1-3].

Treatment of VM and LM were difficult, compose of surgery, laser, steroid therapy, and sclerotherapy[4]. Surgical resection may be hazardous, leading to major blood loss, and incomplete resection. Recurrence and deformity were also common after surgical resection[1]. Laser therapy often had an extensive scar and may ineffective in some patient especially in deep seated lesion. Sclerotherapy, as an alternative treatment method, has proven its efficacy and now advocate as the treatment of choice[1,3-5]. A variety of sclerosing agents was described in the literature, including ethanol, detergents, hyperosmotic solutions, OK 432, ethibloc, and bleomycin[2,3].

In our institute, percutaneous sclerosing therapy has been operated by using absolute alcohol and bleomycin as the sclerosing agents. With regard to difference of morphology or characteristic of the lesions and response of sclerosing therapy, the objective of this study was to evaluate the predictive factors for successful treatment outcome of venous and lymphatic malformations, and to compare the complications associated with bleomycin versus alcohol treatment.

## Material and methods

**Patients:** A retrospective review of 258 patients with clinical diagnosis of venous and lymphatic malformations who had referred to our Interventional Neuroradiology division, Radiology department, Siriraj hospital, Mahidol university for sclerosing therapy between July 2001 and July 2011 was performed. An informed consent was given to the use of sclerosing therapy after patient's counseling. A data collection in each patient  including age, sex, location of lesion, clinical presenting symptom, dose of sclerosant, number of treatment sessions, clinical response, side effects and follow-up. Colour photographs were taken before treatment and during every follow up period.

The diagnosis was confirmed during the operation by yielding the content either blood or lymphatic fluid aspiration directly from the lesion by percutaneous puncture.

The exclusion criterias were

1.  Patients who refused treatment.

2.  Coexistence to other types of malformation or syndromic disease.

3.  The diagnosis could not be confirmed during operation.

4.  The patients who had less than 6 months follow up after first sclerotherapy.

Of 258 patients, there were 225 patients who met our criteria and enrolled in this study.

The imaging studies were not routinely performed, but requested in cases where boundaries were difficult to evaluate or deep seated locations.

**Technique and sclerosing agents:** The procedure was performed under general anesthesia or

regional block depending on site of each lesion and anesthesiologist's decision. Each lesion was assessed percutaneously by using a 20 to 22 gauze Teflon-sheathed needle canula puncture needle through a normal skin. Once venous blood or thin yellow fluid was freely aspirated, contrast medium was injected to evaluate the characteristic and to estimate the volume of the lesion.

The characteristic of the lesions were categorized to be

- Focal; if involvement of one region of the body such as finger, lip.

- Diffuse, if involvement of more than one region, such as hand and forearm, lip and tongue

- Isolate: if there were no venous outlet connecting to systemic circulation

- Systemic venous connection

Before June 2008, all VMs were treated solely by absolute alcohol while no percutaneous treatment for LMs, since then, bleomycin was the only agent using for both VM and LM.

For technique of percutaneous sclerosing injection, it was performed similarly, for both ethanol and bleomycin, under fluoroscopic control. Manual compression of venous outlet or venous pressure tourniquet was applied during injection, if systemic venous connection with the lesion was identified on test percutaneous venography, and this was maintained for at least 10 minute after finishing to retain the sclerosing agent and to minimize systemic contamination. Multiple punctures were required in the same session, if the lesion contained several non-communicating cavities.

The absolute alcohol was opacified with non-ionic contrast medium at the ratio of 3:1 by volume. It was slowly injected under fluoroscopic control. The amount of each injection was estimated from prior test injection and termination when near total lesion was opacified or spillage into venous outlet was visualized. The maximum amount of absolute alcohol was 1 ml/ kg body weight but not exceed 40 ml in each session[6].

Prolonged intubation or prophylactic tracheostomy was required, if the lesion located around tongue or oral cavity.

Bleomycin was mixed at the dilution of 1 mg/ ml by normal saline. It was injected under roadmap fluoroscope after contrast test injection. Injecting bleomycin was stopped as soon as the contrast medium column reached the venous outlet. The amount of the injection varies according to the size of the lesion. In children under 1 year of age, the maximum dose per injection was limited to 1 mg/ kg. Patients who were older than 1 year of age, a single dose of 15 mg was never exceed[7]. For LM lesion, before starting bleomycin injection, the lymph fluid was aspirated as much as possible with the aim to minimize dilution effect of the sclerosant.

Repeated maneuver of sclerotherapy were obtained in 6-8 weeks for the large or the remaining lesions which were re-evaluated at 4-week follow up period.

The accumulation dose of bleomycin was collected in each patient, not to exceed 450 mg[7].

**Outcome evaluation:** The result of treatment was evaluated by comparison the size and clinical symptoms preceding treatment and those at the last visit. The size and morphology of the lesion was evaluated by visual assessment from photographs. The clinical responses were included degree of pain, bleeding and ulcer healing, using patient self-assessment, which were evaluated by direct interview with the patients or parents.

Treatment outcome was evaluated by means of clinical response and quantified by grading of the consensus between Interventional Neuroradiologists and the patients or their parents into 4-point scale, as the followings

**Grade 0** = stable or worse

**Grade 1** = < 50% improvement of symptoms

**Grade 2** = 50-75% improvement of symptoms

**Grade 3** = >75% improvement of symptoms

The treatment outcome grade 2 and 3 were defined as good response.

Complications of the treatment by ethanol and bleomycin were recorded separately.

**Statistical analysis:** The factors which may associate with treatment outcome, including gender, period of disease-onset, site, type and characteristics of lesions, preceeding treatment and sclerosants were analyzed, by using chi-square test. The sclerosants were grouped according to period of using as ethanol alone, ethanol and bleomycin and bleomycin alone. The correlation of patient's age and treatment outcome was evaluated by the unpaired t-test. The correlation between treatment outcome and the predictive factors were determined by the multiple logistic regressions. P <.05 was considered statistically significant. Data analysis was conducted by using the PASW statistic 18.8 software.

## Result

Of total 225 patients, there were 197 VMs (87.6%) and 28 LMs. (12.4%). VMS were predominating in female (6.2:3.8). The mean age was 22.9 years, ranging from 5 months to 68 years. The presenting symptoms, locations and characteristics of the lesions were demonstrated on table 1. All pre-

sented with mass whereas 11% of them had additional sequelae of the diseases including pain, bleeding, lymphatic leakage, and ulceration. The lesions were revealed since birth at 48% and later in life at 52%. The locations of the diseases were found more common at extremities (61.33%) than at head and neck region (35.11%), and the other sites (3.6%) were included shoulder, chest wall, back, abdominal wall and glan penis. Focal and diffuse involvements of the diseases were found rather equally (50.7% and 49.3% respectively). Preceding therapy was documented in 35.6%, including surgery, laser and steroid injection.

Concerning characteristic of venography, most lesions (91.1%) had connection of venous drainages into systemic circulations either with or without venous ectasia, whereas 8.9% had isolated lesion.

Among groups of sclerosant using (ethanol only, ethanol and bleomycin, bleomycin only), there is no statistical significant of treatment sessions, dose and treatment outcome. (p = .42)

The average follow-up period was 13.5 months (range 6-90 months). The treatment outcome of those 225 patients were grade 0 at 7.6%, grade 1 at 20%, grade 2 at 26.7% and grade 3 at 45.8%.

Among patients with grade 3 treatment outcome, VM had more response to sclerosing therapy than LM (49.2% and 21.4% respectively p =.002), and focal lesions had more effective than diffuse lesions (64.9% and 26.1% respectively p<.001). The gender, onset of disease, locations, characteristic on venography and preceding treatment showed no association with treatment result. The correlation between treatment outcome and the variable factors were demonstrated on table 4.

The VMs and focal lesions had been con-
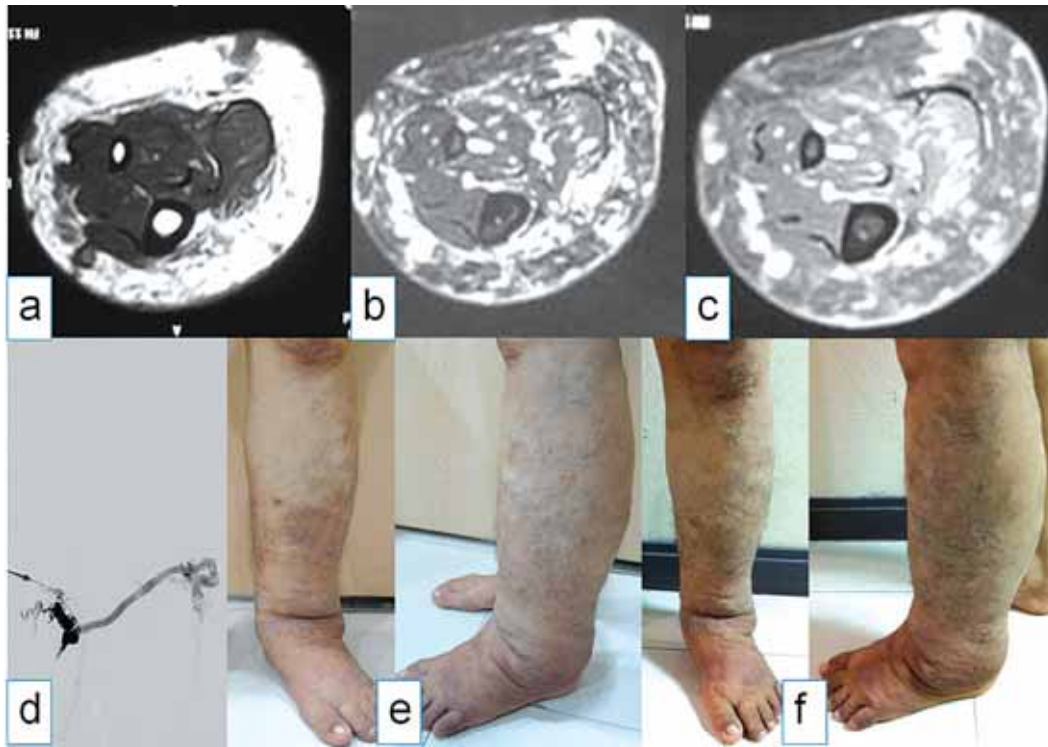
Fig. 1 VM with grade 0 treatment outcome; A 31-year-old male with asymptomatic diffuse type of VM involving left leg, ankle and foot had 3 sessions of bleomycin injection with accumulation dose at 45 mg. (a)T1WI, (b) T2WI/SPAIR (c) T1WI/GD/FS MR imaging of the left leg revealed superficial diffuse venous malformation (d) Percutaneous venography (before sclerosant injection) showed abnormal dilated and tortuous venous structures with systemic venous connection.(e) pre-treatment photograph. (f) Photograph taken at 1 month after last session of sclerotherapy. Note that no significant difference in the appearance.
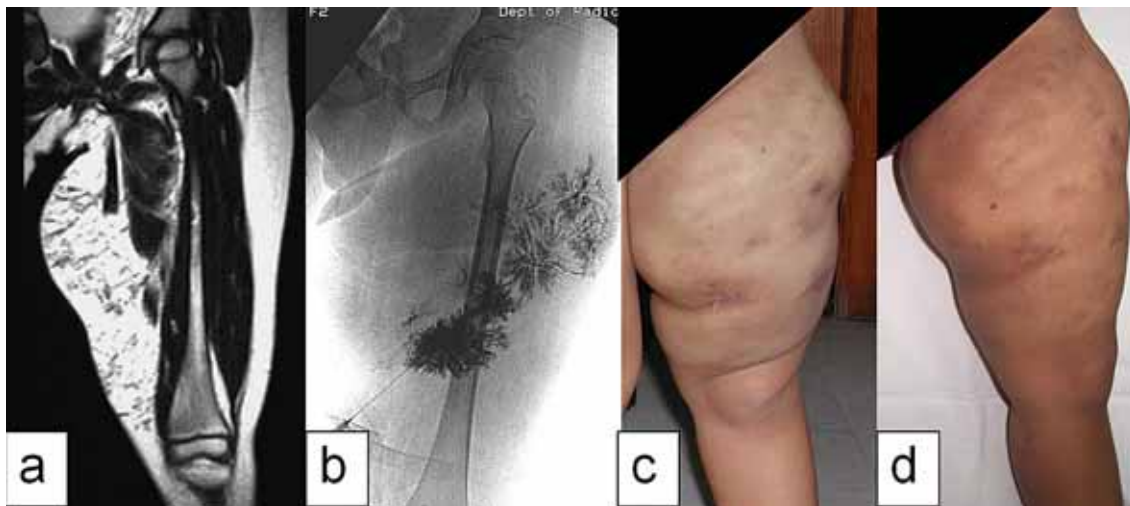


Fig. 2 VM with grade 1 treatment outcome; A 3-year-old girl with diffuse type of VM at left thigh and clinical of pain was treated by one session of 15 mg bleomycin injection. T1WI MR imaging of left thigh revealed diffuse superficial venous malformation (a) that showed abnormal dilated venous structures without systemic venous connection on percutaneous venography - before sclerosant injection (b). The pre-treatment photograph (c) and photograph at 6 months after first session of sclerotherapy (d) show minimal improvement. However the clinical presentation as pain was resolved.
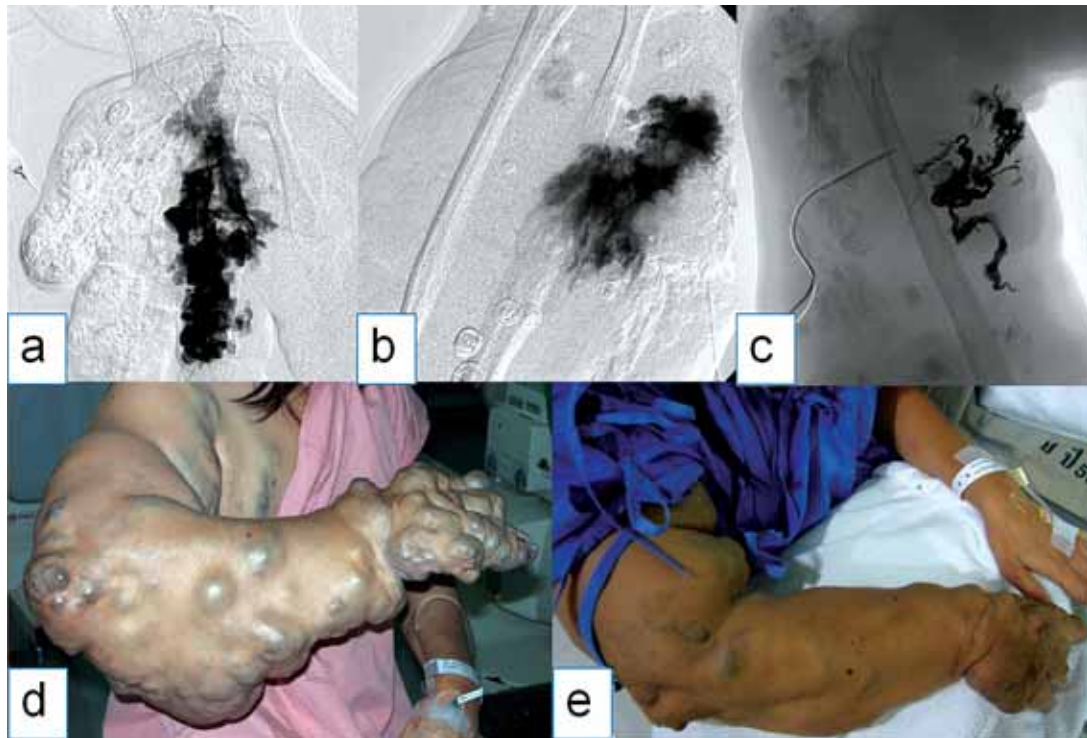
**Fig. 3** VM with grade 2 treatment outcome; A 40-year-old female with cosmetic concerning VM at right hand, forearm, arm and anterior chest wall had 18 sessions of alcohol injection with total dose at 731 ml and 15 sessions of bleomycin injection with total dose at 75 mg. Multiple time of percutaneous venography before sclerosant injection was performed at right hand (a), right forearm (b), and right arm (c) that showed abnormal dilated and tortuous venous structures with systemic venous connection. Pretreatment photograph (d) and photograph taken at 90 months after first treatment (e) showed good response of the disease. Even though still remained some residual malformation but patient had good satisfaction about cosmetic concern.

**Fig. 4** VM with grade 3 treatment outcome; there are nearly obliteration of multiple sites of VM after percutaneous sclerotherapy, (a) pre-treatment photograph of a 30-year-old woman with VM at right lip and cheek, (b) photograph taken after 3 sessions of bleomycin sclerotherapy with total dose at 45 mg. (c) pre-treatment photograph of a 10-year-old girl with focal VM at left little finger, (d) photograph at 6 months after one session of sclerotherapy with 4 ml of alcohol. (e) pre-treatment photograph of a 22-year-old man with focal VM at left foot, (f) photograph taken after 2 sessions of bleomycin sclerotherapy with total dose of 30 mg. (g) pre-treatment photograph of a 5-year-old girl with focal VM at upper lip, (h) photograph taken at 27 months after 5 sessions of bleomycin sclerotherapy with total dose of 56.5 mg.
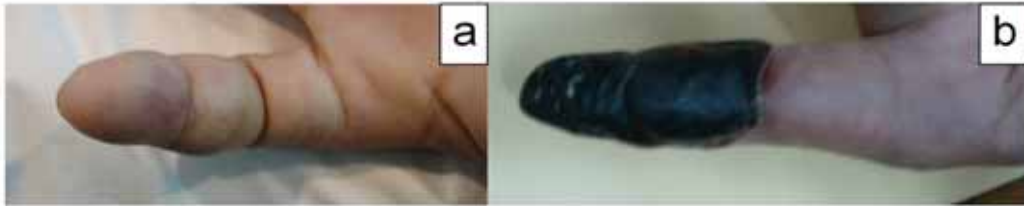
**Fig. 5** Complication of alcohol sclerotherapy; a 31-year-old female with venous malformation at left 2nd finger and had previously surgery; pre-treatment photograph (a), she developed dry finger tip gangrene after one session of 4 ml alcohol injection (b). After 6 months follow up the lesion was not improved then she was consult for amputation.



**Fig. 6** Complication of alcohol sclerotherapy; a 13-year-old boy with VM at upper lip and left cheek, he had severe swelling at puncture site after 12 ml of alcohol injection (a) and 5 days afterthat it showed minimal improvement (b). About 22 months after one session of alcohol injection and three sessions of bleomycin injection, near normal of the lesion was depicted.
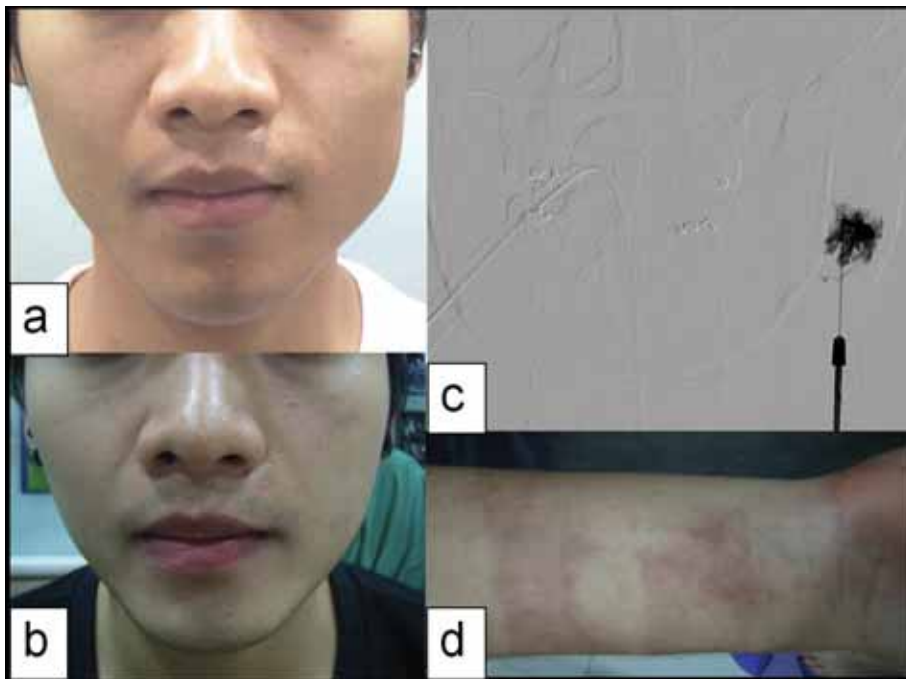


**Fig. 7** Complication of bleomycin sclerotherapy; a 19-year-old male with VM at left cheek had one session of 15 mg bleomycin sclerotherapy (a) pre-treatment photograph, (b) photograph taken at 7 months after first treatment the lesion was markedly regressed. The percutaneous venography revealed malformation without systemic venous drainage (c). He developed hyperpigmentation at right forearm which not improve after 6 months follow up, but the patient was accepting for this complication.

**Table1:** Demographic and characters of venous and lymphatic malformations

| Characteristics | Malformation type | |
|---|---|---|
| | LMs (28) | VMs (197) |
| Sex (n, % within group) | | |
|    Male | 15, 53.57% | 70, 35.53% |
|    Female | 13, 46.43% | 127, 64.46% |
| Mean age (yr) | 15.58 | 23.95 |
| Presentation (n, % within group) | | |
|    Mass | 28, 100% | 197, 100% |
|    Bleeding | 2, 7.14% | 3, 1.52% |
|    Pain | 1, 3.57% | 17, 8.63% |
|    Ulceration | 0, 0% | 1, 0.51% |
|    Lymphatic leakage | 1, 3.57% | 0, 0% |
| Previous treatment (n, % within group) | | |
|    Laser | 1, 3.57% | 3, 1.52% |
|    Laser + surgery | 0, 0% | 4, 2.03% |
|    Surgery | 12, 42.86% | 57, 28.93% |
|    Steroid therapy | 1, 3.57% | 2, 1.02% |
| Site (n, % within group) | | |
|    H&N | 12, 42.86% | 67, 34.01% |
|    Upper extremities | 5, 17.86% | 59, 29.95% |
|    Lower extremities | 9, 32.14% | 65, 32.99% |
|    Other or multiple site | 2, 7.14% | 6, 3.05% |
| Extension of lesion (n, % within group) | | |
|    Focal | 12, 42.86% | 102, 51.78% |
|    Diffuse | 16, 57.14% | 95, 48.22% |
| Morphology of lesion (n, % within group) | | |
|    Isolated without venous drainage | 5, 17.86% | 15, 7.61% |
|    Malformation with systemic venous connection | 23, 82.14% | 182, 92.39% |

**Table 2:** Comparison of treatment sessions, dose and follow-up time among patient-groups treated with sclerosants

| Sclerosing agent | No of sessions | | Dose | | F/U (mo) |
|---|---|---|---|---|---|
| | Alcohol | bleomycin | Alcohol (ml) | Bleomycin (mg) | |
| Alcohol only (64) | | | | | |
|    Range | 1-19 | - | 2-717 | - | 6-74 |
|    Mean | 3.27 | - | 80.5 | - | 14.78 |
| Alcohol+bleomycin (24) | | | | | |
|    Range | 1-18 | 1-8 | 1.3-731 | 0.6-120 | 9-90 |
|    Mean | 3.71 | 4.38 | 110.01 | 56.96 | 38.29 |
| Bleomycin only (137) | | | | | |
|    Range | - | 1-10 | - | 1-150 | 6-70 |
|    Mean | - | 2.26 | - | 28.27 | 10.09 |

**Table 3:** comparison of treatment outcome among patient-groups treated with sclerosants

| Treatment outcome | Sclerosant | | | Total |
|---|---|---|---|---|
| | Alcohol | Alcohol + bleomycin | bleomycin | |
| Grade 0: (n, % within group) | 6, 9.4% | 0, 0% | 11, 8.0% | 17,7.6% |
| Grade 1: (n, % within group) | 9, 14.1% | 4, 16.7% | 32, 23.4% | 45, 20.0% |
| Grade 2: (n, % within group) | 19, 29.7% | 9, 37.5% | 32, 23.4 | 60, 26.7% |
| Grade 3: (n, % within group) | 30, 46.9% | 11, 45.8% | 62, 45.3% | 103, 45.8% |
| Total (n) | 64 | 24 | 137 | 225 |

**Table 4:** correlation of variable factors and treatment outcome grading

| Factors | Outcome grading | | | | Total |
|---|---|---|---|---|---|
| | Grade 0 n (%) | Grade 1 n (%) | Grade 2 n (%) | Grade 3 n( %) | n |
| Gender, n (% within group) | | | | | |
| Male | 9 (10.6%) | 18 (21.2%) | 24 (28.2%) | 34 (40.0%) | 85 |
| Female | 8 (5.7%) | 27 (19.3%) | 36 (25.7%) | 69 (49.3%) | 140 |
| Onset, n (% within group) | | | | | |
| At birth | 7 (6.5%) | 25 (23.1%) | 35 (32.4%) | 41 (38.0%) | 108 |
| Later | 10 (8.5%) | 20 (17.1%) | 25 (21.4%) | 62 (53.0%) | 117 |
| Malformation type, n (% within group) | | | | | |
| VMs | 11 (5.6%) | 36 (18.3%) | 53 (26.9%) | 97 (49.2%) | 197 |
| LMs | 6 (21.5%) | 9 (32.1%) | 7 (25.0%) | 6 (21.4%) | 28 |
| Location, n (% within group) | | | | | |
| H&N | 7 (8.9%) | 11 (13.9%) | 18 (22.8%) | 43 (54.4%) | 79 |
| Upper extremities | 2 (3.1%) | 12 (18.8%) | 16 (25.0%) | 34 (53.1%) | 64 |
| Lower extremities | 7 (9.5%) | 19 (25.7%) | 23 (31.1%) | 25 (33.8%) | 74 |
| Other or multiple site | 1 (12.5%) | 3 (37.5%) | 3 (37.5%) | 1 (12.5%) | 8 |
| Extension , n (% within group) | | | | | |
| Focal | 3 (2.6%) | 13 (11.4%) | 24 (21.1%) | 74 (64.9%) | 114 |
| Diffuse | 14 (12.6%) | 32 (28.8%) | 36 (32.4%) | 29 (26.1%) | 111 |
| Morphology, n (% within group) | | | | | |
| Isolated without venous drainage | 1 (5.0%) | 1 (5.0%) | 4 (20.0%) | 14 (70.0%) | 20 |
| Malformation with systemic venous connection | 16 (7.8%) | 44 (21.5%)\ | 56 (27.3%) | 89 (43.4%) | 205 |
| Previous treatment, n (% within group) | | | | | |
| Yes | 8 (10.0%) | 16 (20.0%) | 24 (30.0%) | 32 (40.0%) | 80 |
| No | 9 (6.2%) | 29 (20.0%) | 36 (24.8%) | 71 (49.0%) | 145 |

**Table 5:**   Multivariate analysis of variables and good response of percutaneous sclerotherapy for venous and lymphatic malformations

| Variable | P value | Odds ratio | 95% confidence interval |
|---|---|---|---|
| Sex; female | 0.271 | 0.716 | 0.395 - 1.299 |
| Onset; at birth | 0.503 | 1.221 | 0.680 - 2.193 |
| Malformation type; venous malformation | 0.001 | 3.682 | 1.635 - 8.290 |
| Location; non-extremity | 0.108 | 0.545 | 0.268 - 1.108 |
| Extension; focal | <.001 | 4.329 | 0.120 - 0.442 |
| Morphology; Isolated without venous drainage | 0.066 | 0.269 | 0.060 - 1.193 |
| Previous treatment; Yes | 0.542 | 0.829 | 0.453 - 1.517 |

firmed to be predictors for good response of sclerosing therapy by the multivariate analysis (table 5). The others were independent factor (p> .05). The mean age of patients with and without good response were 22.8 and 23 years respectively which showed no statistical difference (P = 0.9).

The adverse reactions of bleomycin occurred in 19.8% including hyperpigmentation (either at the site of malformation or remote region) 25 patients (15.5%), localized fibrosis 2 (1.2%) and flu-like symptom 5 (3.1%). However, no serious complication was recognized. In contrast to absolute alcohol, the major complications had happened in 21.8%, including transient hematuria 10 (11.4%), digital gangrene 1 (1.1%), facial paralysis 1 (1.1%), pulmonary embolism 1 (1.1%) and decompensated right heart failure from increased pulmonary pressure with death 1 (1.1%). In addition, swelling at puncture sites were found in nearly all cases, and skin blistering in 20 patients (22.8%).

## Discussion

Although both VMs and LMs are often asymptomatic, however, if there are accompanying pain and functional disturbance or cosmetic concern, treatment is required. The diseases can be found anywhere, in our series, peripheral locations were more common than head and neck region, which was rather different to other reports[3,5,8]. Even there is no predilection exists for either sex in VM and LM(5, 9), but in our study VMs were more frequent in female (64.5%).

Sclerosing therapy by percutaneous injection of liquid agents has been accepted to be the initial treatment of choice and has a high reported success rate[1,10,11], with the aim to eradicate or reduce abnormal vessels by endothelial damage leading to inflammation, thrombosis and fibrosis with obliteration of the lesion finally[2]. Various sclerosing agents have been used including ethanol, ethibloc (radiopaque chemical sclerosant based on ethanol, corn protein, oleum papaveris, and propylene glycol), sodium tetradecil sulphate, polydocanol, ethanolamine oleate, and bleomycin[1-3,10] In our experience, we used only absolute alcohol and bleomycin because of their availability, effectiveness and inexpensive.

Absolute alcohol induces cellular dehydration and endothelial wall protein denaturation resulting to subsequent permanent obliteraion of the vessel lumen[12]. A 75%-95% response rate has been reported for ethanol sclerotherapy of VM[2]. However,

injection of ethanol causes severe pain due to its local tissue reaction resulting in significant tissue swelling or even skin necrosis. Its severe complications can be extremely dangerous including tissue necrosis, permanent peripheral nerve injury, pulmonary hypertension and pulmonary embolism[6]. Similar to our population treated with alcohol, the major complications were recognized at a rate of 21.8%, including hemolysis, gangrene, pulmonary embolism or even one death from uncompensated pulmonary hypertension.

Bleomycin is an antitumor agent, developed by Umezawa in 1966. Its mechanism is inhibition of DNA synthesis and has sclerosing effect on the endothelial cells[4,7]. First use in lymphangioma was reported successfully by Yura et al in 1977. Since that initial report, further studies have confirmed its utility in treating VMs. Thereafter, introduction of bleomycin in the treatment of venous malformations and hemangiomas was described by Muir et al[7] in 2004, with response rate at 84% and minor complication were occurred total 8 in 95 cases including Flu-like symptoms, ulceration, cellulitis, and partial temporary hair loss. Since those reports, further studies have confirmed its utility as a sclerosing agent for lymphangiomas, hemangiomas and venous malformations with good results[1,3-5,13]. To date, no major complications with intralesional bleomycin injection was reported. Even the most concern, regarding the potential development of pulmonary fibrosis, which was dose dependent, found when administered during cancer therapy with accumulation dose higher than 300 mg[3,4], has never been described to its use as a sclerosing agent[5]. However, high incidence of residual disease associated with therapy using bleomycin alone was documented[1,3].

At our institution, absolute alcohol was the only sclerosing agent of choice to treat VMs, until death occurred. In addition, many reports of intralesional bleomycin injection were described with a high success but less complication rates, we started using bleomycin first for LM in June 2008 and increased more in VMs. Until now, it completely replaced the use of ethanol injection. Our total 161 patients with bleomycin injection had the minor adverse reactions occurring in 19.8% with lesser postprocedural swelling, as compared to ethanol. Our experience was similar to those described in the literatures[2].

Currently, regardless complications, between ethanol and alcohol, there is no consensus to the better sclerosant. Although there were reports of more efficacy of ethanol than bleomycin in the aspects of higher success rate and require fewer treatment sessions[2], but the comparison analysis among groups of patients using sclerosant in our study; ethanol alone, ethanol and bleomycin and bleomycin alone, showed no statistical significant in sessions and outcome of treatment. Of our 225 patients treated with sclerosing therapy, satisfactory treatment outcome or good response, (grade 2, 3) was accounted for 72.5%

In this study, we postulated that focal lesions and venous malformations were the predictors of good treatment outcome. This was not surprised since a focal lesion involving only single body part was relatively smaller lesion with lesser extensive, thus it needed fewer session of treatment. In addition, this study was cross sectional study at one point of time, so it was not yet the final outcome of a number of patients with large and diffuse lesions who were still in the treating course.

To our experience, only 46.4% of LMs had good response to bleomycin injection which was

not comparable to the previously published IBI series[4,5,14]. However, our study involved a relatively small group of LMs (28 patients or 12.4%), which was not sufficient for analysis and it needs further study. Nevertheless, on our observation, most lesions were multiple microcysts, with variable in sizes, and we felt that the larger the cystic space, the better response was.

Although our data seemed to have better outcome of treated isolated VMs than lesions with drainage of venous outlet (grade 3 outcome was 70% and 43.4% respectively) but it showed no statistical significant (P = .12 in uni-variate analysis and .066 in multivariate analysis). As such, it was probably due to too different numbers of cases between the two groups (n = 20 and 205 respectively). Puig et al[10] found that VMs with drainage into dysplastic veins and venous ectasia were more difficult to treat with sclerosing agents because of extensive drainage into the normal venous circulation and increased risk of embolic complications. As we performed pressure over venous outlet during injection, it might overcome this problem.

Yun et al[12] reported female gender and not extremity location were significant associated with good response to percutaneous sclerotherapy. This was different from our study. We found no association between age, gender and location of the lesions with good response. However, in our study, the lesions at head and neck region had the highest success rate of sclerosing therapy.

The limitations of this study were retrospective design with a lack of standardized assessment tool, such as imaging study, to compare the result of treatment. The visual assessment on patients' photograph and patient's interview may be not enough statistical reliable.

## Conclusion

Absolute alcohol and bleomycin were proved to be the effective sclerosing agents for percutaneous treatment of venous malformations. Although no significant statistical difference between their degree of success rate, but bleomycin showed superior patient's outcome due to absence of serious complications which could ensure satisfaction for both patients and physicians. Moreover, inferring from our study that the characteristic of focal single lesion, at any region of body part, can be a predictor for good response, and bleomycin provides more successful treatment outcome on VMs than LMs.

## References

1. Jin Y, Lin X, Li W, Hu X, Ma G, Wang W. Sclerotherapy after embolization of draining vein: a safe treatment method for venous malformations. J Vasc Surg. 2008 Jun;47(6): 1292-9.

2. Spence J, Krings T, terBrugge KG, da Costa LB, Agid R. Percutaneous sclerotherapy for facial venous malformations: subjective clinical and objective MR imaging follow-up results. AJNR Am J Neuroradiol. 2010 May;31(5): 955-60.

3. Mathur NN, Rana I, Bothra R, Dhawan R, Kathuria G, Pradhan T. Bleomycin sclerotherapy in congenital lymphatic and vascular malformations of head and neck. Int J Pediatr Otorhinolaryngol. 2005 Jan;69(1):75-80.

4. Sung MW, Chang SO, Choi JH, Kim JY. Bleomycin sclerotherapy in patients with congenital lymphatic malformation in the head and neck. Am J Otolaryngol. 1995 Jul-Aug;16(4):236-41.

5. Rozman Z, Thambidorai R, Zaleha A, Zakaria Z, Zulfiqar M. Lymphangioma: Is intralesional bleomycin sclerotherapy effective? Biomed Imaging Interv J. 2011 Jul;7(3):e18.

6. Mason KP, Michna E, Zurakowski D, Koka BV, Burrows PE. Serum ethanol levels in children and adults after ethanol embolization or sclerotherapy for vascular anomalies. Radiology. 2000 Oct;217(1):127-32.

7.  Muir T, Kirsten M, Fourie P, Dippenaar N, Ionescu GO. Intralesional bleomycin injection (IBI) treatment for haemangiomas and congenital vascular malformations. Pediatr Surg Int. 2004 Jan;19(12):766-73.

8.  Jin Y, Lin X, Chen H, Li W, Hu X, Ma G, et al. Craniofacial venous malformations: magnetic resonance imaging features that predict treatment outcome. J Oral Maxillofac Surg. 2009 Nov;67(11):2388-96.

9.  Som PM. Head and neck imaging. 4th ed. St. Louis.: Mosby.; 2003.

10. Puig S, Aref H, Chigot V, Bonin B, Brunelle F. Classification of venous malformations in children and implications for sclerotherapy. Pediatr Radiol. 2003 Feb;33(2):99-103.

11. Lee KB, Kim DI, Oh SK, Do YS, Kim KH, Kim YW. Incidence of soft tissue injury and neuropathy after embolo/sclerotherapy for congenital vascular malformation. J Vasc Surg. 2008 Nov;48(5):1286-91.

12. Yun WS, Kim YW, Lee KB, Kim DI, Park KB, Kim KH, et al. Predictors of response to percutaneous ethanol sclerotherapy (PES) in patients with venous malformations: analysis of patient self-assessment and imaging. J Vasc Surg. 2009 Sep;50(3):581-9, 9 e1.

13. Kullendorff CM. Efficacy of bleomycin treatment for symptomatic hemangiomas in children. Pediatr Surg Int. 1997 Sep;12(7):526-8.

14. Acevedo JL, Shah RK, Brietzke SE. Nonsurgical therapies for lymphangiomas: a systematic review. Otolaryngol Head Neck Surg. 2008 Apr;138(4):418-24.

Original Article

# The Accuracy of Multidetector Row CT Angiography in the Evaluation of Living Kidney Donors

**Seksan Chitwiset MD**[1]
**Vorapot Choonhaklai**[2]

[1] *Department of Radiology, Rajavithi Hospital, College of Medicine, Rangsit University, Bangkok, Thailand.*
[2] *Division of Urology, Department of Surgery, Rajavithi Hospital, College of Medicine, Rangsit University, Bangkok, Thailand.*

## Abstract

**Purpose:** To assess the value of MDCT in evaluation of the anatomy of living kidney donors and in revealing the prevalence of renal vascular variations.

**Materials and Methods:** This retrospective study was approved by the Ethics committee of Rajavithi hospital(NO.172/2555). The accuracy of the images of vessel structures obtained by using 64-row multidetector computed tomography (MDCT) angiography in comparison with the actual vessel structures observed during surgery was analyzed retrospectively.

We analyzed 20 patients who had undergone donor nephrectomy from 2008 to 2012. Preoperative MDCT angiography was performed, and the surgeons themselves subsequently recorded the operative findings.

**Results:** Nephrectomy was performed on the left side in all 20 patients. The accuracy levels of MDCT for the artery and the vein were 90% and 95% respectively.

**Conclusions:** MDCT angiography is a good investigative technique for the preoperative evaluation of the anatomy of vessels.

*Key Words:* Kidney transplantation; Living donors; Renal artery; Renal veins; MDCT

Correspondence to:
    Jitwiset S.  Diagnostic Radiology, Radiologic department,Rajavithe Gospital, Collecge of Medicine, Rangsit University,
    2 Phyathai Road, Ratchathewi, Bangkok 10400,Thailand
    Phone:0-2354-8180 ext 3025,  Fax:0-2354-8093
    e-mail: seksanchit@hotmail.com

## Introduction

End-stage renal failure is a growing health problem in Thailand. The number of sufferers is increasing due to the prevalence of many underlying diseases and prolonged life expectancy. Patients who suffer from this problem end up having to survive with hemodialysis or continuous ambulatory peritoneal dialysis (CAPD). Renal transplantation is a good treatment choice because it offers improved quality of life and is cost-effective. Cadaveric kidneys available for transplantation are limited: the number of patients waiting for cadaveric kidney transplantation is increasing, and few patients are able to have such transplants because of the lack of availability of cadaveric organs. To make up for this shortage, live kidney donation is now a widely accepted practice, with better recipient tolerance and better renal graft survival than can be achieved with cadaveric donor transplantation[1-3].

Preoperative imaging work-up of living renal donors involves anatomic and functional evaluation of donor kidneys for the selection of a suitable donor and for the planning of surgery. In donor nephrectomy, it is important to understand the exact anatomy of the blood vessels. Information about the number of renal arteries and early division of the main renal artery is important when deciding whether to remove the right or left kidney. This information is also important for minimally-invasive surgery in order to decrease blood loss and the length of hospital stay by reducing complications and accelerating recovery[4,5].

In the past, preoperative evaluation were included intravenous pyelography (IVP), angiography, and abdominal sonography[6,7]. With the introduction of multidetector computed tomography (MDCT), those methods have been replaced by computed tomography (CT) angiography[8]. CT angiography is less invasive than conventional angiography and has the advantage of allowing not only highly accurate assessment of the main vessel (renal vein, renal artery) and ureter structure, but also detection of renal cystic diseases, renal parenchymal lesions, tiny stones, and hilar vessels[9-11].

Many previous studies have been carried out to examine the accuracy of CT angiography in determining vessel structures. The level of accuracy for the main vessels was reported to vary from 90% to 100%, and for the minor vessels from 75% to 100%[12-15]. One reason for the variation in accuracy may be from different CT protocols.

The objective of this study was to assess the accuracy of CTA images for pre-operative evaluation of renal vascular anatomy in comparison with the actual vessel structure observed during surgery.

## Materials and Methods

This retrospective study was approved by the Ethics committee of Rajavithi hospital (NO.172/2555). Between 2008 and 2012, the number of kidney donors who were evaluated with MDCT in our center (Rajavithi Hospital) were 8 males and 12 females (a total of 20 donors) whose ages ranged from 20-53 years old (mean age = 40.6 years old). All 20 donors underwent nephrectomy

### 1. CT protocols

All CT examinations were performed with a standardized examination protocol using a multislice 64 detector-row helical CT scanner (Lightspeed VCT, GE Medical Systems, Milwaukee, USA). Scanning was initiated with a scout image covering the whole abdomen. Precontrast imaging was performed with

5mm slices and the table rotation time was 0.6 sec with 120 kV and automated calculation of mAs. After a plain scan of the abdomen (scout film) had been taken, an 18-20 gauge intravenous catheter was placed in the antecubital vein. Using an automatic injector, 100 ml of the contrast material was injected at a flow rate of 4ml/sec. The arterial phase was obtained after 12 seconds, and the venous phase 60 seconds after the initiation of the contrast bolus. The arterial phase included a volume covering the diaphragm to the pelvis. After acquiring the images, arterial phase and venous phase images were reconstructed by axial 3 mm and 1 mm images and coronal 3 mm images.

The reconstructed images were processed with a commercially available work station (ADW 4.3: GE medical systems). Two- and three-dimensional maps of the renal arteries, renal veins and ureters were generated by using maximum-intensity projection (MIP), volume rendering techniques and multiplanar reformation. In addition, a 3D reconstruction image was acquired with 0.625 mm slice thickness. All CT angiographies were interpreted by a radiologist before donor nephrectomy. During the evaluation, the main vessel structures of the right and left sides were described, together with the path of the hilar veins. Early branching renal artery exists when the first branch of the renal artery originates within 2.0 cm from the lateral wall of the aorta.

## Results

The radiological findings of the CT of the main vessels were compared with the surgical findings of the 20 donors (8 males and 12 females. All nephrectomies were performed on the left side with open flank nephrectomy in 18 donors and with laparoscopic approach in the other 2. The mean age of

the patients was 40.6 years old (range, 20-53 years old). CT showed that a small simple renal cyst (diameter less than 1 cm) was present in one of 20 donor kidneys. None of the selected donor kidneys was noted to have renal stones, fibromuscular dysplasia of renal artery, or any congenital vascular abnormality on multidetector CT images.

### Renal artery

A total of 23 renal arteries in the 20 donor kidneys were depicted with CT. Only 3 kidneys were shown to have more than one renal artery (2 renal arteries in each kidney). During surgery, 23 arteries were also identified in the 20 kidneys, 17 of the 20 kidneys (85%) had a single artery and 3 of the 20 kidneys (15%) had more than one artery. One accessory artery, the superior polar artery, in 1 kidney was initially missed on CT. The sensitivity and specificity of CTA for detection of variant anatomy of renal arteries were 66.66% and 94.11% respectively. The accuracy of CT in detection of renal arteries, positive predictive values, and negative predictive values were 90%, 66.67% and 94.11% respectively, indicating good agreement with surgical findings. The one accessory renal artery that had been missed at the CT initial interpretation was identified in a retrospective review.

### Renal vein

A total of 20 renal veins were identified in CT images of 20 donor kidneys. During surgery, 21 renal veins were identified in 20 kidneys; one kidney had 2 renal veins, and each of the remainder had just one renal vein. The sensitivity and specificity of CT for the identification of variant anatomy of renal veins were 50% and 100% respectively. In surgery, the overall CT findings were concordant in 19 of the

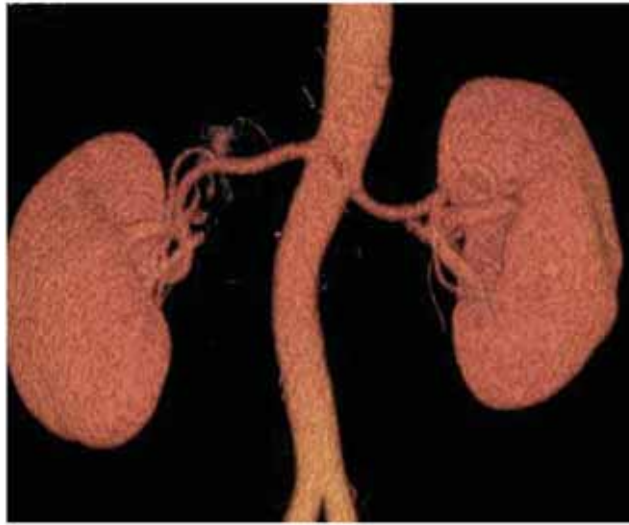**Fig. 1** A 3-D volume-rendered (VR) image  of a 48-year-old female renal donor obtained with a 64-slice MDCT demonstrating single right and left renal artery
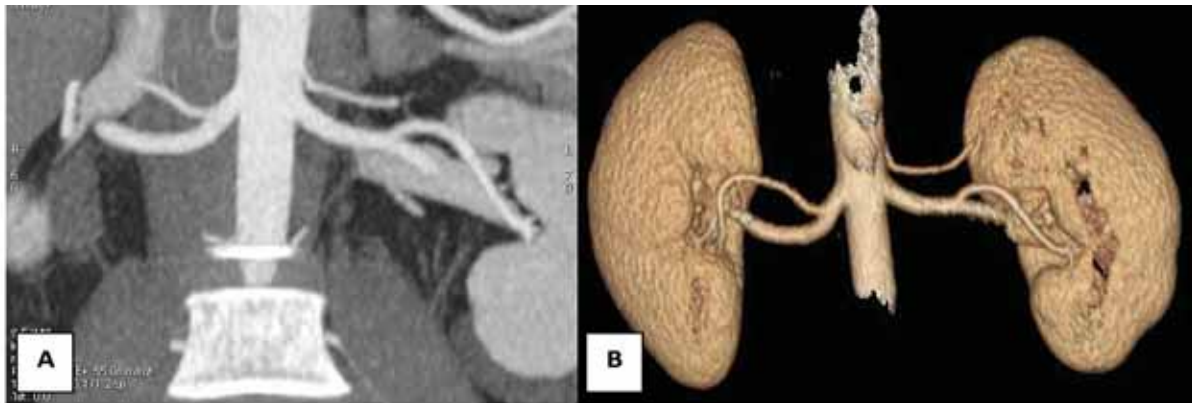


**Fig. 2** (A) A   3-D maximum intensity projection(MIP) image and (B)a 3-D volume-rendered (VR) of a 20-year-old female renal donor obtained with 64-slice CT show  two left renal arteries and early branching  of single right renal artery (7 mm. from aorta)

**Fig. 3** A 3-D maximum intensity projection (MIP) image of a 45-year-old female renal donor obtained with 64-slice MDCT demonstrating double left renal vein with left gonadal vein drain into the inferior left renal vein

20 kidneys (accuracy 95%). The positive predictive and negative predictive values were 100% and 94.73% respectively.

## Discussion

Renal transplantation is a good therapy for patients with end-stage renal disease. Due to the limited number of cadaveric organs available, patients are having to suffer for extended periods of time before undergoing cadaveric kidney transplantation; consequently, the number of living donors has been increasing in recent times[3,12]. It is crucial to evaluate the donor's vascular anatomy before the removal of a kidney with any surgical technique, especially when using a laparoscopic approach because of the limited exposure during the procedure[13,14]. Understanding the vascular anatomy of the kidney is an essential part of pre-operative evaluation of living kidney donors, and it helps the clini-

cians to choose suitable donors and decide whether the left or the right kidney should be used[15]. The anatomic information required before conventional open and minimally-invasive surgery in living kidney donors includes number, length, location and branching patterns of the renal arteries, as well as the status of the donor kidneys and their venous and blood collecting systems[8,16].

In the past, conventional angiography was used to evaluate renal arteries before surgery[10,17,18]. It was a rather invasive procedure and donors had to stay in hospital for a few days after the angiographic procedure with the risk of endothelial damage.

Several investigators have used single-detector row helical CT for predicting renal vascular anatomy[9,14] and some have reported good correlation with both catheter angiography and surgery[5,15-18].

Improvements in CT technology have enabled

multidetector row CT to achieve increased speed of scanning and enhanced spatial resolution with advances in post processing methods[19]. Multidetector row CT provides greater volume coverage with superior quality three-dimensional angiograms. Delayed CT urographic imaging of excretory phase CT is helpful in evaluating pyelocalyceal and ureter anatomy and obviates the need for intravenous pyelography.

The aim of this study was to evaluate the accuracy of renal CT angiography obtained by the use of 64-slice MDCT for prediction of the vascular anatomy and its variations in living kidney donors. It can be concluded that, for renal arteries, CT findings were concordant with those from surgery in 18 of the 20 donors (accuracy 90%). Although one accessory artery of about 1.5mm in diameter had been missed in the initial CT interpretation, it was identified on transverse CT scan alone in a retrospective review of CT data.

Accurate identification of renal veins was achieved in 19 of the 20 donor kidneys (accuracy 95%). The initially-missed accessory renal vein in CT was seen in retrospective review.

The accuracy of the renal vascular anatomy was reported to be high, at 90-100%, and in studies of multidetector row CT, successful identification of minor venous anomalies was reported to be 75-100%. The results of this study correspond well with those of earlier studies with high sensitivity and accuracy in the assessment of renal vasculature[11,21-25].

There have been previous reports about vascular variants in living Thai donors, in which supernumerary renal arteries were found in about 18.5-27% of kidneys. The variations that were found on 64-row MDCT were accessory renal artery = 26.46%;

early branching = 0.62-22.4%; and venous variant = 1.85%[11,26]. Accessory renal arteries were found in about 15% of kidneys in this study.

Preoperative evaluation is important, especially for laparoscopic surgery because of its limited field of view. Conversion to the open approach is not infrequent, the most common reason being vascular injury[27,28]. Therefore, special attention must be paid to the assessment of donor renal vessels and collecting system for selection of suitable kidneys and for planning surgery.

There were some limitations in our study. First the number of donors was low, resulting in a low number of variations. Second, this study was a retrospective one, so many donors were excluded from this study due to incomplete information; furthermore, the study reviewed cases involving many radiologists with varying experience, and it is important to note that we chose to select kidneys with normal anatomy and fewer anomalies for donor nephrectomy. Therefore, the performance of multidetector row CT in the evaluation of more complex vascular and excretory anatomy and anomalies could not be compared.

## Conclusion

MDCT angiography can provide highly accurate assessment of renal vascular anatomy in living kidney donors that will be helpful for preoperative planning.

## Acknowledgement.

## References

1. Poli F, Scalamogna, CariloM, Porta E, Sirchia G. An algo-

rithm for cadaver kidney allocation base on a multivariate kidney graft survival and function. Transpl Int 2000; 13(supple 1):S259-62

2.  Goel C, Modlin Cs, Mottoo AM, Derweesh IH, Flechner SM, Streem S, et al. Fate of donor kidney:laparoscopic versus open technique. J Urol 2004;172(6 pt 1):2326-30.

3.  Annual Report of the U.S Scientific Registry of Transplant Recipients and the Organ Procurement and Trasplantation Network-Transplant Data:1988-1994. UNOS, Richmond,VA and the Division of Transplantation, Bureau of Health Resources and Services Administration,U.S. Department of Health and Human Services, Rockville, MD, 1995

4.  Giessing M. Laparoscopic Living-donor nephrectomy. Nephrol Dial Transplant 2004;19(supple4):iv36-40.

5.  Rydberg J, Kopecky KK, Tann M, Persohn SA, Leapman SB, Filo RS, et al. Evaluation of preoperative of prospective living renal donor for laparoscopic nephrectomy with multisection CT:the marriage of minimally invasive imaging with minimal invasive surgery. Radiographics 2001;21 Spec No:S223-6.

6.  Derauf B, Goldberg ME. Angiographic assessment of potential renal transplant donors. Radiol Clin North Am 1987;25:261-5.

7.  Shaffer D, Sahyoun AI, Madras PN, Monaco AP. Two hundred and one consecutive living-donor nephrectomies. Arch Surg 1998;133:426-31.

8.  Cochran ST, Krasny RM, Danovitch GM, Rajfer J, Barbaric ZM, Wilkinson A, et al. Helical CT angiography for examination of living renal donors. AJR Am J Roentgenol 1997;168:1569-73.

9.  Kawamoto S, Montgomery RA, Lalwer LP, Horton KM, Fishman EK. Multidetector CT angiography for preoperative evaluation of living laparoscopic kidney donors. AJR Am J Roentgenol 2003;180:1633-8.

10. Platt JF, Ellis JH, Korobkin M, Reie K. Helical CT evaluation of potential kidney donors:finding in 154 Subjects. AJR 1997;169:1325-30

11. Raman SS, Pojchmarnwiputh S, Muangsomboon K, Schulam PG, Gritsch HA, Lu DS. Utility of 16-MDCT angiography for comprehensive preoperative evaluation of laparoscopic renal donor. AJR 2006;186:1630-8.

12. Cecka JK, The OPTN/UNOS renal transplant registry, Clin Transpl 2005;1-16.

13. Ratner LE,Ciseck IJ, Moore RG, Cigarroa FG, Kaufman HS,Kavoussi LR. Laparoscopic live donor nephrectomy. Transplantation 1995;60:1047-9.

14. Rubin GD, Alfrey EJ, Dake MD, Semba CP, Sommer FG, Kuo PC, et al. Assessment of living donors with spiral CT. Radiology 1995;195:457-62.

15. Satyapal KS, Haffejee AA, Singh B, Ramasaroop L, Robbs JV, Kalideen JM. Additional renal arteries: incidence or morphometry, Surg Radiol Anat 2001;23:33-8.

16. Del Pizzo JJ, Sklar GN, You-Cheong JW, Levin B, Krebs T, Jacobs SC. Helical computerized tomography arteriography for evaluation of live related donor undergoing laparoscopic nephrectomy. J Urol 1999;162:31-4.

17. Burgos FJ, Pascual J, Mareen R, Garcia-Navas R, Gomez V,Ortuno J. The role of imaging techniques in renal transplantation. World J Urol 2004;22(5):399-404.

18. Leim YS, Kock MC, Ijzermans JN, Weimar W, Visser K, Hunink MG. Living renal donors:optimizing the imaging strategy-decision and cost-effectiveness analysis. Radiology 2003;180(6):53-62

19. Rydberg J, Laiang Y,Teague SD. Fundamentals of multichannel CT. Radiol Clin North Am 2003;41:465-74.

20. Holden A, Smith A, Dukes P, Pilmore H, Yasutomi M. Assessment of 100 Live Potential Renal Donors for laparoscopic nephrectomy with multidetector row helical CT. Radiology 2005;237:973-80.

21. Sahani DV, Rastogi N, Greenfield AC, Kalva SP, Ko D, Saini S,  Multidetector row CT in evaluation of 94 living renal donors by readers with varied experience, Radiology 2005;235:905-10.

22. Raman SS, Pojchamarnwiputh S, Muangsomboon K, Schulam PG, Gritsch HA, Lu DS. Utility of 16-MDCT angiography for comprehensive preoperative vascular evaluation of Laparoscopic renal donors, AJR 2006;186: 1630-8.

23. Apisarnthanarak P, Suvannarerg V, Muangsomboon K, Taweemonkongsap T, Hargrove NS. Renal vascular variants in living related renal donors: evaluation with CT angiography, J. Med Assoc Thai. 2012;95(7):941-8.

24. Kim JK, Park SY, Kim HJ, Kim CS, Ahn HJ, Ahn TY, et al. Living donor kidneys:usefulness of multidetector row CT for comprehensive evaluation. Radiology 2003;229: 869-76.

25. Namasivayam S, Small WC, Kalra MK,Torres WE, Newell KA, MIttal PK. Multidetector-row CT angiography for pre-operative evaluation of potential laparoscopicrenal donors:how accurate are we? Clin imaging. 2006;30: 120-6.

26. Ekkasit S, Chutcharn K,Supakajeee S. Anatomical Cariation of Renal Vessels by 64 Slices Multidetector Computed Tomography(MDCT) Scan of abdomen at Pramongkutklao Hospital.RTA Med J;664:75-83.

27. Rydberg J, Kopecky KK, Tann M, Persohn SA, Leapman SB, Filo RS, et al. Evaluation of prospective living renal donors for laparoscopic nephrectomy with multisection CT;the marriage of minimally invasive imaging with minimally invasive surgery. Radiographics 2001;21:223-36.

28. Richstone L, Seideman C, Baldinger L, Permpandkosol SS, Jarrett TW, Su LM, et al. Conversion during laparoscopic surgery:frequency,indication and risk factors. J Urol 2008;80:855-9.

Original Article

# Magnetic Resonance Imaging Features of Intramedullary Spinal Cord Tumors with Pathological Correlations

**Jureerat Thammaroj, MD**

**Amnat Kitkhandee, MD**

**Parinyaporn Tumkot, MD**

**Pichayen Duangtongpol, MD**

**Sakda Waraosawapati, MD**

*Department of Radiology, Neurosurgery, Pathology*

*Faculty of Medicine, Khon Kaen University, Khon Kaen, Thailand, 40002*

## Abstract

**Objective:** The purpose of this study was to determine characteristic imaging findings of intramedullary spinal cord tumor in magnetic resonance imaging (MRI).

**Material and Methods:** We retrospectively analyzed MRI in 15 patients with histologicaly proven intramedullary spinal cord tumors. The demographic data, MRI findings with histological findings were recorded in terms of age, location, length, morphology, signal intensity, the presence or absence of cyst and hemorrhage, enhancement pattern, other associated findings, necrosis, vascular proliferation and WHO grading.

**Results:** Among the 15 patients, spinal cord ependymomas were eccentric 75%, well-define border 62.5% and cervicothoracic spine located 37.5%.

Spinal cord astrocytomas were eccentrically located and ill-define border 85.7%, cervicothoracic and thoracic spine located 28.5%. A cystic component was seen in 87.5% of spinal cord ependymoma and 71.5% of astrocytomas. Intratumoral hemorrhage occurred in 75% of spinal cord ependymomas, and 57.1% of astrocytomas. In 12.5% of spinal cord ependymomas, a curvilinear low T2 signal, suggesting marginal hemorrhage, was seen at the upper and/or lower margins of the tumors. Twenty-five percent of spinal cord ependymoma and 57.2% of astrocytomas showed heterogeneous enhancement, while in 12.5% of spinal cord ependymomas, enhancement was homogeneous.

**Conclusion:** Although no statistically significant characteristic MRI feature to distinguish between ependymoma and astrocytoma is detected. By percentage we found that border, length and signal intensity of tumors may help diagnosis. With pathological correlation, all of spinal cord ependymomas are mark hypervascular tumor, but astrocytomas never showed.

## Introduction

Intramedullary spinal cord tumors account for approximately 25% of spinal tumors. Ependymoma is the most common intramedullary cord tumors, account for about 60%[1]. Whereas astrocytoma for approximately 30%[2]. The differential diagnosis of spinal tumors is primarily based on location, but the clinical presentation, age, and gender of the patient are also important factors in determining the diagnosis[3].

Magnetic resonance imaging (MRI) has been the sensitive tool for detection and diagnosis of intramedullary spinal cord tumors. With its multiplanar capabilities and high contrast resolution, it allows identification and characterization of the lesion as a noninvasive modality. The addition of intravenous contrast administration allows further delineation of the mass, separating tumor from edema and cysts. The exact histologic diagnosis of tumors remains elusive on the basis of MR signal intensity and enhancement alone. However, there are some imaging characteristics which can be suggest the diagnosis[4].

The goals of surgery are to obtain a tissue diagnosis and to improve neurological function by removing the tumor. It is important to identify type of spinal cord tumors, because proper treatment of different subtypes can reduce the rate of disability and functional impairment. Proper preoperative diagnosis is crucial for neurosurgeon, because most ependymoma is well demarcated from cord tissue, can be totally removed and usually result in cure, whereas astrocytoma always infiltrate the surrounding cord tissue, making total resection is impossible[1]. The traditional treatment of intramedullary astrocytoma has been biopsy or debulking followed by radiation therapy[5]. Outcome for intramedullary spinal cord astrocytoma is significantly worse than that of ependymoma and is most closely predicted by pathological grade[6]. The purpose of this study was to determine characteristic imaging findings of intramedullary spinal cord tumor in magnetic resonance imaging (MRI).

## Material and methods

We retrospectively analyzed MRIs in 15 patients with intramedullary spinal cord tumors from 1st January 2006 to 31th October 2011 at Srinagarind Hospital, KhonKaen University, Thailand. All patients were treated surgically, and pathological confirmations were obtained.

All MRI studies had been obtained by using a 1.5T scanner (GE; Signa Horizon). The protocol included spin-echo T1 weighted, fast spin-echo T2 weighted images in axial and saggital plane, proton density image in saggital plane and post contrast-enhanced (0.2 mmol per kilograms of body weight) fat suppressed fast spin-echo T1 weighted image in axial and saggital plane. Section thicknesses were about 4 mm. and 5 mm. in sagittal and axial images, respectively.

All of MRI studies and proven histological data were evaluated by a fourteen years experienced radiologist and pathologist by single blind technique. The tumor characteristic were recorded in term of location, length, morphology, signal intensity, the presence or absence of cyst and hemorrhage, enhancement pattern, and other associated findings. Additional the results of histology were assessed with cystic component, intratumoral hemorrhage, necrosis, vascular proliferation and WHO grading.

For each imaging sequences, the signal intensity of spinal tumors was compared with spinal cord. The location of the solid tumors was classified as

central or eccentric on the axial image, eccentric indicating that the whole of tumor was laterally placed. In addition, intramedullary spinal cord tumors were assessed with anatomical location (cervical, thoracic, lumbar, cervicothoracic, thoracolumbar, thracolumbosacrum), longitudinal length (number of vertebral segments involving tumor), T1 and T2 signals relative to the spinal cord (hypointense, isointense, hyperintense, hypo-isointense and hypo-hyperintense).

Peritumoral cyst was defined as a cyst at caudal or rostral to the solid tumors without contrast enhancement of its wall, while an intratumoral cyst was define as a cyst within the tumor with enhancement of its wall(If areas of high signal intensity were obscured at non-enhanced T1-weighted image, intratumoral hemorrhage was thought to be present). The presence or absence of a low signal intensity rim at the boundaries of the tumor at T2-weighted imaging, suggesting marginal hemorrhage, was evaluated. The tumor enhancement patterns were classified into the following categories according to the area of solid tumor enhancement and homogeneity: 1) no enhancement, 2) focal nodular enhancement, 3) patchy enhancement (enhancement of less than one-half of the solid portion of the tumor), 4) heterogeneous enhancement (inhomogeneous enhancement of one-half or more of the solid portion of the tumor), and 5) homogeneous enhancement (homogeneous enhancement of one-half or more of the solid portion of the tumor).

## Result

Of 15 patient intramedullary spinal cord tumors, 8 patients were ependymomas and 7 patients were astrocytomas.

## Age and Gender

The patient age ranged from 26 to 60 years (mean = 43) of spinal cord ependymoma and 3 to 47 years (mean = 23) of spinal cord astrocytoma, respectively. The demographic data are summarized in Table 1.

## Tumor morphology and location

Spinal ependymoma appears eccentric located 6/8 (75%), well-defined border 5/8 (62.5 %), ill-defined border 3/8 (37.5) and central located 2/8 (25%), whereas astrocytoma shows eccentric located 6/7 (85.7%), ill-define border 6/7 (85.7%), well-define border 1/7 (14.3%) and central located 1/7 (14.3%).

Spinal cord ependymoma locate at CT spine 3/8 (37.5 %), lumbar spine 2/8 (25 %), TL spine 1/8 (12.5 %), cervical spine 1/8 (12.5%), and TLS spine 1/8 (12.5%), respectively. Spinal cord astrocytomas locate at CT spine 2/7 (28.5%), thoracic spine 2/7 (28.5%), cervical spine 1/7 (14.3% ), lumbar spine 1/7 (14.3%), and TL spine 1/7 (14.3%), respectively. The findings appear in Table 2.

## Tumor length

The lesions varied from 2 to 18 vertebral segments (mean = 7.8 vertebral segments) in length along the neuraxis of spinal cord ependymomas and 3 to 8 vertebral segment (mean=5.4 vertebral segments) of spinal cord astrocytomas. The findings appear in Table 2.

## Signal Intensity

At TI-weighted imaging, 3/8 (37.5%) spinal cord ependymomas were iso-hyperintense and 3/7 (42.9%) were low-isointense of spinal cord astrocytomas.

At T2-weighted imaging, 6/8 (75%) of spinal cord ependymoma were hyperintense and 4/7

(57.2%) of spinal cord astrocytomas were hyper-intense relative to the signal intensity of spinal cord.

### Enhancement Pattern

Among the 15 patients who underwent contrast-enhanced scanning, tumor enhancement was demonstrated in all spinal cord tumors. Enhancement pattern was focal nodular in three (37.5%), heterogeneous enhancement in two (25%), patchy enhancement in two (25%) and homogeneous enhancement in one (12.5%) of eight spinal cord ependymomas (Fig 1), while among seven spinal cord astrocytomas, the observed pattern was heterogeneous in 4 (57.2%). In two cases (28.5%) were focal nodular enhancement (Fig 2) and one case (14.3%) was patchy enhancement. The MR imaging findings of spinal ependymomas and astrocytomas are summarized in Tables 2.

### Cyst and Hemorrhage

Seven of 8 spinal cord ependymomas (87.5%) had reactive cystic component, both rostral and caudal cysts 3/8 (37.5%), caudal 2/8 (25%) and rostral 1/8 (12.5%) cysts (Fig 3 and 4) and intratumoral cyst 1/8 (12.5%) were present. Among spinal cord astrocytomas had cysts 4/7 (57.2%), cyst type was rostral 1/7 (14.3%), caudal 1/7 (14.3%), syringohydromyelia 1/7 (14.3%) and intratumoral cyst 1/7 (14.3%).

Intratumoral hemorrhage occurred in 6 of 8 (75%) spinal cord ependymoma (Fig 5), while 4 of 7

(57.1%) astrocytomas occurred. At T2-weighted imaging, rim(s) of low signal intensity, suggesting marginal hemorrhage between normal and tumoral tissue, were seen at the upper or lower margins of 1 (12.5%) of 8 spinal cord ependymoma.

### Histological findings

Eight spinal ependymomas were tanocytic type 12.5% (1) and myxopapillary type 12.5% (1). All of ependymomas were WHO grade II. Low grade (I-II) spinal cord astrocytomas were 4/7 (57.1%), three were pilocytic astrocytoma grade I (42.8%), one was astrocytoma grade II (14.3%). High grade (III-IV) were 3/7 (42.9%) of spinal astrocytomas, two were anaplastic astroctyma grade III (28.6%) and one was glioblastoma multiforme grade IV (14.3%).

There had intratumoral cysts about four (57.1%) of seven spinal astrocytomas (Fig 6) and three (37.5%) of eight spinal ependymomas. Intratumoral hemorrhage were found six (85.7%) of seven spinal astrocytomas and four (50%) of eight spinal ependymomas. Vascular proliferation found 42.9% of three high grade astrocytomas. Necrosis areas were found one (14.7%) of seven spinal astrocytoma and one (12.5%) of eight spinal ependymoma. All of ependymomas show mark hypervascularity, while two of seven (28.5%) spinal astrocytomas appear moderate hypervascularity. The others associated findings such as true ependymal rosette and/or perivascular rosette found about two (25%) of eight of spinal cord ependymomas. Rosenthal fiber was found three

**Table 1.** Patient Information

| Diagnosis | Age (mean) | Male (%) | Female (%) |
|---|---|---|---|
| Ependymoma | 26-60 years (43) | 12.5 | 87.5 |
| Astrocytoma | 3-47 years (23) | 28.6 | 71.4 |

**Table 2.** Summary of MR Imaging Findings of Spinal Cord tumor

| | Ependymoma (n=8) | Astrocytoma (n=7) | p-value |
|---|---|---|---|
| **Morphology** | 37.5 % | 14.3 % | 0.569 |
| Well-define | 62.5 % | 85.7 % | |
| Ill-define | | | |
| **Axial location** | 75% | 85.7% | >0.999 |
| Eccentric | 25% | 14.3% | |
| Central | | | |
| **Longitudinal location** | | | |
| Cervical spine | 12.5% | 14.3% | |
| Thoracic spine | 0% | 28.5% | |
| Lumbar spine | 25% | 14.3% | 0.874 |
| Cervicothoracic spine | 37.5% | 28.5% | |
| Thoracolumbar spine | 12.5% | 14.3% | |
| Thoracolumbarsacral spine | 12.5% | 0% | |
| **Length of tumors** | 2-18 vertebral | 3-8 vertebral | |
| (mean) | segments | segments | |
| | (mean=7.8 ) | (mean=5.4) | |
| **Signal intensity** | | | |
| **T1W** | | | |
| Isointense | 12.5% | 28.5% | |
| Hypointense | 25% | 28.5% | |
| Hyperintense | 0% | 0% | |
| Iso-hypointense | 25% | 42.9% | 0.483 |
| Iso-hyperintense | 37.5% | 0% | |
| **T2W** | | | |
| Isointense | | | |
| hypointense | | | |
| Hyperintense | 75% | 57.2% | |
| Iso-hypointense | | | 0.608 |
| Hypo-hyperintense | 25% | 42.8% | |
| **Cystic component** | | | |
| None | 12.5% | 42.8% | |
| Rostal | 12.5% | 14.3% | |
| Rostal with caudal | 37.5% | | |
| Caudal | 25% | 14.3% | |
| Syringohydromyelia | | 14.3% | |
|    Intratumoral cyst | 12.5% | 14.3% | 0.096 |
|    Intratumoral hemorrhage | 75% | 57.1% | |
| Hemosiderin cap | 12.5% | - | |
| **Enhancement pattern** | | | |
| No enhancement | | | |
| Homogeneous | 12.5% | | |
| Heterogeneous | 25% | 57.2% | > 0.999 |
| Focal nodular | 37.5% | 28.5% | |
| Patchy enhancement | 25% | 14.3% | 0.720 |

**Table 3.** Summary of pathological findings of spinal cord tumor

| | Ependymoma (n=8) | Astrocytoma (n=7) |
|---|---|---|
| WHO grading | Tanocytic type; 12.5% | Grade I; 42.8% |
| | Myxopapillary type; 12.5% | Grade II; 14.3% |
| | Other type; 75% | Grade III; 28.6% |
| | | Grade IV; 14.3% |
| Cystic component | 37.5% | 57.1% |
| Intratumoral hemorrhage | 50% | 85.7% |
| Necrosis | 12.5% | 14.7% |
| Vascular proliferation | - | 42.8% |
| Calcification | - | - |
| Other findings | Mark hypervascularity; 100% | Moderate hypervascularity; 28.5% |
| | True ependymal rosette or | Rosenthal fiber; 42.8% |
| | perivascular rosette; 25% | |

(42.8%) of seven spinal cord astrocytomas. Neither spinal cord ependymomas nor astrocytoma had intratumoral calcification. The histological findings of spinal ependymomas and astrocytomas are summarized in Tables 3.

## Discussion

Ependymomas are the most common spinal cord tumors in adults, with a peak incidence in the fourth and fifth decades, and account for 60% of all intramedullary tumors[3]. Spinal cord astrocytomas are the most commonly occurring intramedullary tumors in children and the second most common spinal cord tumor in adults, age at presentation is 30 years[3,7,8]. Consistent with our series, we found spinal ependymomas occurred between 26 and 60 years (mean age 43 years) where as spinal astrocytomas occurred in the younger age group patient ranged from 26 to 60 years, mean age 23 years.

The majority of ependymomas arise in the cervical spinal cord, with 44% in the cervical cord alone and 23% involving the upper thoracic spinal cord as well[3]. The myxopapillary ependymomas are commonly present in the conus medullaris and the filum terminale[3,7]. Ependymomas originate from the ependymal walls and as such are more centromedullary located compared with astrocytomas[9]. They are usually well circumscribed and do not infiltrate adjacent cord tissue. Astrocytomas are more frequent in the cervical and the thoracic regions[10]. The typical astrocytoma is large, eccentrically located and frequently ill-defined margin[9]. The mean size of the ependymoma corresponds to a mean height of three to four vertebral bodies (min. 2, max. 13), whereas astrocytomas are usually more extension, with a mean height of 5.6 vertebral bodies (min. 2, max. 19)[9]. In contrast, we found that most of spinal cord ependymomas and astrocytomas were eccentric location, 6/8 (75%) and 6/7 (85.7%), respectively. Spinal cord ependymomas had longer extension than spinal cord astrocytomas, 7.8 and 5.4 vertebral segments, respectively.

Ependymomas commonly are hyperintense on T2WI. Myxopapillary ependymoma is usually hyperintense on T1 because of mucinous content or hemorrhage content[10], whereas most non-myxopapillary
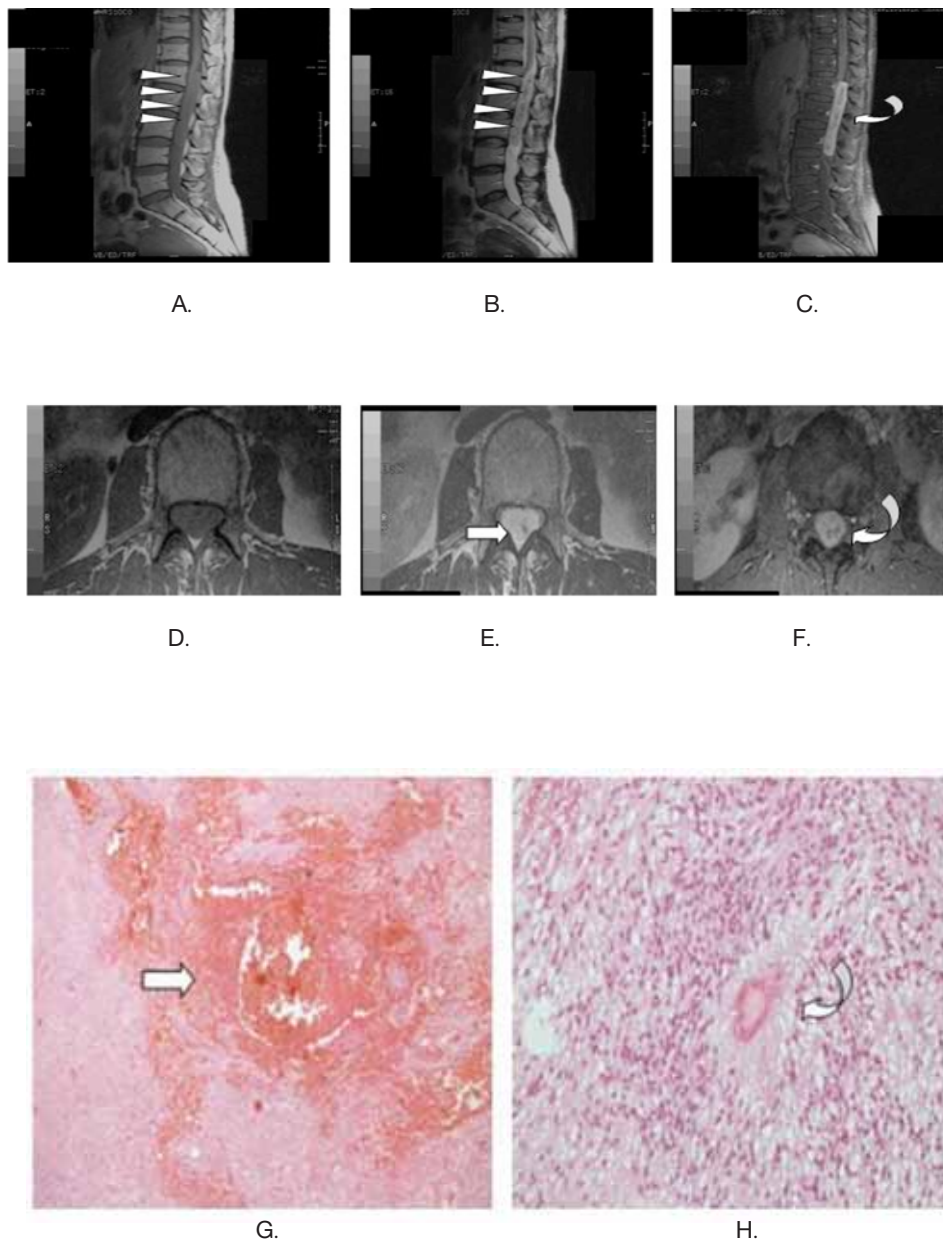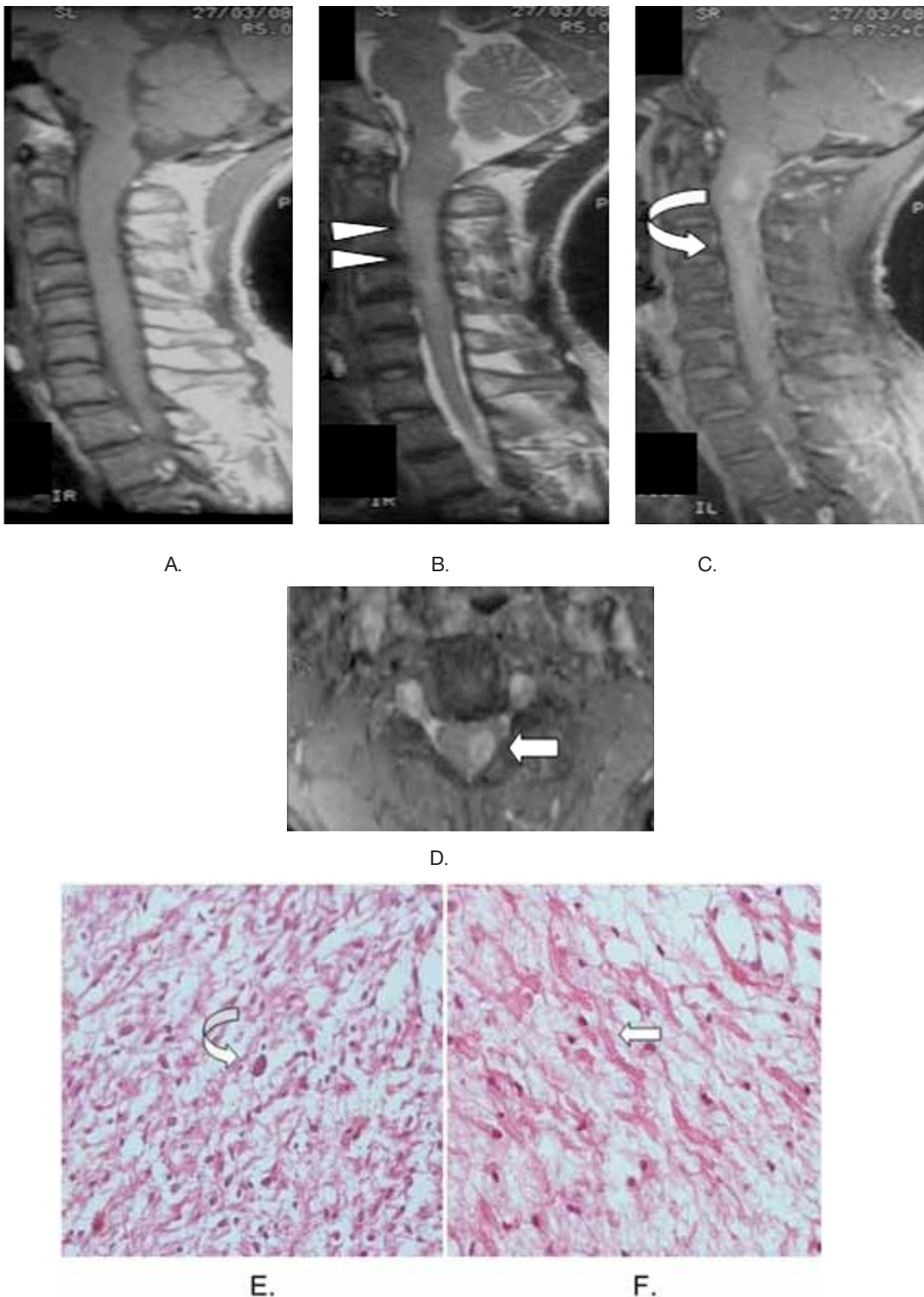
**Fig 1** Typical spinal cord ependymoma ( WHO grade II) in 49 year-old woman. (A) T1-weight sagittal image show well-define iso SI intramedullary tumor from L1-L4 spine epiconus region and exhibit mix hypo-hyper SI on (B) T2-weight sagittal image (arrow head). (C) Fat suppressed CE T1-weight axial image show intense homogeneous enhancement (curve arrow). (D) T1-weight axial image show small area of iso SI and exhibits low SI area on (E) T2-weight gradient axial image, representing intratumoral hemorrhage (white arrow). (F) Fat suppressed CE T1-weight axial image show intense enhancement. (G) and (H) Histology show area of intratumoral hemorrhage (arrow) and perivascular rosette formation (curve arrow).

A.

B.

C.

D.

E.

F.

**Fig 2** Typical spinal cord pilocytic astrocytoma (WHO grade I) in 47 years old woman. (A) T1-weight sagittal image show ill-define iso SI intramedullary spinal cord tumor and exhibit heterogeneous hyper SI on (B) T2-weight sagittal image (arrow head). (C) and (D) Fat suppressed CE T1-weight sagittal and axial image show focal nodular enhancement of tumors (white arrow). (E), (F) and (G) Histology show atypical astrocyte (curve arrow) and rosenthal reaction (arrow).

A.                    B.                    C.



D.
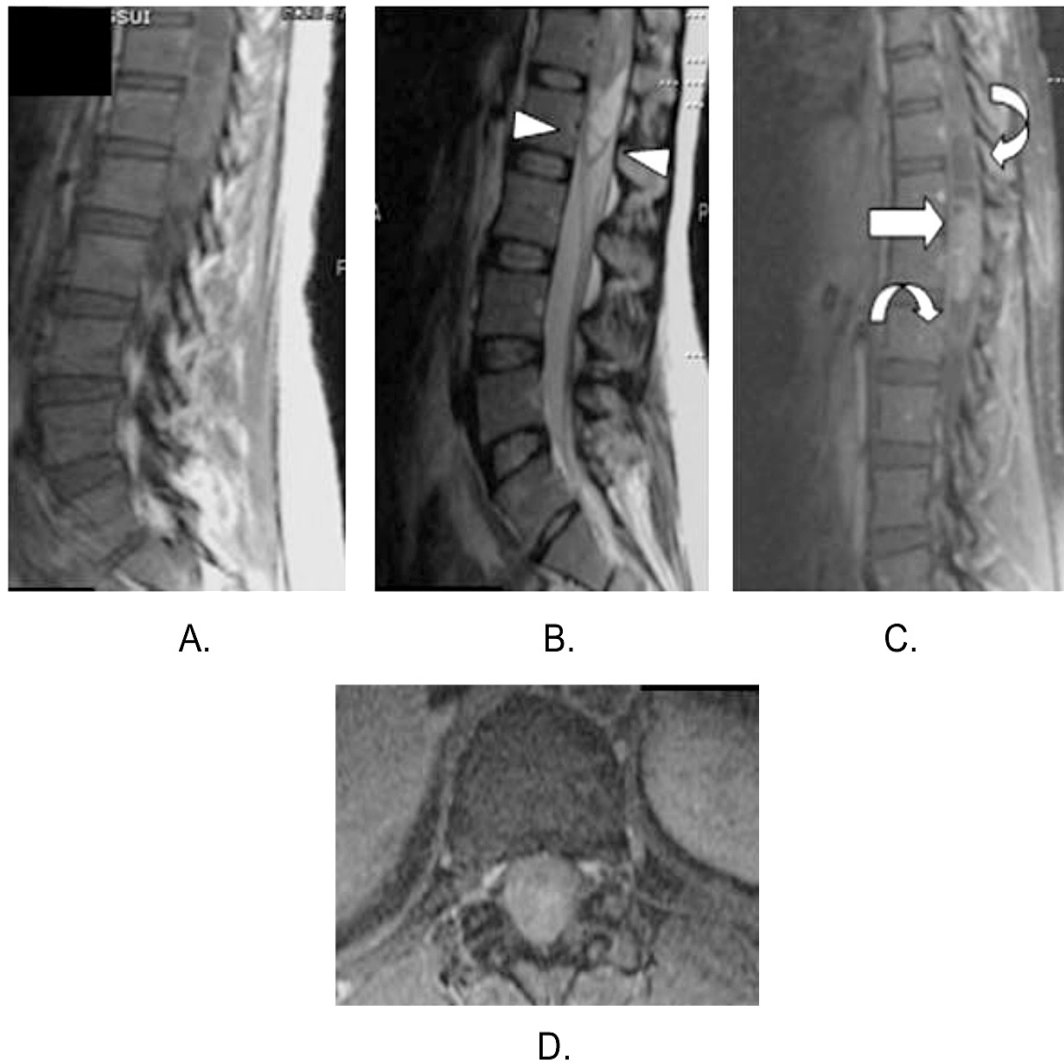
**Fig 3** Spinal cord tanocytic ependymoma with rostral and caudal cysts (WHO grade II) in 36 year-old woman. (A) T1-weight sagittal image show heterogeneous iso-hypo signal intensity at conus medullaris region and exhibit hyper SI on (B) T2-weight sagittal image with peritumoral low SI (arrow head), representing hemosiderin cap sign. (C) and (D) Fat suppressed CE T1-weight sagittal and axial image show intense enhancement (white arrow) with rostral and caudal cysts (curve arrow).

A.

B.

C.

D.

E.

F.

**Fig 4** Spinal cord ependymoma with syringohydromyelia (WHO grade II) in 39 year-old woman. (A) T1-weight sagittal image show low signal intensity intramedullary tumors form C2-T12 spine and exhibit high signal intensity in (B) T2-weighted image. (C) Fat-suppressed CE T1-weighted sagittal image show patchy enhancement of intramedullary spinal cord lesions (curved arrow). (D) T1-weighted sagittal image (E) T2-weighted sagittal image and (F) Fat-suppressed CE T1-weighted sagittal image show intramedullary tumors extending to the thoracic spine with syringohydromyelia at T11/12 spine (white arrow).

**A.**

**B.**

**C.**             **D.**             **E.**
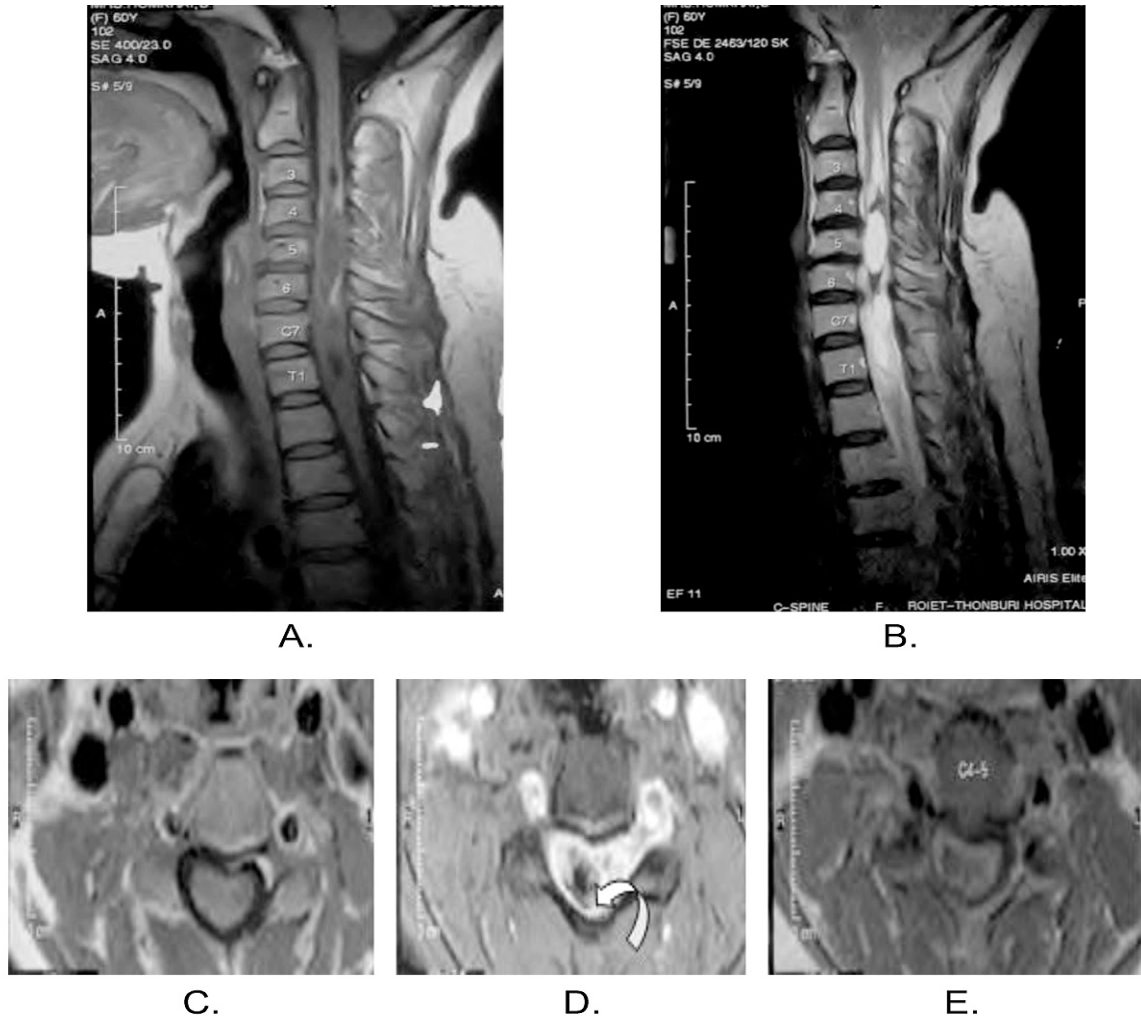
**Fig 5**   Spinal cord ependymoma with intratumoral hemorrhage ( WHO grade II) in 60 year-old woman. (A) T1-weight sagittal image show well-defined mix iso-hyper SI intramedullary tumor from C3-T1 spine and exhibit hyper SI on (B) T2-weight sagittal image (arrow head). (C) T1-weight axial image show small area of hyper SI and exhibits low SI area with blooming artifact on (D) T2-weight gradient axial image, representing intratumoral hemorrhage (curved arrow). (E) Fat suppressed CE T1-weight axial image show heterogeneous enhancement pattern.

A.
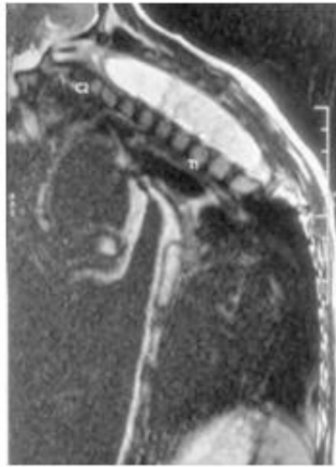


B.



C.
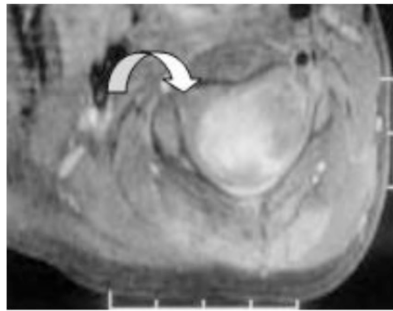


D.



E.
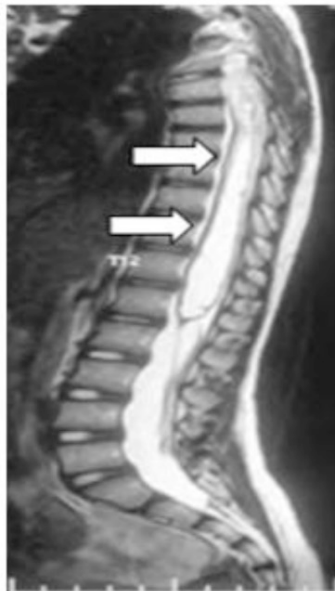


F.



G.
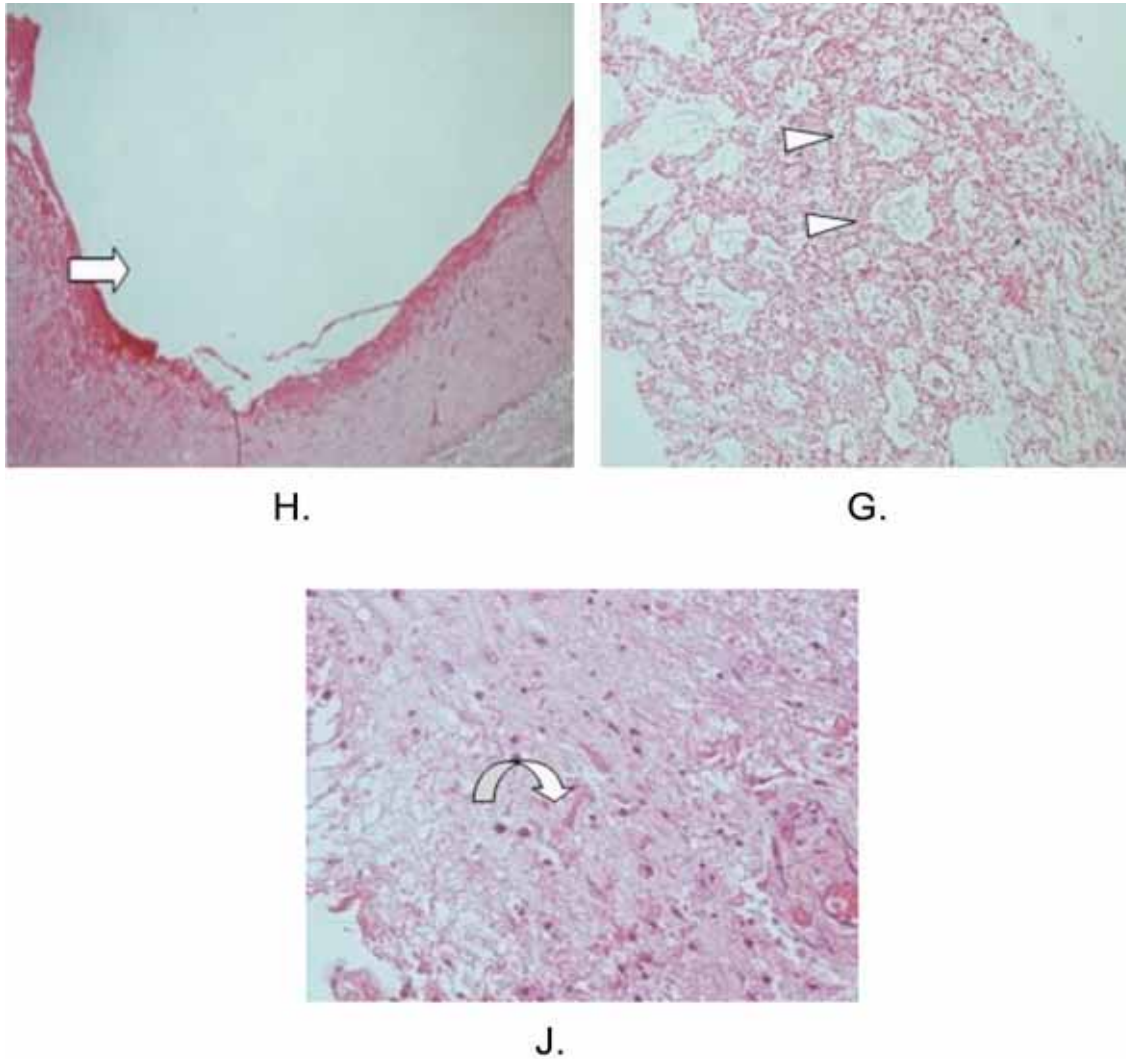
**Fig 6** Spinal cord pilocytic astrocytoma (WHO grade I) in 9 years old girl presenting with scoliosis. (A) T1-weight sagittal image (TR/TE=700/12.5) show ill-define iso SI intramedullary spinal cord tumor form C2-T1 and exhibit heterogeneous hyper SI on (B) T2-weight sagittal image. (C) and (D) Fat suppressed CE T1-weight sagittal and axial image show heterogeneous enhancement of tumors (arrow head and curve arrow). (E) T1-weight sagittal image shows long segment of syringohydromyelia entire thoracic extending to lower lumbar spine and exhibit hyper SI on (F.) T2-weight sagittal image (white arrow). (G) Fat suppressed CE T1-weight sagittal image shows no enhancement of this lesions. (H), (I) and (J) Histology show a large cystic area (arrow), microcystic area (arrow head) and rosenthal fiber (curve arrow).

ependymomas are hypointense[8]. These tumors are sometimes heterogeneous due to hemorrhage. Sometimes dark caps were seen, especially on T2WI, rostral and caudal of the tumor representing hemosiderin deposits. Cyst formation and hemorrhage is common, especially at the tumor margins. Hemorrhage and calcification are more common than in astrocytomas[10]. After contrast administration intense enhancement is the rule, sometimes homogeneous, but often also heterogeneous of rim-like[8]. Most astrocytomas were iso- or hypointense relative to the spinal cord on T1-weighted imaging and hyperintense on T2-weighted imaging[2,8]. The enhancement patterns of the intramedullary astrocytomas, were evenly distributed with focal nodular, patchy, and inhomogeneous diffuse enhancement; however, non demonstrated a homogeneously diffuse enhancing pattern[2]. These patchy or irregular enhancements are one of the MR imaging characteristics of astrocytomas, differentiating them from ependymoma and are supposedly the result of the pathologic features of astrocytomas that tend to have an infiltrative nature extending far beyond the gross tumor margin. Therefore, patients with astrocytomas have a worse prognosis and survival rate than those with ependymomas.

At T2 imaging, the presence of a low-signal rim along the rostral or caudal margin of a spinal cord tumor is a fairly specific indicator of ependymoma, and was found in 17%, 20%, 20% and 64% of cases in the series investigated, respectively, by Choi et al.[11], Fine et al.[12], Alice et al.[13], and Nemoto et al[14]. The rim is due to the presence of hemosiderin at the margin of the tumor, arising, presumably, from prior subclinical tumoral hemorrhage, and is often referred to as a 'hemosiderin cap'. In our series was found only 1/8 (12.5%) of spinal cord ependymoma.

In the next category, the published literature states that 50% of spinal ependymomas will demonstrate associated cysts[7]. There are two basic types of cysts: tumoral and nontumoral. Cysts located at the poles of the solid portion of the tumor usually represent simply reactive dilatation of the central canal (syringomyelia). Approximately 60% of all intramedullary spinal tumors demonstrate these rostral or caudal[15]. In these cases, only the solid component of a spinal cord tumor must be resected; the rostral and caudal cysts will either decompress upon removal of the solid portion or they can be aspirated by the surgeon at resection[7,15]. In fact, rostral and caudal cysts have been shown to contain either hemorrhagic or xanthochromic fluid, but never tumor cells[7]. These cysts are not part of the tumor itself and should not enhance on imaging studies. They are not septated and do not show echogenicity within their walls at intraoperative ultrasonography (US)[15]. Rostral or caudal cysts are believed to arise from the egress of fluid produced by these neoplasms through the central canal and may also explain the relative lack of symptoms seen in cases of intramedullary spinal neoplasms. In contrast, tumoral cysts are contained within the tumor itself and frequently show peripheral enhancement[7,15]. They tend to be more commonly seen in astrocytomas than in ependymomas[15]. Identification of the location of the solid enhancing portion of the tumor (including enhancing tumoral cysts) is vital because current neurosurgical techniques allow laminotomy or laminectomy to be limited only to this zone, thereby decreasing potential surgical morbidity[7,15]. Balériaux et al, intratumoral cysts appeared in 4 astrocytomas (21%) and peritumoral cysts appeared in 3 (16%) patients[9]. In our series, patho-

logical findings show cystic component 57.1% of seven spinal cord astrocytomas and 37.5% of eight spinal cord ependymomas. Whereas MRI findings show rostal or caudal reactive cyst 87.5% of spinal cord ependymomas more common than spinal cord astrocytomas 28.6%.

### Histological findings

Most ependymomas are histologically benign and well demarcated and compress the adjacent cord rather than infiltrating it. WHO grade is one component of a combination of criteria used to predict a response to therapy and outcome[16]. There are four histologic subtypes of ependymomas: cellular, papillary, clear cell, and tanocytic. The cellular form is the most common intramedullary variant. On histologic evaluation, perivascular pseudorosettes are the cardinal histologic feature (Fig 1), and there is moderate cellularity with low mitotic activity. The most common histologic subtypes are pilocytic astrocytomas (World Health Organization [WHO] grade I) and fibrillary astrocytomas (WHO grade II). Glioblastoma (WHO grade IV) rarely occurs in the spine, accounting for only 0.2-1.5% of cord astrocytomas. On histologic evaluation, fibrillary astrocytomas show widespread parenchymal infiltration with variable degrees of nuclear atypia and increased cellularity. Histologically, they are often biphasic with dense and looser areas. Pilocytic astrocytomas generally lack mitotic figures and other high-grade features and may harbor Rosenthal fibers (intracytoplasmic proteinaceous inclusions) (Fig 4) and thickened vascular walls. We found that in every cases ependymomas were mark hypervascularity, while 2/7 (28.2%) of astrocytoma were moderate hypervascularity. Therefore spinal cord ependymomas show homogeneous intense enhancement, but astro-

cytomas never. In our series, we found homogeneous enhancement of spinal cord ependymoms 1/8 (12.5%). Most of spinal cord ependymomas had cystic and hemorrhage component, possibly other enhancement patterns such as focal nodular, heterogeneous or patchy enhancement. Spinal cord astrocytomas show heterogeneous enhancement 4/7 (57.2%). Two of 15 cases (13.3%) were misinterpreted, the fist one of spinal cord ependymoma at cervical spine and the last one of hemorrhagic astrocytoma.

In our study, there are some limitations as following. The sample size was too small. The MRI was interpreted by one experienced neurological radiologist without intraobserver variability assessment. MRI gradient sequence was not performed in all cases which may lower sensitivity to detected intratumoral hemorrhage.

## Conclusion

The correct diagnostic spinal cord tumor is important because the treatment and prognosis are different. MRI has significantly changed the detection and diagnosis of intramedullary spinal cord tumors. Although no statistically significant characteristic MRI feature to distinguish between ependymoma and astrocytoma is detected. By percentage we found that border, length and signal intensity of tumors may help diagnosis. With pathological correlation, all of spinal cord ependymomas are mark hypervascular tumor, but astrocytomas never showed.

## References

1.  Sun, B., Wang, C., Wang, J. MRI features of intramedullary spinal cord ependymomas. Journal of Neuroimaging 2003;13(4):346-51.

2.  H.S. Seo, J.-h. Kim, D.H. Lee. Nonenhancing Intramedullary Astrocytomas and Other MR Imaging Features: A Retrospective Study and Systematic Review. AJNR 2010; 31:498-503.

3.  Kasim Abul-Kasim, Majda M. Thurnher. Intradural spinal tumors: current classification and MRI features. Neuroradiology 2008;50:301-14.

4.  Lowe, G.M. Magnetic resonance imaging of intramedullary spinal cord tumors. Journal of Neuro-Oncology 2000; 47(3):195-210.

5.  Fred J. Epstein, Jean-Pierre Farmer, F.R.C.S., and Diana Freed. Adult intramedullary astrocytomas of the spinal cord. J Neurosurg 1992;77:355-9.

6.  John K. Houten and Paul R. Cooper. Spinal cord astrocytomas: presentation, management and outcome. Journal of Neuro-Oncology 2000;47:219-24.

7.  Heather Kahan, Evelyn M. L. Sklar. MR Characteristics of Histopathologic Subtypes of Spinal Ependymoma. AJNR 1996;17:143-50.

8.  J.W.M. Van Goethem et al. Spinal tumors. European Journal of Radiology 2004; 50:159-76.

9.  Balériaux, D.L.F.Spinal cord tumors. European Radiology 1999;9(7):1252-8.

10. Bloomer, C.W., Ackerman, A., Bhatia, R.G. Imaging for spine tumors and new applications. Topics in Magnetic Resonance Imaging 2006;17(2):69-87.

11. Choi, J.-Y., Chang, K.-H. Intracranial. Spinal Ependymomas: Review of MR Images in 61 Patients. Korean Journal of Radiology 2002;3(4):219-28.

12. Fine MJ, Kricheff II, Freed D, Epstein FJ. Spinal cord ependymomas: MR imaging features. Radiology 1995; 197:655-8.

13. Alice Boyd Smith. Karl A. Soderlund. Radiologic-Pathologic Correlation of Pediatric and Adolescent Spinal Neoplasms. AJR 2012;198:34-43.

14. Nemoto Y, Inoue Y, Tashiro T, et al. Intramedullary spinal cord tumors: significance of associated hemorrhage at MR imaging. Radiology 1992;182:793-6.

15. Kelly K. Koeller, CDR, R. Scott Rosenblum. Neoplasms of the Spinal Cord and Filum Terminale: Radiologic-Pathologic Correlation. RadioGraphics 2000;20:1721-49.

16. Louis, D.N., Ohgaki, H. The 2007 WHO classification of tumours of the central nervous system. Acta Neuropathologica 2007;114(2):97-109.

# A Nine Case Series of Ultrasound-Guided Hydrostatic Reduction of Intussusception by Saline Enema

**Sornsupha Limchareon[1], Adisorn Boonyarit[2]**

[1] *Division of Radiology and Nuclear Medicine, Faculty of Medicine, Burapha University, Chonburi, Thailand*
[2] *Department of Radiology, Phyathai-Sriracha Hospital, Chonburi, Thailand*

## Abstract

Non-surgical reduction of the intussusception is the first line treatment in children with intussusception. Among various radiological reduction techniques, barium enema reduction of the intussusception under fluoroscopy has been widely used in Thailand while pneumatic reduction under fluoroscopy has become popular in teaching hospitals. To our knowledge, ultrasound-guided hydrostatic reduction of the intussusception by saline enema (UGHSE) has never been used in Thailand. We reported 9 cases using UGHSE with 100% success rate without complication.

## Introduction

Intussusception is the invagination of one bowel segment into the lumen of the other. It is a common cause of the intestinal obstruction in infants and children. It frequently occurs in well-nourished infants, mostly are 4 to 12 months old [1]. The majority of the causes are idiopathic[2]. The remaining causes are the pathologic lead points such as polyp, Meckel's diverticulum, duplication cyst[1,2]. US is the modality of choice for the diagnosis of intussusception [3]. The traditionally barium enema was used to diagnose and reduction of intussusception[1]. If the attempt of reduction was failed, surgery was subsequently indicated. There have been various techniques mentioned in the literature that improved the success rate and less perforation rate[4-6]. The advantages and disadvantages of each technique has been discussed [2,4-6]. The technique of radiological reduction in daily practice depends on the radiologist's preferences[7]. In Thailand barium enema reduction of intussusception under fluoroscopy has been widely used and pneumatic reduction under fluoroscopy is popular in teaching hospitals, while UGHSE has never been used.

## Case series

From January 1, 2011 to July 31, 2013, we performed UGHSE in 9 children. The detail of each patient is shown in table 1. There were 5 boys and 4 girls, aged 4-36 months (average 19.6 months). All except one patient had no fever on the presentation. The most common symptom was abdominal pain (56%), followed by fever (44%), vomiting (33%), diarrhea (22%), and bloody stool (22%). The maximum duration of the symptoms was 6 days,average 2.28 days. Seven out of 9 nine (78%) patients had negative physical examinations. White blood count was done in 8 patients. All of them showed no leukocytosis or neutrophil shift. Five patients had abdominal radiographs but intussusception was suspected in only two (22%). All the intussusceptions was diagnosed by US, showing target sign in short-axis view. The most common locations of the intussusception apices was hepatic flexure in 7 (78%).

The average axial diameter of the intussusception was 2.41 cm (range 1.9-3.2 cm). Reduction was successful by the first attempt in 7 of 9 (78%) and the second attempt in 2 (22%). All children was free from complication or recurrence in at least 48-hour follow up.

## Technique

We informed parents, pediatricians with/or without surgeons before the procedure. The procedure was performed in the US room. An enema bag was filled with 1,000 ml of normal saline that was warmed at the temperature of 37$^{\circ}$C and was kept at 100-120 cm above the table top. The upper end of the saline bag remained open. A well-lubricated Foley's catheter (12-16 F was introduced transrectally) with balloon inflation. The buttocks was firmly taped together with adhesive tape and by manually during the procedure. No sedation, muscle relaxant or prophylaxis antibiotic was administered. The reduction was observed under the guidance of US by using a 5-12MHz linear transducer (Toshiba Aplio, XG SSA-790A, Japan). Successful reduction was determined when the IC valve and terminal ileum were visualized associated with fluid reflux into the small bowel. During the reduction, we intermittently observed US findings of perforation including sudden collapse of the colon, and rapid increased intraperitoneal free fluid.

**Table 1.** Details of 9 patients.

| Case No. | Sex | Age (mo) | Symptoms | BT (°C) | PE-abdomen | WBC/N | Abd film | US intus location+size | Successful reduction |
|---|---|---|---|---|---|---|---|---|---|
| 1 | M | 5 | Fever+ vomiting 1 day | 36.9 | neg | 14600 ( N 59 , L39 , Mo 2) | Suspected mass at RUQ | Hepatic flexure 2.1 cm | 1st attempt |
| 2 | M | 34 | Abdominal pain 9 hours | 36.1 | Mass ? | 8900 (N 42 L 47 Mo 11 ) | - | Mid ascend 2.2 cm | 1st attempt |
| 3 | F | 4 | Fever 3 days, Bloody stool + vomiting 1 day | 36.9 | neg | 3800 (N 60 L 32 Mo 7 ) | Unremark-able | rectosig moid | 1st attempt |
| 4 | M | 25 | Abdominal pain 1 day | 37.2 | neg | 5500 (N 73 L 23 Mo 3 ) | - | Hepatic flexure 2.1 cm | 1st attempt |
| 5 | M | 36 | Abdominal pain 4 days | 36.0 | neg | 10300 (N 49 L 47 Mo 3 ) | - | Hepatic flexure 3.1 cm | 1st attempt |
| 6 | F | 26 | Abdominal pain + vomiting 2 days, diarrhea ? day | 37.0 | neg | 11600 (N 46 L 51 Mo 3 ) | Suggestive of intussucep-tion | Hepatic flexure 2.7 cm | 1st attempt |
| 7 | M | 10 | Abdominal pain 1 day | 36.5 | neg | 9400 (N 54 L 39 Mo 7 ) | - | Hepatic flexure 2.1 cm | 2nd attempt |
| 8 | M | 28 | Fever 6 days, diarrhea 2 days | 39.1 | neg | 3400 (N 25 L 61 Mo 13 ) | - | Hepatic flexure 2.3 cm | 2nd attempt |
| 9 | F | 8 | Fever + bloody stool 2 days | 36 | RLQ mass | - | Unremark-able | Hepatic flexure | 1st attempt |

Note : abdominal film - 5 cases in written part, but show only 4 cases in table

## Discussion

There is a wide variation in the techniques of non-surgical reduction of the intussusception[7]. Variation refers in two aspects. The first variation depends on guidance method either fluoroscopy or US. The other variation depends on material used either liquid or gas. Pneumatic reduction under fluoroscopy has become popular nowadays because of higher success rate than barium[5,6]. However it still has radiation hazard. Hydrostatic reduction by saline enema is quite popular in Eastern world[2]. In the large series of Bai YZ et al.[2], they reported UGHSE in 5218 cases and the success rate was 95.5% with 0.17% perforation rate. The only disadvantage of US is operator dependent. Thus learning curve is needed to perform with confidence. Newer techniques such as US-guided pneumatic reduction[8], external manual reduction with US assistance[9] have been presented recently. The best technique has not been in consensus yet. US criterion for successful reduction were disappearance of the intussusceptions, and fluid reflux into the terminal ileum[2]. We observed that visualization of the IC valve made us more confident in distinguishing between

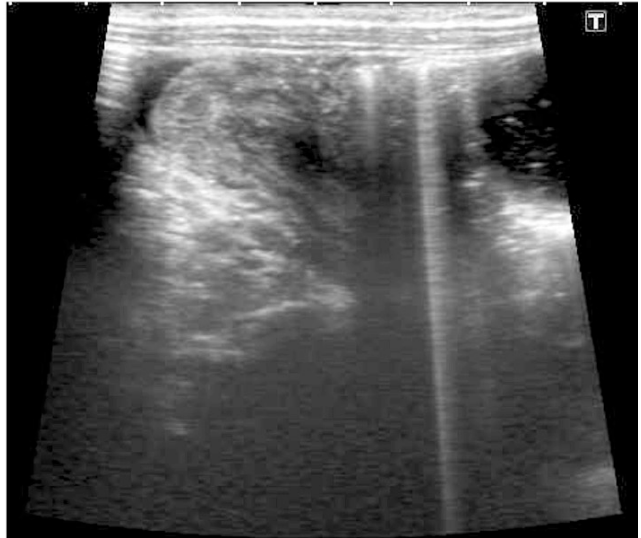**Fig. 1** Normal saline at the apex of intussuception



**Fig. 2** Intussusceptum at IC valve



**Fig. 3** Intussusceptum passing IC valve



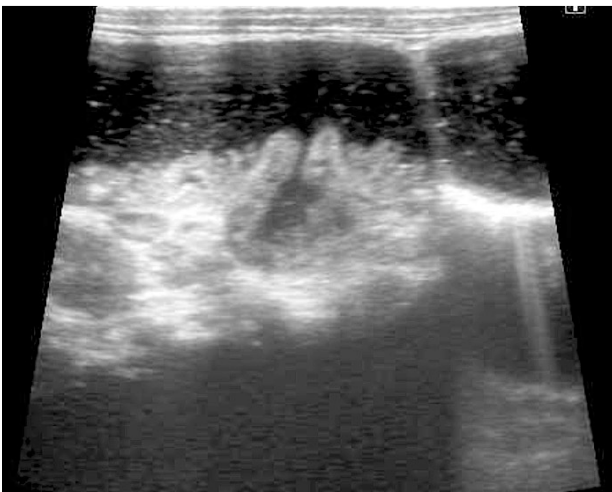**Fig. 4** Intussusceptum almost passed IC valve



**Fig. 5** IC valve post reduction



**Fig. 6** Swollen terminal ileum with gradual transition to normal wall

colon and ileal loops. Yoon CH, et al.[8] proposed the other criteria as abrupt transition between the swollen terminal ileum and the proximal normal ileal loop in long-axis scan could rule out any residual ileoileal intususception.

We did not use any sedation in this our series as well as in the report of 194 cases by Gonzalez-Spinola, et al.[10] which showed success rate in almost 90%. However In the recent report of Ilivitzki A, et al.[11] claimed that using deep sedation with propofol during reduction of intussusceptions was safe and effective.

## Conclusion

In our 9 case series, UGHSE is feasible with high success rate without complication. The benefit is no radiation which is a point of our concern. We would like to encourage radiologists to perform this technique. If we have enough number of patients, we can generalize the advantages or disadvantages of this technique.

## References

1. Kobayashi Y, ShimiZu N, Matsuda R. Thirty -seven years of experience in the treatment of intussusceptions in infants and children. Yonago Acta Med 1987;30 Suppl: 193-202.

2. Bai YZ, Qu RB, Wang GD, Zhang KR, Li Y, Huang Y, et al. Ultrasound-guided hydrostatic reduction of intussusep- tions by saline enema: a review of 5,218 cases in 17 years. Am J Surg 2006;192:273-5.

3. Hryhorezuk AL, Strouse PJ. Validation of US as a first- line diagnostic test for assessment of pediatric ileocolic intussusceptions. Pediatr Radiol 2009;39(1):1075-9.

4. Chan KL, Saing HS, Peh WC, Mya GH, Cheng W, Khong PL, et al. Childhood intussusceptions: ultrasound-guided Hartmann's solution hydrostatic reduction or barium enema reduction? J Pediatr Surg 1997;32(1):3-6.

5. Hannon EJ, Allan RA, Negus AS, Murphey F, Okoye BO. Air enema reduction of intussuception: a registrar-led, protocol driven service is safe and effective. Pediatr Surg Int 2013;29:805-9.

6. Hadidi AT, Shal NE. Childhood intussusceptions: a com- parative study of non surgical management. J Pediatr Surg 1999;34(2):304-7.

7. Rosenfeld K, McHugh K. Survey of intussusceptions re- duction in England, Scotland and Wales: how and why we could do better.Clinical Radiology 1999;54:452-8.

8. Yoon HC, Kim HJ, Goo HW. Intussusception in children: US-guided pneumatic reduction-initial experience. Radio- logy 2001;218:85-8.

9. Vazquez JL, Ortiz M, Doniz MC, Monterio M, Campo VM. External manual reduction of paediatric idiopathic ileo- colic intussusceptions with US assistance: a new, stan- dardized, effective and safe manoeuvre. Pediatr Radiol 2012;42:1197-204.

10. Gonzalez-Spinola J, Pozo GD, Tejedor D, Blanco A. Intussuception: the accuracy of US-guided saline enema and the usefulness of a delayed attempt at reduction. J Pediatr Surg 1999;34(6):1016-20.

11. Ilivitzki A, Shtark LG, Arish K, Engel A. Deep sedation during pneumatic reduction of intussusceptions. Pediatr Radiol 2012;42:562-5.

# Color Doppler Ultrasound and MRI Findings of Vein of Galen Malformation in a Newborn, a Case Report.

Jiraporn Srinakarin[1], Jureerat Thammaroj[1], Ratana Kumwilaisak[2]
Waranon Munkong[1], Junya Jirapradittha[3]

[1] Department of Radiology, Faculty of Medicine, Khon Kaen University, Thailand.
[2] Department of Obstetrics and Gynecology, Faculty of Medicine, Khon Kaen University, Thailand.
[3] Department of Pediatrics, Faculty of Medicine, Khon Kaen University, Thailand.

## Abstract

The Vein of Galen aneurysmal malformation (VGAM) is a rare intracranial arteriovenous anomaly that has usually been diagnosed prenatally. We reported a near term boy, 2,140 grams body weight, with a large VGAM, who was diagnosed prenatally by color Doppler ultrasound. After birth, his APGAR scores were 2, 4, and 8, respectively. An emergency cranial ultrasound was performed promptly when his vital sign began to be stable. The image revealed a huge dilatation of the great vein of Galen, measured about 1.9 x 2.0 x 3.8 cm. in diameter, with mixed venous and arterial flow profiles. Abnormal dilatation of the right internal carotid artery, and circle of Willis were also identified and likely to be an arterial feeder to choroidal artery which directly draining into the great vein of Galen. MRI, MRA, and MRV of the brain were performed on the following day and also showed a huge aneurysmal dilatation of a median vein of prosencephalon (precursor of the great vein of Galen) and marked dilatation of falcine sinus. Torcular herophili, both transverse / sigmoid sinuses and both internal jugular veins showed abnormal dilatation on MRA and MRV. Endovascular transarterial embolization was planned to performe on this patient but his vital sign was not stable. He finally expired from severe congestive heart failure after 5 days of life.

*Keywords:* Color Doppler ultrasound, MRI, VGAM

## Introduction

The Vein of Galen aneurysmal malformation (VGAM) is a rare congenital disease with an incidence of 1:25000. It was first described by Steinhel et al in 1895[1]. The VGAM is located in the midline in the choroidal fissure. It consists of multiple feeding arteries including anterior and posterior choroidal arteries, anterior cerebral artery. The feeding arteries drain directly into a large venous pouch called the vein of Galen. Raybaud et al reported that malformation develops between the 6th and 11th weeks of gestation and thought to result from the development of an arteriovenous connection between primitive choroidal vessels and the median prosencephalic vein of Markowski[2]. Base on angioarchitecture association, the VGAM are divided into choroidal and mural types. The Vein of Galen aneurysmal malformation (VGAM) can be diagnosed by many imaging modalities such as color Doppler sonography, CT scan and MRI. It is usually or accidentally been diagnosed prenatally[3,4]. Identification of the type of the VGAM by the imaging helps us to know clinical outcome and prognosis of the neonate. It is also very important to distinguish the VGAM from aneurysmal dilatation of the true vein of Galen caused by an adjacent brain AVM called VGAD (vein of Galen aneurysmal dilatation) which has a higher risk of hemorrhage[5].

We reported a 37 weeks gestation age boy with 2,140 grams body weight, who was diagnosed VGAM prenatally by color Doppler ultrasound. The boy was delivered by Cesarean section with APGAR scores of 2, 4, and 8, respectively. Prenatal diagnosis of a large (5 mm) patent ductus arteriosus (PDA) was reported with mild dilated coronary sinus and cardiac chambers. Tricuspid regurgitation was also identified with pressure gradient of 37 mm Hg and

EF 32%. An emergency transcranial Doppler sonography was performed in the NICU when his vital sign began to be stable. The color Doppler ultrasound (LOGIQ P6, GE Medical System, Milwaukee, WI, USA) revealed a huge dilatation of the great vein of Galen, measured about 1.9 x 2.0 x 3.8 cm. in diameter, with mixed venous and arterial flow profiles (Fig.1). Multiple high velocity (> 100 cm/s) and dilated feeding vessels were clearly identified draining directly into the great vein of Galen (Fig.2). MRI, MRA, and MRV of the brain (Philips Achieva 3.0T TX, Netherlands) were performed on the following day and also showed a huge aneurysmal dilatation of a median vein of prosencephalon (precursor of the great vein of Galen) and marked dilatation of falcine sinus (Fig.3). Torcular herophili, both transverse/sigmoid sinuses and both internal jugular veins also showed abnormal dilatation on MRA and MRV. The diagnosis of VGAM was reported with likely be a choroidal type. We planned to perform endovascular transarterial embolization when his clinical and vital sign were stable. His parents were referred for consultation with a pediatric specialist, a cardiovascular surgeon, a neurointerventionist and a palliative team in order to plan an optimal management and let them know the prognosis. Clinically, his heart failure was progressing and superimposed with anemia and septicemia. Finally, he expired on the 5th day of life from cardiovascular failure.

## Discussion

The vein of Galen malformation is actually a misnomer term because the ectatic vein we identified was the median mesencephalic vein of Markowski, the embryonic precursor of the vein of Galen and is normally absent in the adult[2]. It's divided into two types; the choroidal and mural types. The former

**Fig 1.** Transcranial color Doppler sonogram shows turbulent flow (Yin-Yang sign) in the aneurysmal dilatation of the great vein of Galen (arrow).
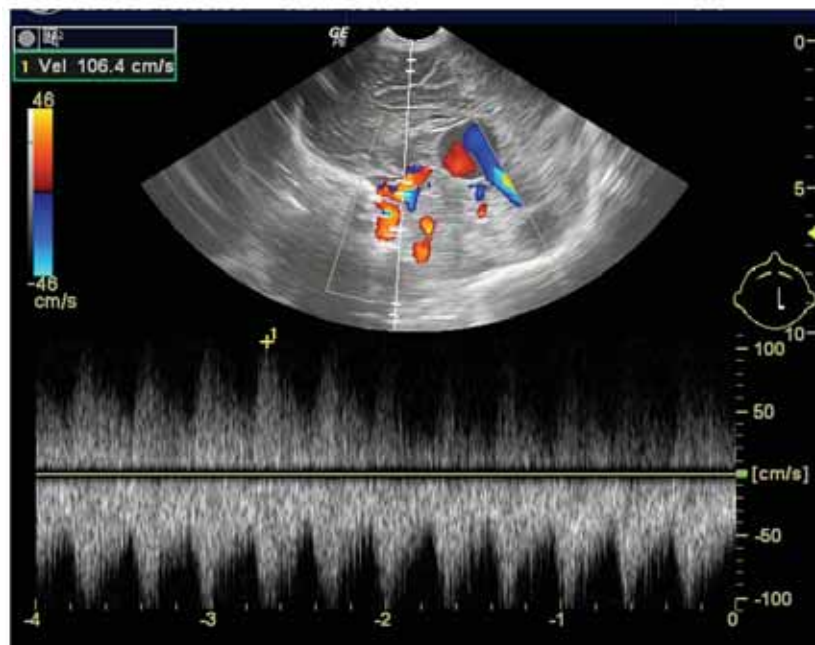


**Fig 2.** Transcranial color Doppler sonogram shows abnormal high velocity of the spectral waveform of the feeding artery (arrow).

**Fig 3.** A sagittal T2-weighted MRI of the brain shows a markedly enlarged median prosencephalic vein of Markowski, or the great vein of Galen (arrow) with marked dilatation of the straight sinus and the Torcular herophili.

type receives feeding arteries from choroidal arteries before emptying into a venous pouch, and is a primitive condition associated with poor clinical outcome in neonates[6-9]. The latter type is characterized by direct AVFs within the wall of the median prosencephalic vein of Marlowski and is found in infants with better prognosis. We reported a choroidal type of VGAM in the neonate associated with severe high output heart failure. Transcranial sonography is the best imaging modality for definite diagnosis as well as during late prenatal ultrasound scanning[10]. MRI with MR angiography helps us identifying the arterivenous malformations and a huge great vein of Galen (in fact it is the median prosencephalic vein of Markowski). MRA is also useful as a preliminary noninvasive imaging plan, and a follow up before performing endovascular transarterial embolization. The therapy of choice is the endovascular embolization using a special glue[6-9]. The therapeutic efficacy of the treatment reported by Lasjaunias et al, using the 21-point scale in neonate based on a number of factors, including cardiac, cerebral, hepatic, respiratory, and renal function those help a neurointerventionist and a pediatrician to predict the proper time to perform endovascular embolization for a good outcome[9]. In a large scale study by Lasjaunias et al reported a mortality rate of 10.6% overall, and 52% for neonate[9]. In our case report, he expired from severe high output heart failure, regarded 21-point scale by Lasjaunias. His scale was less than 8 suggested that endovascular therapy would be unsuccessful and thus treatment was not indicated.

## Acknowledgment

# References

1. Dandy W.E., "Experimental hydrocephalus," Annals Surgery, 1919;70(2)129-42.

2. Raybaud CASC, Strother CM, Hald JK. Aneurysms of the vein of Galen: embryonic considerations and anatomical features relating to the pathogenesis of the malformation. Neuroradiology 1989;31:109-28.

3. Beucher G, Fossey C, Belloy F. Richter B, Dreyfus M. Antenatal diagnosis and management of vein of Galen aneurysm: review illustrated by a case report. Journal de Gynecologie Obstetrique et Biologie de la Reproduction;2005:34(6);613-9.

4. Yamashita Y, Abe T, Ohara N, et al. Successful treatment of neonatal aneurymal dilation of the vein of Galen: the role of prenatal diagnosis and trans-arterial embolization. Neuroradiology1992;34(5):457-9.

5. Bhattacharya J J, Thammaroj J. Vein of Galen Malformations. J Neurol Neurosurg Psychiatry 2003;74(Suppl I):i42-i44.

6. Lasjaunias PL, Ter Brugge K, Lopez Ibor L, et al. The role of dural anomalies in vein of Galen aneurysm: report of six cases and review of literature. AJNR Am J Neuroradiol 1987;8:185-92.

7. Lasjaunias PL, Garcia-Manaco R, Rodesch G, Ter Brugge K, Zerah M, Tardieu M, et.al. Vein of Galen Malformation. Endovascular management of 43 cases. Childs Nerv Syst 1991;7:360-7.

8. Lasjaunias PL, Hui F, Zerah M, Garcia-Manaco R, Malherbe V, Rodesch G, et al. Cerebral arteriovenous malformations in children. Management of 179 consecutive cases and review of the literature. Childs Nerv Syst1995;11:66-79.

9. Lasjaunias PL, Chng SM, Sachet M, Alvarez H, Rodesch G, Garcia-Manaco R. The management of vein of Galen aneurysmal malformations. Neurosurgery 59 (5 Suppl 3); 2006:S3-113,S184-94.

10. Stephen S, Rodesch G, Elolf E, Wiemann D, Jorch G. Vein of Galen aneurysmal malformations: an ultrasonographic incidental finding-a case report. Pediatrics 2012; doi:10.1155/2012/824284(6pages).

# The Committee of Royal College of Radiologists of Thailand and Radiological Society of Thailand

## Apr 2013-Mar 2015

# The Journal of the Royal College of Radiologists & Radiological Society of Thailand

## (2013 - 2015)

**Office:**

The Royal college of Radiologists & Radiological society of Thailand. 9th Floor,
Royal Golden Jubilee Building, 2 Soi Soonvijai, Petchburi Road, Bankok, 10320
Tel 02-716-5963,    Fax 02-716-5964
E-mail pusjeckchon@hotmail.com.

# Instructions for Authors

1. The Asean Journal of Radiology publishes the papers on Radiological Sciences, such as research work, reviews articles case reports, innovations in medical Sciences related to all branches of Radiology, and letters to the editor. The aforementioned materials can be written in English only.

2. The authors have to submit 2 copies of the manuscript and a CD :to Assoc. Prof. Sirintara   Singhara Na Ayudya, Department of Radiology, Faculty of medicine, Ramathibodi hospital 270, Rama VI Road, Toong Phayathai, Ratchathewi, Bangkok, 10400. Tel 02-2011259#110, Fax 02-2011297, E-mail Sirintarapongpech2@hotmail.com

3. The original copy to be submitted must be typed in a double space on one of the page 8.5"x11" (A4) paper.

4. The format of the article must include:

    a. Title page and address of the author (s)

    b. Abstract (Objective, Methods, Results and conclusion)

    c. Introduction

    d. Material and Method

    e. Results and discussion

    f. Acknowledgment (if any)

    g. References (Follow the Vancouver style)

5. We will provide 5 copies of reprints for the author (s) an article for publication in the Asean Journal.

6. The illustrations and table must be clearly prepared with legends in English as they are the art works to be reproduced

7. The authors are responsible for the contents of the article as to its facts and findings.

8. Ethics

    Paper reporting studies which might be interpreted as human experimentation (e.g. controlled trials) should conform to the standards of the Declaration of Hilsinki (see British Medical Journal 1964:2:177) and should indicate that, approval that such studies may proceed, has been granted by the local or hospital Ethics Committee.

    When reporting experiments on animal indicate whether the institution's or the National Research Council's guide for, or any national law on, the care and use of laboratory animals was followed.

# THE ASEAN JOURNAL OF RADIOLOGY

## Instructions for Authors.

1. The Asean Journal of Radiology publishes the papers on Radiological Sciences, such as research work, reviews articles case reports, innovations in medical Sciences related to all branches of Radiology, and letters to the editor. The aforementioned materials can be written in English only.

2. The authors have to submit 2 copies of the manuscript and a CD : to 9th Floor,Royal Golden Jubilee Building, 2 Soi Soonvijai,New Petchburi road,Bangkok 10310,Thailand. Tel 02-2011259 #110, Fax 02-2011297, E-mail Pusjeckson@hotmail.com

3. The original copy to be submitted must be typed in a double space on one of the page 8.5 x11 inch (A4) paper.

4. The format of the article must include :
   a. Title page and address of the author (s)
   b. Abstract (Objective, Methods, Results and conclusion)
   c. Introduction
   d. Material and Method
   e. Results and discussion
   f. Acknowledgment (if any)
   g. References (Follow the Vancouver style)

5. We will provide 5 copies of reprints for the author (s) an article for publication in the Asean Journal.

6. The illustrations and table must be clearly prepared with legends in English as they are the art works to be reproduced

7. The authors are responsible for the contents of the article as to its facts and findings.

8. Ethics

Paper reporting studies which might be interpreted as human experimentation (e.g. controlled trials) should conform to the standards of the Declaration of Hilsinki (see British Medical Journal 1964:2:177) and should indicate that, approval that such studies may proceed, has been granted by the local or hospital Ethics Committee.

When reporting experiments on animal indicate whether the institutionûs or the National Research Council's guide for, or any national law on, the care and use of laboratory animals was followed.

## Website   http://www.rcrt.or.th